CHAPTER SEVENTEEN

THEORETICAL STUDIES OF THE ELECTRONIC STRUCTURE OF COMPOUNDS OF THE ACTINIDE ELEMENTS

Nikolas Kaltsoyannis, P. Jeffrey Hay, Jun Li,
Jean-Philippe Blaudeau, and Bruce E. Bursten

17.1   INTRODUCTION

In this chapter, we will present an overview of the theoretical and computational developments that have increased our understanding of the electronic structure of actinide-containing molecules and ions. The application of modern electronic structure methodologies to actinide systems remains one of the great challenges in quantum chemistry; indeed, as will be discussed below, there is no other portion of the periodic table that leads to the confluence of complexity with respect to the calculation of ground- and excited-state energies, bonding descriptions, and molecular properties. But there is also no place in the periodic table in which effective computational modeling of electronic structure can be more useful. The difficulties in creating, isolating, and handling many of the

actinide elements provide an opportunity for computational chemistry to be an unusually important partner in developing the chemistry of these elements.

The importance of actinide electronic structure begins with the earliest studies of uranium chemistry and predates the discovery of quantum mechanics. The fluorescence of uranyl compounds was observed as early as 1833 (Jørgensen and Reisfeld, 1983), a presage of the development of actinometry as a tool for measuring photochemical quantum yields. Interest in nuclear fuels has stimulated tremendous interest in understanding the properties, including electronic properties, of small actinide-containing molecules and ions, especially the oxides and halides of uranium and plutonium. The synthesis of uranocene in 1968 (Streitwieser and Müller-Westerhoff, 1968) led to the flurry of activity in the organometallic chemistry of the actinides that continues today. Actinide organometallics (or organoactinides) are nearly always molecular systems and are often volatile, which makes them amenable to an arsenal of experimental probes of molecular and electronic structure (Marks and Fischer, 1979). Theoretical and computational studies of the electronic structure of actinide systems have developed in concert with the experimental studies, and have been greatly facilitated by the extraordinary recent advances in high-performance computational technology.

We will focus on computational studies of the electronic structure of discrete (molecular or ionic) actinide-containing systems. We begin by discussing some of the general tenets of bonding that are relevant to the actinide elements and some of the challenges that are unique to this field. We then present the results of computational electronic structure studies on a variety of molecular actinide systems. The literature of molecular electronic structure of actinide systems has been compiled by Pyykkö (1986, 1993, 2000b), as well as being available as a database on the web (http://www.csc.fi/rtam). Pepper and Bursten (1991) reviewed the methodology and applications in the field in 1991. The reader is referred to those reviews for some of the details on earlier studies in this field. We restrict our discussion in this chapter to molecular actinide systems and do not discuss the extensive body of research in the use of theoretical electronic structure methods to model solid-state actinide chemistry. The reader is referred to Chapter 21 and some recent review articles (Lander *et al.*, 1994; Soderlind, 1998; Wills and Eriksson, 2000) for discussions of theoretical electronic structure methods applied to the metallic actinide elements and solid-state actinide compounds. We will also have minimal discussion of compounds of the transactinide elements in this chapter. The electronic structure of compounds of the transactinides is discussed in Chapter 14 and in the excellent review by Pershina (1996).

17.1.1 Electronic structure of actinide atoms

The challenge in undertaking theoretical studies of actinide complexes begins, of course, with the complex electronic structure of the actinide atoms. The lanthanide and actinide elements are distinct from the p- and d-block elements

in having f-orbitals as part of the active valence orbitals of the atom. The methodologies that can be successful in describing the electronic structure of such systems must obviously be able to accommodate valence f-orbitals. The historical development of methods that could handle f-electrons has been discussed by Pepper and Bursten (1991) and will be briefly recounted later in this chapter.

The most common representation of the angular functions of the seven real f-orbitals is presented in Table 17.1 and Fig. 17.1. Real orbitals are constructed by forming linear combinations of the spherical harmonics $Y_{l,m_l}(\theta,\phi)$ with common $|m_l|$ values, such as $Y_{3,1} \pm Y_{3,-1}$. The resulting real orbitals can be described with Cartesian labels in the same way we do for p- and d-orbitals. They are characterized by a distinct $|m_l|$ value, giving axially quantized orbitals of σ ($m_l = 0$), π ($|m_l| = 1$), δ ($|m_l| = 2$), and ϕ ($|m_l| = 3$) symmetry with respect to the z-axis. In addition, a set of f-orbitals convenient for systems with cubic symmetry can be formed via linear combinations of these real f-orbitals (see, for example, Cotton, 1990).

Both the lanthanide and actinide elements have valence f-orbitals, but they have distinct differences that originate in electronic structure. The 5f orbitals of the actinide elements are in close energetic proximity to other valence orbitals, which leads to complex and fluctuating electron distributions for the early actinide elements. Table 17.2 compares the ground electron configurations of isovalent lanthanide and actinide atoms. It is evident that, when comparing the early members of each series, the 6d orbitals of the actinide elements are more energetically accessible than are the 5d orbitals of the lanthanide elements. The radial functions for the outer orbitals of actinide atoms also indicate that the characterization of these elements as ones for which the chemistry is dominated by the behavior of the 5f electrons might be considered somewhat of a misnomer. Fig. 17.2 shows the radial functions obtained for the Pu atom from recent relativistic Cowan–Griffin *ab initio* atomic calculations of Seijo *et al.* (2001). As expected, the 7s and 6d radial functions are significantly more diffuse than the 5f radial function. Somewhat more surprising, the 6s and 6p orbitals, which are typically considered to be core orbitals, have radial functions of comparable or greater extension than the 5f radial function. These results underscore the fact that the electronic structure of actinide atoms can involve complex electron occupancies that span several different n and l values, even in the absence of spin–orbit effects.

The fact that there are so many atomic orbitals (AOs) in spatial and energetic proximity near the highest valence level of the actinide atoms leads to another complicating factor in describing the electronic structure of actinide systems, namely the presence of a large number of electronic states close to the ground state. Particularly for the early actinides and their simple ions, the presence of multiple $5f^n6d^m7s^k$ configurations of comparable energy, and the energetically close multiplets that can arise from each of these configurations, leads to the enormously complex state energetics and optical spectra observed for these

Table 17.1 *The angular functions of the seven real f-orbitals in the axially quantized representation.*

Axial symmetry	Spherical harmonics	Cartesian representation	Usual label
σ	$Y_{3,0}$	$z(5z^2-3r^2)$	f_{z^3}
π	$Y_{3,1} \pm Y_{3,-1}$	$x(5z^2-r^2)$, $y(5z^2-r^2)$	f_{xz^2}, f_{yz^2}
δ	$Y_{3,2} \pm Y_{3,-2}$	$z(x^2-y^2)$, zxy	$f_{z(x^2-y^2)}$, f_{zxy}
ϕ	$Y_{3,3} \pm Y_{3,-3}$	$x(x^2-3y^2)$, $y(3x^2-y^2)$	$f_{x(x^2-3y^2)}$, $f_{y(3x^2-y^2)}$
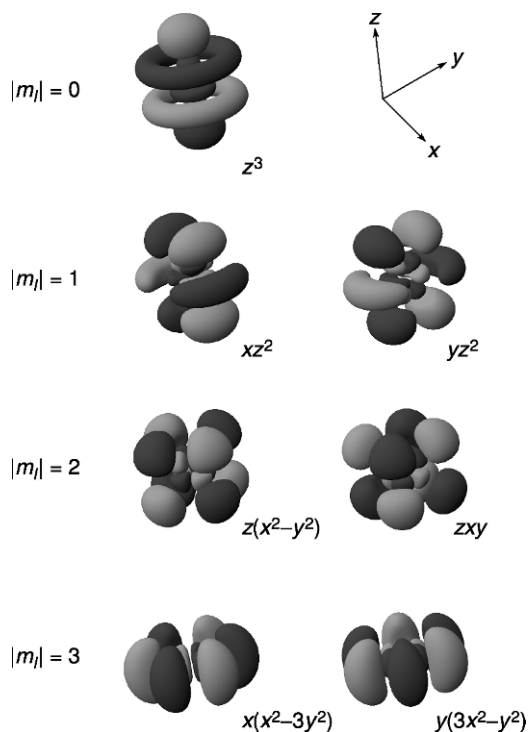
Fig. 17.1 *Representation of the angular functions for the seven real 5f-orbitals in the axially quantized representation.*

systems (Wybourne, 1965; Dieke, 1968; Carnall and Crosswhite, 1986). With the exception of $5f^1$ complexes (Kaltsoyannis and Bursten, 1995; Seijo and Barandiarán, 2001), the various multiplets of actinide systems in general cannot be described within a single-configuration framework, which has greatly hindered the use of first-principles calculations of the electronic state energies. As a result, until recently most efforts to understand the optical spectra of actinide ions involved crystal-field models that incorporated empirically obtained parameters (Crosswhite and Crosswhite, 1984; Carnall, 1992). In

Table 17.2 *Ground state electron configurations of the lanthanide and actinide atoms.*[a]

La	$[Xe]5d^16s^2$	Ac	$[Rn]6d^17s^2$	Gd	$[Xe]4f^75d^16s^2$	Cm	$[Rn]5f^76d^17s^2$
Ce	$[Xe]4f^15d^16s^2$	Th	$[Rn]6d^27s^2$	Tb	$[Xe]4f^96s^2$	Bk	$[Rn]5f^97s^2$
Pr	$[Xe]4f^36s^2$	Pa	$[Rn]5f^26d^17s^2$	Dy	$[Xe]4f^{10}6s^2$	Cf	$[Rn]5f^{10}7s^2$
Nd	$[Xe]4f^46s^2$	U	$[Rn]5f^36d^17s^2$	Ho	$[Xe]4f^{11}6s^2$	Es	$[Rn]5f^{11}7s^2$
Pm	$[Xe]4f^56s^2$	Np	$[Rn]5f^46d^17s^2$	Er	$[Xe]4f^{12}6s^2$	Fm	$[Rn]5f^{12}7s^2$
Sm	$[Xe]4f^66s^2$	Pu	$[Rn]5f^67s^2$	Tm	$[Xe]4f^{13}6s^2$	Md	$[Rn]5f^{13}7s^2$
Eu	$[Xe]4f^76s^2$	Am	$[Rn]5f^77s^2$	Yb	$[Xe]4f^{14}6s^2$	No	$[Rn]5f^{14}7s^2$

[a] There have been discussions about whether the lanthanide and actinide series should begin with La and Ac, respectively, as has been done here, or with Ce and Th, respectively. See Jensen (1982).
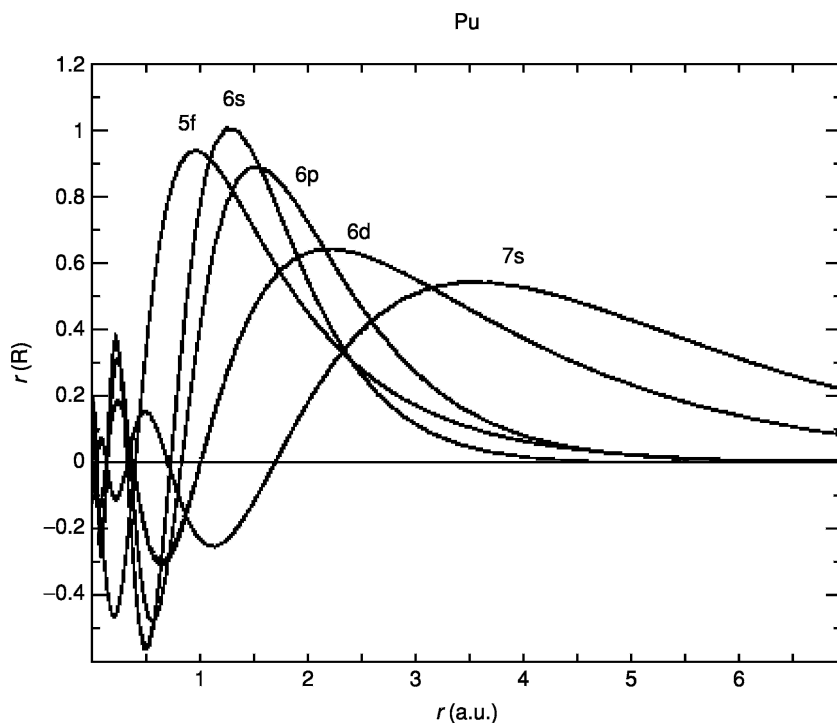
Fig. 17.2 *Radial functions for the outer orbitals of a Pu atom from relativistic atomic calculations (reproduced from Seijo* et al., *2001).*

recent years, correlated electronic structure methods with spin–orbit operators have been used to address optical excitations in f^n ($n > 1$) actinide-containing systems (Matsika and Pitzer, 2000; Gagliardi *et al.*, 2001b; Matsika *et al.*, 2001; Mochizuki and Tatewaki, 2002), but this still remains as one of the biggest challenges in computational actinide chemistry.

17.1.2 Relativistic effects

Another challenge in describing the electronic structure of the actinide and transactinide elements is the necessity to include the effects of relativity on the behavior of the electrons. Although Dirac (1929) merged special relativity and quantum mechanics in 1929, and Breit (1932) extended Dirac's ideas to many-electron systems shortly thereafter, the importance of relativistic corrections in molecular quantum chemistry was not fully appreciated until the 1970s. Dirac himself was not convinced of the importance of relativistic effects, which he said would be ''of no importance in the consideration of atomic and molecular structure and ordinary chemical reactions'' (1929). Dirac clearly understated the chemical consequences of his discovery! Beginning with the third-row transition metal atoms, and even more so for the actinide and trans-actinide atoms, the high kinetic energy of the core electrons, which correspond to classical speeds close to the speed of light, leads to large relativistic effects. Powell (1968) presented an early and readily understood introduction to the derivation of Dirac's relativistic quantum mechanics and its impact on chemistry, and a number of more detailed reviews (Pyykkö, 1978, 1988; Pitzer, 1979; Pyykkö and Desclaux, 1979; Christiansen *et al.*, 1985; Balasubramanian and Pitzer, 1987; Ermler *et al.*, 1988; Balasubramanian, 1989; Schwarz, 1990; Kaltsoyannis, 1997; Bond, 2000) and monographs (Malli, 1983; Balasubramanian, 1989, 1994, 1997; Dolg and Stoll, 1996; Schwerdtfeger, 2002, 2004; Hess, 2003; Hirao and Ishikawa, 2004) over the last 25 years discuss the chemical consequences of relativistic effects in greater detail. We provide a brief recap here of the major relativistic effects that influence the electronic structure of actinide complexes.

Because most of the chemical distinctiveness of the actinide elements results from the presence of valence f-electrons, much of our focus will be on the effects of relativity on the 5f orbitals. The magnitude of many of the relativistic effects increases as Z^n (Z = atomic number; $n > 1$). Hence, relativistic effects are more pronounced for the actinide elements than for the lanthanide elements. This trend is apparent in Fig. 17.3, in which the nonrelativistic and Dirac–Fock relativistic atomic orbital energies obtained by Desclaux (1973) for lanthanide and corresponding actinide atoms are compared. This figure illustrates the two general classes of relativistic effects on the electronic structure, both of which are greater for the actinides than for the lanthanides. The first effect is the increase in the energies of the nf and $(n + 1)$d orbitals relative to the $(n + 1)$p and $(n + 2)$s orbitals ($n = 4$ and 5). These overall changes in the orbital energies are primarily due to 'classical' relativistic effects, such as the relativistic mass correction for core electrons, that lead to greater shielding of the higher l-value orbitals. The 5f orbitals in actinides are more destabilized by relativistic effects than are the 4f orbitals of the lanthanides. As a result, the valence 5f electrons in the actinide elements are more weakly bound, and hence more chemically active, than the 4f electrons in the lanthanide elements.
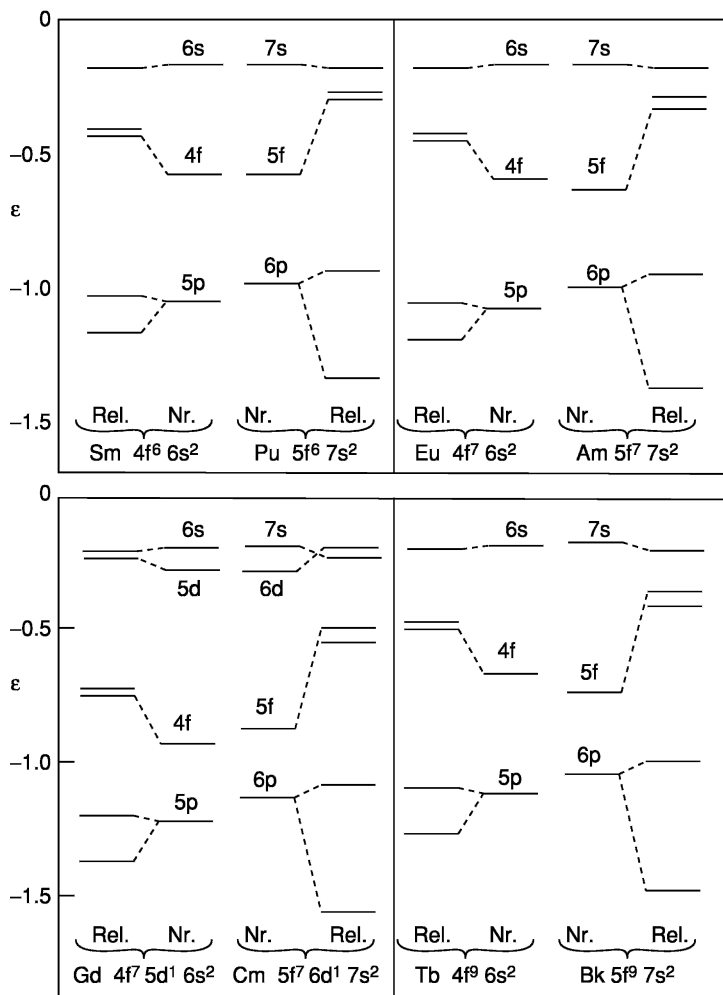
Fig. 17.3 *The Dirac–Fock average of configuration orbital energies* (a.u.) *obtained by Desclaux* (1973) *for the lanthanides Sm, Eu, Gd, and Tb and for the corresponding actinides Pu, Am, Cm, and Bk. The inner columns for each lanthanide–actinide pair denote nonrelativistic orbital energies. The shifts in energy due to the relativistic effects are evident in the relativistic orbital energies, displayed in the outer columns for each lanthanide–actinide pair* (*adapted from Pyykkö,* 1978).

The second relativistic effect is the splitting of subshells with $l \geq 1$ because of spin–orbit coupling, which can be considered a 'quantum' relativistic effect. The spin–orbit splitting generally decreases with the increase of l and with increasing orbital energy. In Fig. 17.3, for example, the $(n + 1)$p orbitals are split more

than the nf orbitals. These two classes of relativistic effects are lucidly discussed in a review by Pitzer (1979) and spin–orbit effects in molecules have recently been reviewed by Marian (2001).

The various methods for the inclusion of relativistic effects in electronic structure calculations have been discussed briefly by Pepper and Bursten (1991) and in greater detail by Balasubramanian (1997). They will also be developed more fully in Section 17.2. In general, the methods can be separated into two broad classes depending on how the relativistic effects are incorporated into the molecular Hamiltonian. In the so-called *scalar* relativistic methods, the relativistic mass–velocity and Darwin terms are incorporated into the Hamiltonian in such a way that preserves the separation of the spatial and spin components of the resultant wavefunction. Scalar relativistic methods thus generate wavefunctions that are bases for the representations of the familiar single point groups used in nonrelativistic calculations. Spin–orbit effects are not explicitly included in scalar-relativistic calculations, although they can be included via perturbative methods.

In the second general approach to relativistic molecular electronic structure calculations, the full Dirac equation is solved using a variety of simplifying formalisms, such as the Dirac–Fock approach that is the relativistic analog to nonrelativistic Hartree–Fock (HF) methods. Spin–orbit coupling is explicitly included in these methods, which yield four-component wavefunctions. The two small components, which are usually needed only for calculations involving electromagnetic field interactions, are often omitted from the molecular wavefunction. Because the spatial and spin components of the electronic wavefunction are coupled in these approaches, the calculated orbitals are bases for the less-familiar double point groups, which sometimes complicates the interpretation of the results.

As this chapter develops, we will see that scalar-relativistic methods, which use LS labels for the molecular states, are generally adequate for the calculation of many of the ground state properties of actinide systems, including molecular geometries and vibrational frequencies, although the reader is referred to the discussion concerning the plutonyl (PuO_2^{2+}) ion below. The calculation of excited state properties, especially optical excitation energies, almost always demands an approach that includes spin–orbit effects explicitly. When these effects are included, double-group labels are required. For example, for linear molecules, the states are labeled based on Ω values rather than on Λ values.

17.1.3 Actinide–ligand bonding: General considerations

In this chapter, we will address a number of different molecular and ionic systems that contain a variety of ancillary atoms and ligands bonded to an actinide center. Although these systems might appear at first glance to be very different, there are some general observations that can be made about the nature of the ligand-to-actinide bonding.

The actinide elements are classified as hard Lewis acids, especially in their more positive oxidation states (Katz *et al.*, 1986; Kaltsoyannis and Scott, 1999). The interactions of ligands with an actinide center are conventional Lewis acid–base interactions in which the ligand serves as an electron donor to a vacant acceptor orbital on the metal. In this sense, the formation of actinide–ligand complexes is entirely analogous to the formation of metal–ligand bonds in transition-metal coordination chemistry. There are several general factors that distinguish actinide coordination chemistry from that of the transition metals and the lanthanide elements:

(1) As hard Lewis acids, both the actinide and lanthanide ions generally prefer to coordinate hard Lewis bases such as F^-, O^{2-}, and other O-containing ligands, including OH^- and H_2O. Indeed, the chemistry of the actinides tends to be dominated by aqua complexes, fluorides, oxides, and oxyfluorides, although much of our subsequent discussion will involve different types of ligands, such as hydrocarbyls.

(2) The 4f orbitals of the lanthanides are too contracted in their radial distributions to be involved to any significant extent in covalent interactions with ligands, particularly in the +3 oxidation state that dominates lanthanide chemistry. The 5f orbitals of the early actinide elements are less contracted and can therefore have significant overlap with ligand orbitals. The 5f orbitals contract as one moves across the actinide series, which is consistent with the observation that the chemistry of the later actinides is similar to that of the lanthanides. As a consequence, the bonding in the lanthanides and the later actinides tends to be largely ionic, whereas significant covalent character can be found in the early actinides (Burns and Bursten, 1989).

(3) For most of the actinide (An) systems, we will see that the An 6d orbitals serve as more effective acceptor orbitals than the An 5f orbitals because the former are more diffuse than the latter. Thus, if a choice is allowed by symmetry, the ligands tend to interact more strongly with the 6d orbitals than the 5f orbitals. In centrosymmetric systems, such as the actinyl ions(AnO_2^{q+}), the actinide hexafluorides (AnF_6) and the actinocenes (An (η^8-C_8H_8)$_2$), interactions of the ligands with the An 6d and 5f orbitals will be partitioned based on the inversion symmetry of the ligand group orbitals.

(4) In most cases, any metal-based electrons will reside primarily in the 5f orbitals of the An center. For example, in U(IV) complexes the two electrons formally remaining on the U atom will be localized within the U 5f orbitals.

As noted earlier, the large number of An atomic orbitals generally leads to a large number of electronic states close to the ground state. Strong interactions of the An center with ligands serve to destabilize some of the An orbitals and greatly increase the energy of configurations that involve those orbitals. Thus, the distribution of states near the ground state can be somewhat simpler than that for free ions or atoms of the elements.

17.2 RELATIVISTIC APPROACHES FOR ELECTRONIC STRUCTURE OF ACTINIDES

A variety of methods are used in electronic structure calculations on actinide molecules. Some of these methods and their historical development were outlined in the 1991 review by Pepper and Bursten (1991). In this section, we will touch upon some of the salient features covered in that review as well as address recent developments and applications over the past decade. In discussing these theoretical approaches, it is useful to categorize them according to three aspects: (a) whether the electronic structure calculation is based on wavefunction-based *ab initio* approaches, such as Hartree–Fock and CI, or by density functional theory (DFT) approaches, such as local density and generalized-gradient methods; (b) the manner in which relativistic effects are included; and (c) whether the approach explicitly involves all-electron or only valence-electron character.

17.2.1 Hartree–Fock and density functional approaches

While electronic structure approaches for molecules differ in their methodologies, they share many common features. The starting point is the molecular energy expressed in terms of the total wavefunction for the molecule and a Hamiltonian describing the interactions. The total wavefunction, in turn, is comprised of an antisymmetrized product of one-electron molecular orbitals (ϕ_i). By applying the variational principle to the expression for the molecular energy, one obtains a set of self-consistent field (SCF) equations that are solved iteratively to obtain the molecular orbitals (MOs). The MOs are typically represented as linear combinations of atomic orbitals (LCAO), which may be expanded in terms of Gaussian- or Slater-type functions. From the molecular orbitals, one can then calculate the energy of the molecule, the total charge density, and other molecular properties.

In Hartree–Fock calculations, the exchange interaction is treated explicitly in the expression for the molecular energy:

$$E_{HF} = E_{kin} + E_{coul} + E_{exch}$$

where E_{HF}, E_{kin}, E_{coul}, and E_{exch} are the Hartree–Fock total energy, the electron kinetic energy, the Coulomb repulsion energy, and the exchange energy, respectively. The nonlocal Hartree–Fock exchange operator is associated with interchanging electrons of the same spin. Electron correlation effects are treated by including excitations from occupied to virtual levels by perturbation theory (e.g. second-order Møller–Plesset perturbation theory (MP2) to fourth-order Møller–Plesset perturbation theory (MP4)) (Møller and Plesset, 1934; Pople *et al.*, 1977), coupled-cluster theory (Bartlett, 1981, 1989), including coupled cluster with single and double excitations (CCSD; Purvis and Bartlett, 1982) and coupled cluster singles, doubles and perturbative triples (CCSD(T); Raghavachari *et al.*, 1989; Watts *et al.*, 1993), and configuration interaction

(CI, e.g. configuration interaction with single and double excitations [CISD]) (Shavitt, 1977; Szabo and Ostlund, 1989; Jensen, 1999).

DFT is based on the famous Hohenberg–Kohn theorem (Hohenberg and Kohn, 1964), which states that the electronic ground state of a molecule can be obtained uniquely from knowledge of the electron density $\rho(r)$ at all points in the molecule. Exchange and correlation effects are treated by the use of exchange and correlation functionals, which depend on the density, and lead to an expression for the energy similar to that for Hartree–Fock except for the 'exchange-correlation' energy, E_{xc}:

$$E_{DFT} = E_{kin} + E_{coul} + E_{xc}(\rho)$$

By expanding the electron density via a set of Kohn–Sham (KS) orbitals, one can derive the one-electron KS equation, similar to the Hartree–Fock equation (Kohn and Sham, 1965; Koch and Holthausen, 2001).

At the time of the 1991 review by Pepper and Bursten, DFT methods were very much in their infancy. At that time the majority of DFT methods used the local density approximation (LDA), in which the functional depends only on the density. Among the early LDA approaches that were widely applied to inorganic systems including actinides were the Xα-scattered wave (Xα-SW) and Dirac–Slater (DS) discrete variational (DV) methods, including early versions of the quasi-relativistic Hartree–Fock–Slater (HFS) approach (see relativistic methods in next section). At that time, the Xα variant of the LDA methods had questionable reliability with respect to the calculation of total energy and could not be used generally to determine geometries and vibrational properties. Pepper and Bursten (1991) made the following statement about DFT in the conclusion of their review:

> "Recent developments in density functional theory, including improved functionals and methods for the accurate calculation of binding energies, also bode well for computational actinide chemistry. These methods have the advantage of providing easily interpreted information about bonding interactions in actinide systems, and have proved useful for many years in organotransition metal and organoactinide chemistry. Again, the improved approaches are just beginning to be applied to actinide systems, with promising results."

Indeed, as will be evident in this chapter, DFT methods have become a major contributor to our understanding of actinide electronic structure. We will briefly discuss some of the major developments in DFT since the 1991 review, including the improved accuracies of molecular energies and other quantities using DFT methods as well as the development of improved functionals for DFT calculations.

Among numerous efforts in developing 'good' exchange-correlation functionals beyond the LDA, Becke (1988) developed a gradient-corrected exchange functional in 1988. This exchange functional depends both on the density, ρ, and on its gradient, $\nabla\rho$, at any point in space. In the past decade, developments by many individuals, including Lee *et al.* (1988), Perdew and Wang (1992),

Perdew *et al.* (1992), Becke (1993a), and others have led to new functionals [often known as generalized-gradient approximations (GGA)] for both exchange and correlation that have received wide usage by the community because of the improvements in orbital energies, bond energies, structures, and other properties.

In 1993 Becke launched another revolution in the density functional world by developing a 'hybrid' functional (Becke, 1993b). The hybrid approach differs in the treatment of exchange by adding a certain amount of the nonlocal exact exchange calculated in Hartree–Fock formalism to the local and gradient-corrected terms of the exchange functional of traditional DFT. Overall the form of the functional had three linear parameters that determined the amount of exact exchange as well as the relative amounts of local and gradient-corrected terms in the exchange and correlation functionals. The parameters were determined for a set of small organic molecules by the best fit to a set of experimental energies. When combining with appropriate correlation functionals (e.g. LYP and PW91), these functionals, denoted as B3LYP and B3PW91, have achieved great success in the computational chemistry of organic and inorganic molecules. The performance of these hybrid functionals in the prediction of thermochemical properties and molecular structures has led numerous investigators to apply these functionals to actinide chemistry as well.

Finally, another crucial development in the past decade for both Hartree–Fock and DFT methods has been the implementation of techniques for calculating the gradient and second derivative of the molecular energy as a function of nuclear coordinates. The information on the gradient gives directly the forces on the nuclei for a particular molecular configuration and this, in turn, enables the optimization of molecular geometries to be carried out routinely for various functionals, Hartree–Fock methods, and the hybrid approaches. Similarly the second derivatives provide the vibrational frequencies at the equilibrium structure and the Hessian matrix to characterize stationary points (e.g. minima and saddle points) and to move along molecular potential energy surfaces.

17.2.2   Relativistic effects

Relativistic effects are incorporated into electronic structure calculations by a variety of techniques that are partially summarized in Table 17.3. They are categorized on the basis of whether they are Hartree–Fock- or DFT-based, on how many components of the wavefunction are treated (see below), and on other characteristics.

The formal starting point for most relativistic methods is the Dirac equation (Dirac, 1929). In the previous section, each molecular orbital ϕ_i was a scalar function associated with either up or down spin. In relativistic theory ϕ_i is represented as a four-component spinor comprised of 'large' (or *electronic*) and 'small' (or *positronic*) components with each component having spin up (α) and spin down (β). For a one-electron system the Dirac equation is

Table 17.3 *Summary of theoretical methods for treating molecules including heavy atoms divided according to wave-function-based (Hartree-Fock) or density-functional-based approaches.*

Wave-function-based approaches	Density functional approaches
nonrelativistic	
HF	LDA, GGA, hybrid functional, meta-GGA
MP2–MP4	(all-electron, frozen-core, and ECP)
CCSD(T)	
scalar relativistic	
HF with RECP	quasi-relativistic Pauli formalism
MPn, CCSD(T) with RECP	ZORA
CASPT2, MRCI with RECP	LDA, GGA, hybrid, meta-GGA with RECP
two-component relativistic	
SO multi-configuration SCF	SO DFT
SO-CASPT2, SO-MRCI	two-component ZORA
	two-component DKH
four-component relativistic	
Dirac–Hartree–Fock	Dirac–Kohn–Sham

$$H\Psi = \left[\vec{\alpha} \cdot \vec{p} + (\beta - 1)mc^2 + V \right]\Psi = i\hbar \frac{\partial \Psi}{\partial t}$$

The $\vec{\alpha}$ and β are the Dirac matrices and are 4×4 dimensional (the $\vec{\sigma}$ are the familiar 2×2 Pauli matrices and I is the 2×2 identity matrix):

$$\vec{\alpha} = \begin{pmatrix} 0 & \vec{\sigma} \\ \vec{\sigma} & 0 \end{pmatrix} \qquad \beta = \begin{pmatrix} I & 0 \\ 0 & -I \end{pmatrix}$$

For many-electron systems, in analogy to the nonrelativistic many-electron Schrödinger equation, the relativistic equation is termed the Dirac–Coulomb equation (here h_{D} is the one-electron Dirac equation):

$$H_{\mathrm{Dirac}} = \sum_i h_{\mathrm{D}}(i) + \sum_{i>j} \frac{1}{r_{ij}}$$

Analogous to the nonrelativistic Hartree–Fock (for wavefunction methods) and Kohn–Sham (for DFT methods) equations, these equations are the bases for the Dirac–HF and Dirac–Kohn–Sham methods, respectively. Dirac-based codes are thus four-component methods that are computationally extremely demanding and, for this reason, such methods have been applied to relatively few actinide molecules. There are several well-known codes [e.g. MOLFDIR (MOLFDIR), DIRAC (DIRAC; Saue *et al.*, 1997)], Beijing density functional code (BDF; Liu *et al.*, 2004), BERTHA (BERTHA; Grant and Quiney, 2000), and PORPHET4R (Matsuoka and Watanabe, 2004) that have been developed for these methods (Hirao and Ishikawa, 2004).

Several techniques exist to separate the large and small components, thus enabling a formal treatment of only the electronic (i.e. large) components and resulting in two-component methods (one for spin up and one for spin down). One such method is the Foldy–Wouthuysen transformation (Foldy and Wouthuysen, 1950; Foldy, 1956), which results in a two-component Hamiltonian (to order α^2, where α is the fine structure constant) called the Pauli Hamiltonian:

$$H = H_{NR} + H_{mv} + H_D + H_{so}$$

In the Pauli Hamiltonian, H_{NR}, H_{mv}, H_D, and H_{so} are the nonrelativistic Hamiltonian, the mass–velocity term, the Darwin term, and the spin–orbit coupling term, respectively:

$$H_{mv} = \frac{-p^4}{8m^3c^2}$$

$$H_D = \frac{1}{8m^2c^2}\left(p^2 V_{ext}\right)$$

$$H_{so} = \frac{1}{4c^2}\left(\nabla(V_N + V_{el}) \times \overrightarrow{p}\right) \bullet \overrightarrow{s}$$

Baerends and coworkers have developed a zeroth-order regular approximation (ZORA) that overcomes some of the problems of the Pauli formalism (*vide infra*). Rösch and coworkers (Knappe and Rösch, 1990; Rösch *et al.*, 1996) have developed a linear combination of Gaussians DFT method in the PARAGAUSS program (PARAGAUSS) that implements the all-electron second-order Douglas–Kroll–Hess (DKH) scheme (Douglas and Kroll, 1974; Jansen and Hess, 1989) for transforming the Dirac equation. The DKH method has also been implemented by de Jong and coworkers and Hirata *et al.* (de Jong *et al.*, 2001a; Hirata *et al.*, 2004) in the software package NWChem (NWChem) in scalar form and by Peralta and Scuseria (2004) in Gaussian in both scalar and spin–orbit forms. Dyall (1997, 2001) proposed an alternative series of transformations via so-called normalized elimination of the small components (NESC) from the four-component wavefunctions. Nakajima and Hirao (1999) suggested a formalism named relativistic scheme by eliminating small components (RESC).

As noted in Section 17.1.2, when spin–orbit coupling effects are ignored or averaged out, the relativistic methods reduce to scalar relativistic (one-component) methods. The vast majority of electronic structure calculations on actinide species use these simpler 'scalar relativistic' methods in which the wavefunction has the same form as in nonrelativistic quantum chemistry and each orbital has either α or β spin. In these scalar relativistic methods, only the mass–velocity and Darwin terms are included in addition to the usual nonrelativistic Hamiltonian. Scalar relativistic methods include calculations

with effective core potentials (ECPs; see next section), where the relativistic terms are implicitly incorporated into the potential.

Among density functional approaches the quasi-relativistic (QR) and ZORA are popular relativistic methods that are included in the Amsterdam Density Functional (ADF) software. The quasi-relativistic method of Ziegler *et al.* (1989) is based on the Pauli formalism, where only the first-order terms are retained. These methods treat the relativistic terms self-consistently and are typically employed with frozen relativistic core orbitals to reduce variational instabilities. The ZORA method (van Lenthe *et al.*, 1993, 1994), which is equivalent to the earlier CPD (Chang, Pelissier, and Durand) method (Chang *et al.*, 1986), includes higher order effects in a slightly different manner. ZORA is also implemented by van Wullen (1999), by the Li group in BDF (Wang *et al.*, 2000; Hong *et al.*, 2001), and Gagliardi *et al.* (1998, 2001c) in three other DFT codes. These QR, ZORA, and DKH approaches can utilize either the LDA or GGA DFT functionals. Such approaches are beginning to be applied to the chemistry of heavy atoms, including the two-component ZORA method, implemented in ADF (ADF) and MAGIC (MAGIC), and spin–orbit DFT, which is now part of NWChem (NWChem).

17.2.3   Relativistic effective core potentials

An alternative approach to including relativistic effects is to replace the inner core electrons using relativistic effective core potentials (RECPs) derived from all-electron relativistic atomic calculations. RECPs have been recently reviewed by Dolg (2002). With these methods, the quantum chemical calculations are carried out in nonrelativistic fashion without any explicit relativistic terms in the calculation. In addition to including the effects of the core electrons, the RECPs implicitly treat the relativistic effects on the valence orbitals, since relativistic orbitals were used to construct the RECPs. A major question, especially for actinides, concerns which electrons should be included in the core. For an atom such as U, the 'large core' would treat the outer $6s^2 6p^6 7s^2 5f^3 6d^1$ electrons as valence electrons and treat the remaining 78 electrons as core electrons. Note that the 'large core' approach actually includes a smaller number of electrons than are in the noble gas configuration of [Xe], which includes the so-called semi-core 6s and 6p electrons. As noted elsewhere, the 6s and 6p electrons are energetically and spatially in the same region as the other valence electrons and play an important role in the valence electronic structure. The other common choices for core size are a 68-electron core (with the 5d shell in the valence space) and a 60-electron core (with the 5s and 5p shells in the valence).

RECPs have been developed starting with numerical Dirac–Fock orbitals by Pitzer, Christiansen, Ermler and colleagues (Lee *et al.*, 1977; Christiansen *et al.*, 1979). After transforming to a two-component 'spinor' equation, they obtain two spin–orbit-coupled RECPs for each orbital (such as $6p_{1/2}$ and $6p_{3/2}$), except for the case of s orbitals. The two RECPs can be combined in a weighted

average to obtain an average RECP (AREP) to facilitate calculations in scalar relativistic mode. The other combination of RECPs yields a rigorous spin–orbit potential that can be used in two-component SCF or spin–orbit CI calculations. Atomic RECPs for the entire periodic chart have been derived according to this procedure. Of interest for 5f elements are potentials for Fr–Pu by Ermler *et al.* (1991) and for Am through element 118 by Nash *et al.* (1997, 1999).

Starting from a scalar relativistic Cowan–Griffin numerical atomic wavefunction (Cowan and Griffin, 1976), Hay, Wadt, Kahn and coworkers developed the first RECPs for uranium and applied it to UF_6 (Hay *et al.*, 1979). They have subsequently developed RECPs for much of the periodic table (Hay and Wadt, 1985). In their approach, an 'average' RECP is directly obtained because there is only one radial function for, for example, the 6p shell of U atom. Spin–orbit effects have been treated by an approximate operator. The most recent versions of these potentials have been reported for U, Np, and Pu (Hay and Martin, 1998).

Alternative approaches developed by Preuss, Stoll, Dolg and coworkers fit the RECP parameters to calculated levels from all-electron relativistic methods (Küchle *et al.*, 1994). The atomic results can be obtained either from Dirac-based methods or an alternative scalar-relativistic method developed by Wood and Boring (1978), which is analogous to the Cowan–Griffin method. In addition to 'large core' actinide RECPs, 'small-core' RECPs have been developed in which the 5s, 5p, and 5d shells are also treated as valence electrons, because they are in the same principal quantum shell as the 5f electrons, even though these electrons are 'deep' in terms of energy. Among the codes that have capabilities for relativistic ECPs are GAUSSIAN (GAUSSIAN), GAMESS (GAMESS), TURBOMOLE (TURBOMOLE), NWChem (NWChem), and COLUMBUS (Pitzer and Winter, 1988; Shepard *et al.*, 1988).

An alternative to RECPs are those based on the Huzinaga–Cantu equation (Huzinaga and Cantu, 1971) and are known as model potentials. For these potentials, the valence-space orbitals, unlike those previously discussed, preserve the nodal (radial) structure of the all-electron orbitals. The most commonly used form is the so-called *ab initio* model potentials (AIMP) of Seijo, Barandiarán, and coworkers (Huzinaga *et al.*, 1987; Seijo and Barandiarán, 1999), who have recently published a set of AIMPs, with appropriate basis sets, for lanthanides and actinides (Seijo *et al.*, 2001). These potentials are based on a spin-dependent relativistic Wood–Boring AIMP Hamiltonian, which can be divided into a Cowan–Griffin spin-free relativistic Hamiltonian and a pure spin–orbit Hamiltonian.

The model potentials are formed by replacement of the core operators in two ways: for local, long-range operators, such as the Coulomb operator, a simple local operator is used. For local, short-range, or non-local operators, such as the exchange or the mass–velocity and Darwin Cowan–Griffin operators, a spectral representation is used (Seijo *et al.*, 2003). Recently, alternate formulations of incorporating relativistic effects, namely the aforementioned relativistic

elimination of small components (RESC) (Motegi *et al.*, 2001) and the DKH approaches (Paulovic *et al.*, 2002, 2003) have been incorporated into AIMP methods.

In the latter of these studies, spin–orbit relativistic (i.e. two-component) calculations are performed in a two-step procedure: a large scalar relativistic (one-component) calculation is used to incorporate electron correlation followed by a smaller spin–orbit (two-component) calculation. There are some important assumptions made in this approach. Its underlying principle is that the correlation calculation converges more slowly than the spin–orbit one, and that the two results are additive. The CIPSO code of Teichteil and coworkers (Teichteil and Spiegelmann, 1983; Teichteil *et al.*, 1983) is a well-known example of this method and has been applied to actinides in several studies (Maron *et al.*, 1999; Vallet *et al.*, 1999a,b). Recently, this method has been extended to the EPCISO code, which accounts for spin–orbit polarization effects (Vallet *et al.*, 2000). Another implementation of the two-step method has been developed by the Roos group; the first step being a complete active space plus second-order perturbation theory (CASPT2) correlation calculation (Andersson *et al.*, 1992), followed by a restricted active space self-consistent field (RASSCF) state interaction (RASSI) method to perform the spin–orbit calculation (Malmqvist *et al.*, 2002).

The COLUMBUS codes of Pitzer *et al.* (Pitzer and Winter, 1988; Shepard *et al.*, 1988) have incorporated RECPs within a two-component approach. Initially their methodology was developed by using the observation that when the calculations are carried out under C^*_{2v}, D^*_2, or D^*_{2h} double-group symmetry (see Section 17.2.5), the spin–orbit integrals are either pure real or pure imaginary, thus allowing the program to use real arithmetic. Recently, Yabushita *et al.* (1999) developed a spin–orbit formalism for the COLUMBUS graphical-unitary group approach (GUGA) CI program. Their method uses configuration state functions (CSFs) based on spatial orbitals (e.g. from a one-component SCF or multi-configuration self-consistent field [MCSCF] calculation) in a CI expansion that uses a spin–orbit Hamiltonian. Thus, the correlation and the spin–orbit effects are treated simultaneously and variationally via the spin–orbit CI approach. This method has been used with CI expansions of the order of a million CSFs on actinide systems, including several of the actinyl ions (Zhang and Pitzer, 1999; Matsika and Pitzer, 2000; Matsika *et al.*, 2001).

17.2.4 Excited electronic states

The preceding discussion has focused primarily on methodologies for calculating properties of the electronic ground state of actinide molecules. There has been considerably less activity involving excited states, in part because of the unique challenges actinides present with respect to the importance of spin–orbit and other relativistic effects, and in part because of the inherent challenge of

many electronic states involving unpaired 5f electrons in multiple electron configurations (Section 17.1.1). For Hartree–Fock-based methods, CI techniques have been the most popular approach to determining excited-state energies. For a ground state with no unpaired electrons, single excitations from occupied MOs to virtual MOs provide a zero-order description of the electronic states. Inclusion of higher order excitations explicitly treats the electron correlation effects needed for more quantitative results. Spin–orbit CI calculations (Pitzer and Winter, 1988; Yabushita *et al.*, 1999) have evolved to the point where fairly accurate calculations can be carried out on complexes of modest size. Illustrations of spin–orbit configuration interaction (SOCI) results will be presented in the section on the spectroscopy of actinyl species. There is also a recent review on the development and application of the multi-configuration-based relativistic quantum chemistry in exploring excited states of heavy elements, including actinides (Roos and Malmqvist, 2004).

While DFT is based on the ground electronic state of a system (or the lowest state of a given spin and symmetry), there have been various developments for treating excited electronic states within a DFT approach. Among the earliest LDA approaches was the transition state theory of Slater (1974), in which the prescription of exciting one-half electron from occupied to virtual level corresponded to the proper excitation energy in DFT. Within the QR and ZORA techniques in the ADF program and others, one can solve self-consistently for the excited states by progressively removing an electron from various occupied orbitals and promoting it into the virtual levels.

More recently, time-dependent DFT (TD-DFT) techniques have been developed (van Gisbergen *et al.*, 1995; Jamorski *et al.*, 1996; Petersilka *et al.*, 1996; Casida *et al.*, 1998) in terms of 'response functions' to provide an alternative description of the excited states in molecules. In TD-DFT, an excited state is made up of all possible particle–hole excitations (as well as counter-intuitive hole–particle 'de-excitations') between occupied and virtual MOs. This approach is applicable to closed-shell ground states to compute excited singlet and triplet excited states, and to open-shell ground states as well. Numerous TD-DFT results with a variety of functionals (LDA, GGA, and hybrid) have been reported for organic molecules and transition metal complexes. To date, very little work has been done on actinide species, mainly because the calculated excitation energies would hardly be useful without including spin–orbit coupling effects. Notably, recent developments by Liu and coworkers that allow calculations of TD-DFT excitation energies with spin–orbit coupling is a highly promising approach for tackling excited states of actinides (Gao *et al.*, 2004).

17.2.5   Double groups

As previously mentioned, the incorporation of a spin–orbit operator in the Hamiltonian requires the use of two-component wavefunctions and double groups, because the operator allows the mixing of functions with different

spins. Thus, one needs to incorporate a framework where spin functions are allowed to transform under symmetry operations of a point group. Originally suggested by Bethe (1929), double groups incorporate such transformations (Wigner, 1959; Herzberg, 1991). Before describing double groups, it is instructive to review some of the tenets of angular momentum coupling and term symbols in atoms and molecules. The following discussion is based on the development in Levine's textbook on quantum chemistry (Levine, 2000); readers are also referred to the classic series of texts by Herzberg (1944, 1989, 1991).

For atoms, the two most common methods for coupling spin and angular momenta are the LS and the j–j coupling schemes. LS, or Russell–Saunders, coupling is used when the electronic repulsion splitting is greater than the spin–orbit splitting, whereas j–j coupling is used if the latter is greater than the former. When coupling two angular momenta $\vec{j_1}$ (characterized by quantum number j_1) and $\vec{j_2}$ (characterized by j_2), one uses vector sums to obtain the possible quantum numbers characterizing the total angular momentum, which are defined by the following relation:

$$j = j_1 + j_2, j_1 + j_2 - 1, j_1 + j_2 - 2, ..., |j_1 - j_2|$$

To couple any number of angular momenta, one first couples two angular momenta according to the formula above, then couples the resulting values with the third angular momentum, and repeats the procedure as needed.

In LS coupling, there is a defined total electronic orbital angular momentum, labeled by $\vec{L}$, characterized by the quantum number L, formed by the vector sum of the individual electron orbital angular momenta, $\vec{l}_i$. Analogously, there is a defined total spin angular momentum, labeled by $\vec{S}$, characterized by S, formed by the vector sum of the individual electron spin angular momenta, $\vec{s_i}$. The total electronic angular momentum, $\vec{J}$, characterized by J, is the vector sum of $\vec{L}$ and $\vec{S}$. The possible J values for a given L and S are:

$$J = L + S, L + S - 1, ..., |L - S|$$

In j–j coupling, the orbital angular momentum, $\vec{l_i}$, characterized by l_i and the spin angular momentum, $\vec{s_i}$, characterized by s_i, for each electron is coupled to form the total angular momentum for the particular electron, $\vec{j_i}$, characterized by j_i. The total angular momentum is the vector sum of these individual angular momenta, the J values are obtained using:

$$\vec{J} = \sum_i \vec{j_i}$$

For a non-spin–orbit Hamiltonian, the total orbital and total spin angular momentum operators, which correspond to the quantum numbers L and S, commute with the Hamiltonian, and are good quantum numbers – enabling their use in the labeling of wavefunctions (i.e. the electronic states). The labels for atomic states, called term symbols, use the multiplicity, defined as

the quantity $2S + 1$, as a left superscript and using a capital letter to represent the total orbital angular momentum: S for $L = 0$, P for 1, D for 2, F for 3, G for 4, and then alphabetically (omitting J). Thus one obtains ^{2S+1}L for the term symbol, and ^{1}P, ^{2}D, and ^{3}S as examples. When one includes the J values, which are subscripts, one would obtain $^{2S+1}L_J$ and for the previous examples: ^{1}P$_1$; ^{2}D$_{3/2}$, ^{2}D$_{5/2}$; and ^{3}S$_1$.

For linear molecules, including diatomics, the total angular momenta are no longer good quantum numbers, but their z-components are. Thus, when coupling angular momenta for linear molecules, algebraic sums are used rather than vector sums. Greek letters are used for the z-component of orbital angular momenta, the total z-component angular momentum is now characterized by the quantum number Λ, and the analogous coupling to LS coupling is referred to as ΛS coupling. To couple two individual electron z-components, one obtains (note that each λ quantum number corresponds to a z-component of $\pm M_\lambda$ where $\lambda = M_\lambda$):

$$\lambda = \lambda_1 + \lambda_2 \quad \text{and} \quad \lambda = \lambda_1 - \lambda_2$$

Again, to couple more than two angular momenta z-components, one uses the above relation repeatedly. The total orbital momentum is now labeled Σ for $\Lambda = 0$, Π for 1, Δ for 2, Φ for 3, Γ for 4, and so on. Since (for a non-spin–orbit Hamiltonian) the total spin is still a good quantum number, the molecular term symbols are $^{2S+1}\Lambda$. For Σ ($\Lambda = 0$) states, there is an additional label, corresponding to reflection symmetry in a mirror plane containing the internuclear axis. Σ states, symmetric with respect to this symmetry operation, have a plus sign as a right superscript and Σ states antisymmetric with respect to this operation have a minus sign. The total component angular momentum is labeled Ω and is obtained by coupling Λ with the z-component of spin (called Σ). The values of $\Lambda + \Sigma$ are thus, note that this value may be negative:

$$\Lambda + S, \Lambda + S - 1, ..., \Lambda - S$$

The possible values of Ω, the total z-component angular momentum are:

$$\Omega = \Lambda + S, \Lambda + S - 1, ..., |\Lambda - S|$$

The molecular term symbol is $^{2S+1}\Lambda_{\Lambda+\Sigma}$, thus a $^4\Pi$ state will split into $^4\Pi_{5/2}$, $^4\Pi_{3/2}$, $^4\Pi_{1/2}$, and $^4\Pi_{-1/2}$ states.

The coupling for linear molecules analogous to j–j coupling for atoms is called ω–ω coupling. The z-component angular momentum for each electron is coupled to the spin z-component to form the individual electron total z-component angular momenta, ω_i. The individual ω_i are then coupled to form the Ω values.

For nonlinear polyatomics, electronic states are labeled by the irreducible representations of the point group of the molecule and the multiplicity of the state, referred to as ΓS coupling. The term symbols are $^{2S+1}\Gamma$. In analogy to j–j and ω–ω coupling, one can incorporate spin into a total symmetry label, but

that involves determining how spin functions transform, invoking double groups.

When spin functions are allowed to transform under symmetry operations, the fact that they are antisymmetric with respect to a rotation of 2π leads to the necessary modification of the identity operator, which now corresponds to a rotation of 4π. The operator corresponding to a rotation of 2π is labeled R, and the number of symmetry operators is now doubled (hence the name *double* group). An alternative perspective for atoms, more mathematical, is use of the nomenclature of Lie groups, for which a 2-to-1 homomorphism can be shown to exist between the two-dimensional special unitary group, SU(2), and the full special three-dimensional rotation group, SO(3) or O_3^+ (Arfken, 1985; Hamermesh, 1989). The resulting double point groups have double the number of operators than the simple groups, although the number of classes is not necessarily doubled. Character tables for these double groups are available in various references (Koster *et al.*, 1963; Pyykkö and Toivonen, 1983; Herzberg, 1991). Due to the additional classes, there are additional irreducible representations in these groups, referred to as double-valued representations, corresponding to states that change sign upon rotation by 2π. It can be shown that odd-electron functions necessarily transform as one of these double-valued representations, while even-electron functions transform as one of the irreducible representations of the simple group, now referred to as single-valued representations. Of particular importance for Hartree–Fock or DFT calculations that include a spin–orbit operator is that, because orbitals are one-electron functions, they now carry labels from the double-valued irreducible representations. Calculations that include only the spin–orbit operator in the subsequent correlation step and perform the Hartree–Fock calculations with a spin-free Hamiltonian retain the single-valued irreducible representation labels for the orbitals.

Of importance for chemical purposes is how functions transform. For example, for two electrons, the singlet spin function transforms as the totally symmetric irreducible representation and the triplet functions transforms in the same fashion as the angular momentum vector operators – e.g. functions with a z-axis projection of zero, such as S_z, transform under the same irreducible representation as L_z does. To obtain the double-group label of a function, the direct product of the irreducible representation for the spatial function and the irreducible representations for the spin function are determined. For atoms, this procedure is analogous to obtaining J values. S^2 and L^2 no longer commute with the Hamiltonian and their magnitudes are no longer good quantum numbers, but the magnitude of the total angular momentum, J, is still good. For example, for a ^{3}P function, one obtains J values of 2, 1, and 0 and the states are labeled ^{3}P$_2$, ^{3}P$_1$, and ^{3}P$_0$. The spin–orbit operator allows mixing of the ^{3}P$_1$ with a ^{1}P$_1$ function. Where the spin–orbit interaction is much larger than electron–electron repulsion, the states are more properly labeled by J values alone, which leads to the progression from Russell–Saunders (or LS) coupling

to j–j coupling. For linear molecules, the double-group irreducible representations correspond to Ω values, where Ω is the z-component of the total angular momentum. The z-component of the orbital angular momentum, Λ, is no longer a good quantum number, Ω is still a valid quantum number. For a $^3\Pi$ state, one obtains Ω values of 2, 1, 0^+, and 0^- and the states are labeled $^3\Pi_2$, $^3\Pi_1$, $^3\Pi_{0+}$, and $^3\Pi_{0-}$. The $^3\Pi_1$ can mix with $^1\Pi_1$. For linear molecules, the analog to j–j coupling is ω–ω coupling. For nonlinear polyatomics, the double-group label is obtained by first determining the representation of the spin functions. For example, in C_{2v}^*, the triplet functions transform as $A_2 + B_1 + B_2$, while the singlet function transforms as the A_1 irreducible representation. Thus, a $^3B_1$ function in ΓS coupling transforms, after the direct product is taken, as the B_2, A_1, and A_2 irreducible representations of the double group. A $^1A_2$ function would transform as the A_2 irreducible representation of the double group and would be able to mix with the A_2 portion of the triplet function. Note that the double-group label does not have an explicit spin label as a superscript; the spin symmetry is incorporated in the label itself.

A final point is that different authors use different labels for the additional irreducible representations of the double group. For example, for the O_h^* group, Herzberg (1991) uses two sets of labels $E_{1/2g}$, $E_{5/2g}$, $G_{3/2g}$, $E_{1/2u}$, $E_{5/2u}$, and $G_{3/2u}$, while other authors use the labels Γ_{6g}, Γ_{7g}, Γ_{8g}, Γ_{6u}, Γ_{7u}, and Γ_{8u}.

17.3 THEORETICAL STUDIES OF THE ACTINYL IONS AND ACTINIDE OXO COMPLEXES

Because the actinide elements, and especially the most studied early actinides, tend to be very electropositive, much of their chemistry is dominated by high positive oxidation states. The electropositive nature of the actinides leads to high oxophilicity, as exemplified by the high-valent (typically +5 and +6 oxidation states) actinide elements in actinyl ions, AnO_2^{q+}. The U(VI) uranyl ion, UO_2^{2+}, is by far the most studied of the actinyl ions, and the electronic structure of this isolated species has been the subject of numerous theoretical studies. In the next section, the bonding in UO_2^{2+} is discussed briefly, followed by discussion of actinyl complexes of the general form $[AnO_2(L)_n]^q$. This is followed by sections on the spectroscopy of 'bare' actinyl species and actinyls in ionic solids. The section ends with discussion of other high-valent actinide oxo compounds and of actinide oxyfluorides.

17.3.1 The uranyl ion and related species

The most common oxidation state for uranium is +6, which corresponds to an f^0 center with a radon-like electron configuration. In the presence of oxygen, the most common discrete ionic and molecular uranium species formed contain the

uranyl ion, UO_2^{2+}, which nearly always has a linear O–U–O linkage. Similarly, neptunium and plutonium commonly form NpO_2^{q+} and PuO_2^{q+} species in which the actinide center is in the +5 or +6 oxidation state. The 'bare' uranyl species has not been isolated in the gaseous state, and can only be approached in matrix isolation studies or in ionic lattices, as will be discussed in later sections.

Electronic structure calculations on UO_2^{2+} have served as benchmarks for theoretical methods as well as a means for understanding the bonding in this relatively simple system and in the complexes it forms with other ligands. As has been detailed by Pepper and Bursten (1991), the electronic structure of UO_2^{2+} has been surprisingly controversial, especially given the apparent simplicity of this symmetric, linear, triatomic system. Among the significant questions addressed by these calculations are the following: (a) how important are relativistic effects on the electronic structure of the uranyl and related ions? (b) how covalent are the U–O bonds? (c) what are the relative contributions of the U 5f and 6d orbitals in the U–O interactions? and (d) what are the bonding principles that cause UO_2^{2+} to favor a linear geometry? Many of these questions are general ones that serve as proxies for the challenges in all electronic structure calculations on molecular actinide systems. Inasmuch as the uranyl ion is the smallest commonly found molecular actinide ion, it is not surprising that it has received intense scrutiny by theoretical methods. To provide an historical framework, the contributions of electronic structure theory in addressing the above questions about the uranyl ion will be briefly discussed here, followed by discussion of some of the recent advances in applications of theoretical methods to the chemistry of the actinyl ions.

The high symmetry and small size of the UO_2^{2+} ion has made it an attractive early candidate for electronic structure calculations of actinide complexes. McGlynn and Smith (1961) presented a nonrelativistic semiempirical MO description of the electronic structure of the uranyl ion in 1961. The importance of relativistic effects in the bonding of the uranyl ion was recognized as early as 1965, and all of the theoretical methods used to study UO_2^{2+} over the last 40 years have included explicit or implicit relativistic corrections. Many of the early and more recent studies of the bonding in uranyl have addressed the debate over 5f contributions to the U–O bonds, a seemingly straightforward question that has led to lively debates among theoretical and experimental actinide chemists.

The question of 5f covalency in actinide systems is not a new one. Chemical evidence for f-orbital covalency in actinyl nitrates was provided in 1950 by Glueckauf and McKay (1950), but was disputed shortly thereafter by Katzin (Glueckauf and McKay, 1950; Katzin, 1950). In 1952, Connick and Hugus used experimental data for UO_2^{2+} to propose U 5f orbital participation in the U–O bonds (Connick and Hugus, 1952). In 1953, Elliott used a model involving 5f interactions to explain the temperature dependence of paramagnetism in NpO_2^{2+} and PuO_2^{2+} (Elliott, 1953). Eisenstein proposed group theoretical arguments in favor of 5f and 6d covalency in uranyl and other actinide compounds (Eisenstein and Pryce, 1955; Eisenstein, 1956). Coulson and Lester (1956) soon

after proposed that f-orbital interactions must contribute to the bonding in hexavalent actinyl complexes, but that ionic interactions are probably dominant. They surprisingly proposed that the 6f orbitals of the actinides would dominate any f-orbital interactions because of the contracted nature of the 5f orbitals. At roughly the same time, Seaborg and coworkers attributed the difference in the ion-exchange behavior of analogous lanthanide and actinide complexes to significant 5f orbital contributions in the actinide systems (Diamond *et al.*, 1954).

Although relativistic quantum chemical methodology continued to grow in sophistication from the 1960s through the 1980s, there was still surprisingly little agreement among quantum chemists concerning the 5f contributions to and the energetic ordering of the highest occupied orbitals in UO_2^{2+}. Because it is an f^0 ion, the highest-energy orbitals of UO_2^{2+} are predominantly O 2p in character. For the linear ion, the formally filled O $2p\sigma$ orbitals lead to group orbitals of σ_g and σ_u symmetry. Likewise, the formally filled doubly-degenerate O $2p\pi$ orbitals generate filled doubly-degenerate π_g and π_u orbitals of UO_2^{2+}. Because of the centrosymmetric symmetry of the linear ion, the allowed interactions of the U 6d and 5f orbitals are mutually exclusive; the gerade $6d\sigma$ and $6d\pi$ orbitals can interact with the O 2p σ_g and π_g combinations, whereas the ungerade $5f\sigma$ and $5f\pi$ orbitals can interact with the σ_u and π_u ligand group orbitals. A qualitative MO diagram for UO_2^{2+} is presented in Fig. 17.4. All of the orbital methods agree that the four highest occupied MOs are the O 2p-based σ_g, σ_u, π_g, and π_u MOs, followed by low-lying U 5f virtual orbitals. There has been marked disagreement over the actual ordering of the highest filled orbitals, however. The disagreements about the orbital orderings in UO_2^{2+} were especially marked in the late 1970s and early 1980s when a number of relativistic methods were applied to the ion, including the relativistic extended Hückel (REX) calculations of Pyykkö and Lohr (1981), the quasi-relativistic multiple-scattering (QR-MS) Xα calculations of Wood and Boring (Boring *et al.*, 1975; Boring and Wood, 1979; Wood *et al.*, 1981), the Dirac–Slater multiple-scattering (DS-MS) Xα calculations of Yang *et al.* (1978), the Dirac–Slater discrete-variational (DS-DV) Xα calculations of Ellis *et al.* (1975), the Hartree–Fock calculations with RECPs by Wadt (1981), and the relativistic HFS calculations of DeKock *et al.* (1984). Jørgensen and Reisfeld (1983) compared the lack of quantitative agreement among these various methods for the orbital ordering in UO_2^{2+} to the 'effect of throwing dice'. Most of these early calculations predict a σ_u highest occupied molecular orbital (HOMO), as shown in Fig. 17.4. A detailed discussion of the lively debate over the ordering of the O 2p-based orbitals in linear UO_2^{2+} is given in the review by Pepper and Bursten (1991). As an illustrative example of a very recent calculation, the following ordering was obtained in a hybrid DFT calculation (Sonnenberg *et al.*, 2005) for the highest occupied orbitals for the bare uranyl ion: π_g (–24.91 eV) $<$ π_u (–24.56) $<$ σ_g (–24.27) $<$ σ_u (–23.63). The 5f-based virtual orbitals had the ordering ϕ_u (–18.38) $<$ δ_u (–17.95) $<$ π_u (–15.49).
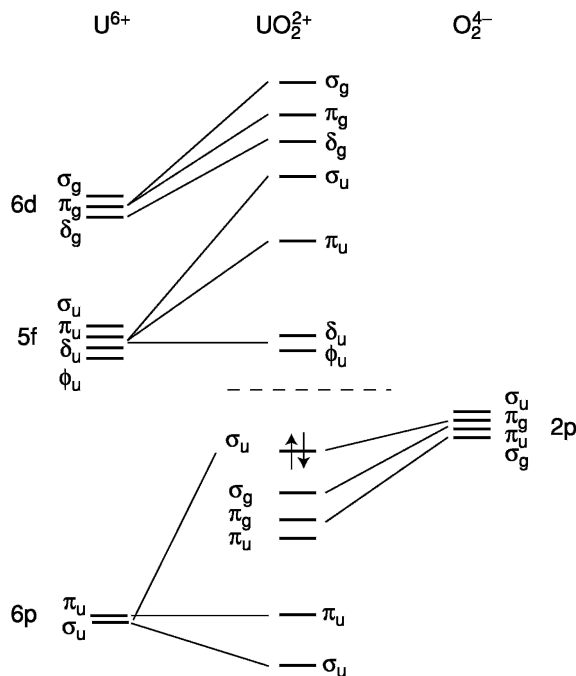
Fig. 17.4   *Schematic diagram of the MO interactions in* UO_2^{2+}, *showing the interaction of the U 6d and 5f atomic orbitals with the oxygen 2s and 2p orbitals* (*adapted from Pepper and Bursten*, 1991).

It is now clear that accurate accounting of both electron correlation and relativistic effects are essential for the prediction of the ordering of these frontier orbitals.

The electronic structural origins of the nearly invariably linear geometry of the UO_2^{2+} ion have been the focus of many theoretical studies, especially given that isoelectronic ThO_2 and the analogous transition metal ion MoO_2^{2+} typically exhibit bent geometries. The issue was first addressed on the basis of extended Hückel calculations by Tatsumi and Hoffmann (1980) and later using REX by Pyykkö *et al.* (1989) The factors include the relative admixture of $5f(\sigma_u)$ vs 6d as the ion bends, the role of the filled 'outer core' U 6p shell, and the relative contributions of covalent and ionic bonding. RECP calculations at the Hartree–Fock level by Wadt correctly predicted bent ThO_2 and linear UO_2^{2+} but disagreed in the interpretation of the role of U 6p orbitals (Wadt, 1981).

Dyall (1999) has carried out Dirac–Hartree–Fock calculations on ThO_2, PaO_2^+, and UO_2^{2+} and has analyzed in detail the role of the actinide 6p, 6d, and 5f orbitals across the series on the basis of the more sophisticated results.

He observes that the energy of the U 6d orbitals remain roughly unchanged across this region of the actinide series whereas the 5f orbitals drop in energy and becoming more radially contracted. For Th, the 5f orbitals lie above the 6d and it is favorable to bend and use f–d hybrids in the bonding, while for U the lower energy of the 5f orbitals favors linearity. In Fig. 17.5, the energy of the orbitals (actually spinors from the Dirac–Hartree–Fock [DHF] results) as a function of bending is shown. The highest-energy spinor, which corresponds to the σ_u orbital, increases in energy with bending for UO_2^{2+} but decreases for ThO_2.

A summary of the results of recent theoretical calculations on UO_2^{2+} using a variety of methods (Wahlgren *et al.*, 1998; Dyall, 1999; Ismail *et al.*, 1999; Vallet *et al.*, 1999b; Han and Hirao, 2000; Zhou *et al.*, 2000; de Jong *et al.*, 2001b; Garcia-Hernandez *et al.*, 2002), is given in Table 17.4. The methods are grouped into Hartree–Fock-based and density functional theory categories. Both of these include all-electron (AE) calculations along with calculations employing RECPs. The latter include two types denoted 'large core' with 78 electrons replaced by the RECP (Ermler *et al.*, 1991; Hay and Martin, 1998) and 'small core' with 60 electrons replaced (Küchle *et al.*, 1994). Among all-electron calculations, the U=O bond length is calculated to be about 1.65 Å from the various Hartree–Fock-based methods (DHF and DK-HF). With the small-core
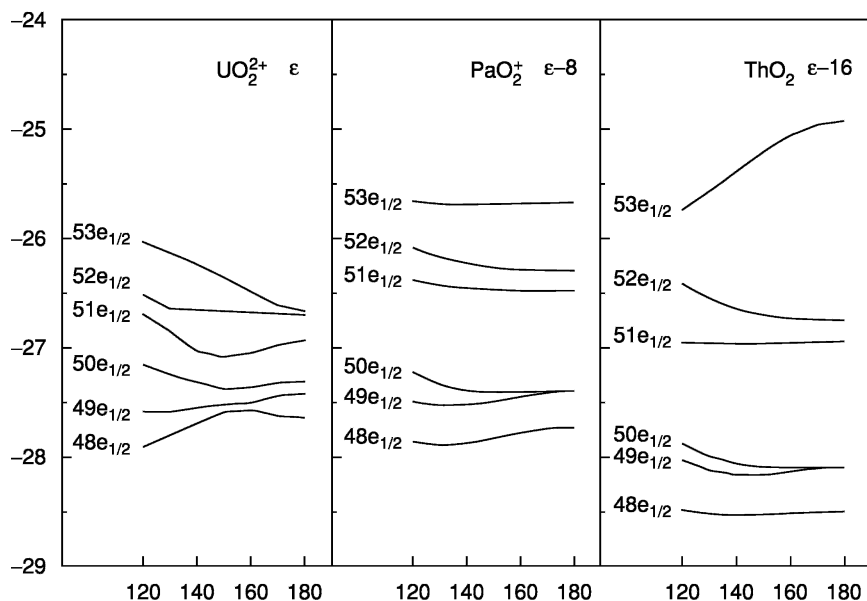
Fig. 17.5 *Valence spinor energies* (eV) *energies as a function of bending angle* (*degrees*) *for ThO₂, PaO₂⁺, and [UO₂]²⁺ from relativistic calculations at M–O = 1.9 Å* (*adapted from Dyall*, 1999).

Table 17.4 *Comparison of the calculated properties of UO_2^{2+} from various theoretical methods using all-electron (AE) approaches or employing using either small core (SC) or large core (LC) relativistic effective core potentials (RECP).*

Method	AE or ECP	$R_{U=O}$ (Å)	v_1 (cm^{-1})	v_2 (cm^{-1})	v_3 (cm^{-1})	References
HF-based						
DK-HF	AE	1.651				Wahlgren *et al.* (1998)
	AE	1.647				Vallet *et al.* (1999b)
DHF	AE	1.651	1240	241	1326	de Jong *et al.* (2001b)
	AE	1.650	1234	246	1294	Dyall (1999)
HF	SC KDSP[a]	1.643				Vallet *et al.* (1999b)
	SC KDSP[a]	1.642	1243	268	1394	Han and Hirao (2000)
	SC KDSP[a]	1.654	1221	260	1301	Ismail *et al.* (1999)
	LC K[b]	1.613	1275	287	1321	Zhou *et al.* (2000)
	LC K[b]	1.631	1250	271	1301	de Jong *et al.* (2001b)
	LC HM[c]	1.646	1228	270	1280	de Jong *et al.* (2001b)
correlated						
DK CCSD(T)	AE	1.706				Vallet *et al.* (1999b)
DHF CCSD(T)	AE	1.715	974	164	1121	de Jong *et al.* (2001b)
CCSD(T)	SC KDSP	1.702	1025	192	1113	Han and Hirao (2000)
DFT scalar						
DK SVWN	AE	1.705	1034	263	1142	Garcia-Hernandez *et al.* (2002)
SVWN	SC KDSP	1.697	1029	134	1124	Zhou *et al.* (2000)
		1.709	1059	65	1165	Ismail *et al.* (1999)
		1.698	1031	221	1133	Garcia-Hernandez *et al.* (2002)
	LC K	1.670	1056	87	1138	Zhou *et al.* (2000)
	LC HM	1.728	931	84	961	Garcia-Hernandez *et al.* (2002)
	LC ERC[d]	1.691	1005	34	1096	de Jong *et al.* (2001b)
DFT hybrid						
B3LYP	SC KDSP	1.694	1051	174	1142	Ismail *et al.* (1999)
	SC KDSP	1.705	1041	161	1140	Zhou *et al.* (2000)
	SC KDSP	1.696	1049	163	1142	de Jong *et al.* (2001b)

Table 17.4 (*Contd.*)

Method	AE or ECP	$R_{U=O}$ (Å)	ν_1 (cm^{-1})	ν_2 (cm^{-1})	ν_3 (cm^{-1})	References
	LC K	1.661	1090	181	1166	Han and Hirao (2000)
	LC HM	1.704	1011	139	1101	de Jong *et al.* (2001b)
	LC ERC	1.679	1047	166	1135	de Jong *et al.* (2001b)

[a] Küchle *et al.* (1994).
[b] RECP for U:http://www.theochem.uni-stuttgart.de/pseudopotentials/index.en.html
[c] Hay and Martin (1998).
[d] Ermler *et al.* (1991).

relativistic effective core potentials (RECPs), Hartree–Fock calculations lead to similar bond lengths to those found using the all-electron DHF method, while there are slightly greater differences noted with the large-core RECPs. When correlation effects are explicitly included, as in CCSD(T) approaches, the bond length increases to 1.71 Å. The density functional results (for the LDA and B3LYP functionals summarized in the table) that incorporate correlation effects through the exchange-correlation functional reasonably reflect this with predicted U=O bond lengths ranging from 1.69 to 1.71 Å. Again larger discrepancies arise with the large core RECP.

The calculated vibrational stretching frequencies generally follow the trend that higher frequencies are associated with shorter U=O bond lengths. DHF calculations, with shorter bond lengths, predict symmetric and asymmetric stretching frequencies of 1240 and 1300 cm^{-1}, while the correlated methods and DFT approaches give 1020–1050 and 1110–1140 cm^{-1} for the same values. Comparison with experiment is problematic in the absence of isolated gas-phase spectroscopic studies, but comparisons with observed frequencies will be given below for uranyl complexes.

Garcia-Hernandez *et al.* (2002) examined the Np(VI) analog [NpO$_2$]$^{2+}$ with a 5f^1 configuration using all-electron Douglas–Kroll–Hess approaches. For the Np–O bond length they obtained 1.698, 1.716, and 1.718 Å using the VWN, BP, and PBEN functionals, respectively. Results with spin–orbit DKH showed practically no change in the computed bond lengths. For symmetric stretch frequencies, the same calculations predicted 1009 cm^{-1} (VWN), 972 cm^{-1} (BP), and 969 cm^{-1} (PBEN).

17.3.2 Actinyl complexes

In solution and the solid state, additional ligands bind to the actinyl ions in the equatorial plane of the O=An=O unit. Among the most common characterized species are the aqua complexes [UO$_2$(H$_2$O)$_5$]$^{2+}$ found at low pH, the hydroxo

complexes $[UO_2(OH)_4]^{2-}$, $[UO_2(OH)_5]^{3-}$, and $[UO_2(OH)_4(H_2O)]^{2-}$ found at high pH, and the halide species $[UO_2X_4]^{2-}$ found in crystals (Fig. 17.6). In this class of $[UO_2L_n]$ complexes, the equatorial ligands are weak σ-donors. In this case, the U atom can use acceptor orbitals oriented in the equatorial plane that are not utilized in the bonds with the actinyl oxo atoms. The orbitals that in principle can act as acceptors in the equatorial plane include the $6d(x^2-y^2)$, $6d(xy)$, $5f(x^3-3xy^2)$ and $5f(y^3-3x^2y)$, and, to a lesser extent, the 7s and 7p orbitals. In the case of hydroxo complexes, the OH$^-$ ligands can be π-donors and can compete with the metal orbitals involved in the U=O π_u and π_g bonds.

Clavaguéra-Sarrio *et al.* (2003b) have recently reported a DFT study of the binding energies and geometries of $UO_2L_2^{q+}(q=0,2)$ complexes with 33 different ligands L with the goal of predicting preferred coordination geometries. They determined that ligand polarization and charge transfer to the uranyl ion are likely to be necessary in any force-field model for uranyl–ligand bonding.

(a) Aqua complexes

Aqua complexes of actinyls have been studied in solution and the solid state using extended X-ray absorption fine structure (EXAFS) spectroscopy (Allen *et al.*, 1997), X-ray crystallography (Alcock and Esperas, 1977; Aaberg *et al.*, 1983), and X-ray scattering (Neuefeind *et al.*, 2004). The experimental studies show a preferred coordination number of five water molecules. The $[UO_2(H_2O)_5]^{2+}$ ion is the commonly observed U(VI) species in aqueous solution at low pH (Fig. 17.6) and consequently this complex has been the subject of several recent theoretical studies (Gropen, 1999; Spencer *et al.*, 1999; Tsushima and Suzuki, 1999; Wahlgren *et al.*, 1999; Hay *et al.*, 2000; Fuchs *et al.*, 2002; Clavaguéra-Sarrio *et al.*, 2003a) including DFT-based approaches and model potentials with Douglas–Kroll corrections. The oxygen atoms of the five water molecules are coordinated in nearly perfect five-fold symmetry about the uranyl ion, with the water molecules nearly perpendicular to the equatorial plane. Subtle differences in the structure of this complex are obtained among the calculations (Table 17.5). The AIMP-DK and DFT calculations with LDA and B3LYP functionals all predict U=O bond lengths in the range 1.75–1.78 Å. These theoretical results are in good agreement with the EXAFS solution bond length of 1.76 Å, which is slightly longer than the solid state value of 1.71 Å. The U-OH$_2$ bond lengths are predicted to be 2.42–2.52 Å in the DFT calculations, which compare favorably with the experimental bond lengths of 2.41–2.45 Å (Hay *et al.*, 2000). In the DKH studies (Fuchs *et al.*, 2002), the effects of solvation were included where the U=O bond length decreased from 1.771 to 1.662 Å while the U–OH$_2$ bond length increased from 2.530 to 2.639 Å.

Several studies have addressed the issue of why five is the preferred coordination number for H$_2$O with UO_2^{2+} (Spencer *et al.*, 1999; Tsushima and Suzuki, 1999; Hay *et al.*, 2000). In particular, several groups have explored the relative
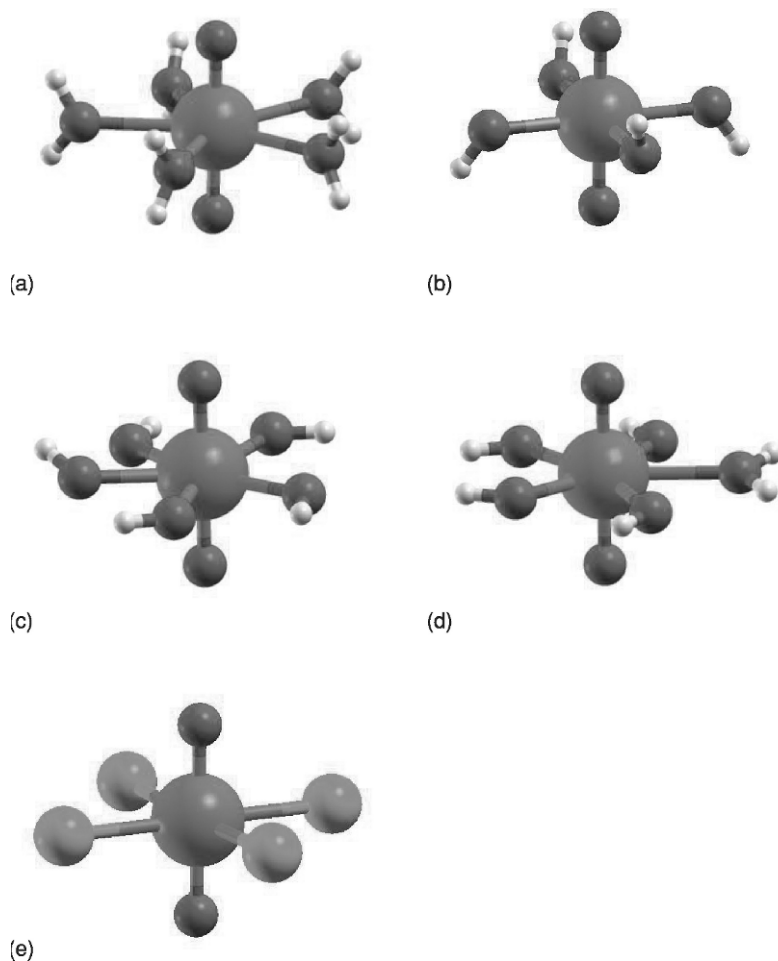
Fig. 17.6 *Structures of (a)* $[UO_2(H_2O)_5]^{2+}$, *(b)* $[UO_2(OH)_4]^{2-}$, *(c)* $[UO_2(OH)_5]^{3-}$, *(d)* $[UO_2(OH)_4(H_2O)]^{2-}$, *and (e)* $[UO_2Cl_4]^{2-}$ *as determined by DFT calculations (rendered from results reported in Schreckenbach* et al.*, 1998, 1999; Wahlgren* et al.*, 1999; Clavaguéra-Sarrio* et al.*, 2003a; Sonnenberg* et al.*, 2005).*

energetics of binding four, five, or six water molecules to various actinyl ions. These approaches used a combination of energies from density functional calculations, thermodynamic quantities derived from calculated vibrational frequencies, and solvation energies from dielectric continuum models. Spencer *et al.* (1999) used DFT (Becke–Lee–Yang–Parr functional [BLYP]) calculations to obtain the relative ordering 5 < 4 (+7.2 kcal mol^{-1}) < 6 (+18.5) for $[UO_2(H_2O)_n]^{2+}$ species. They obtained a similar ordering pattern for $[PuO_2(H_2O)_n]^{2+}$ ions. Calculations using DFT (B3LYP) and different solvent

Table 17.5 *Calculated properties of $[UO_2(H_2O)_5]^{2+}$ from various theoretical methods, compared to experimental values for the uranyl aqua complex.*

Method	$R_{U=O}$ (Å)	$R_{U-O(H)}$ (Å)	v_{sym} (cm^{-1})	v_{asym} (cm^{-1})	References
BLYP	[1.746]	2.550			Spencer *et al.* (1999)
AIMP-DK	1.750	2.421			Wahlgren *et al.* (1999)
HF RECP	1.694	2.545	1091	1149	Hay *et al.* (2000)
LDA RECP	1.778	2.423	854	945	Hay *et al.* (2000)
BLYP RECP	1.803	2.516	787	893	Hay *et al.* (2000)
B3LYP RECP	1.756	2.516	910	1003	Hay *et al.* (2000)
PBEN (AE)	1.771	2.530			Fuchs *et al.* (2002)
PBEN (AE+solv)	1.662	2.639			Fuchs *et al.* 2002
Expt.	1.76	2.41	869	965	Allen *et al.* (1997)

models gave a slightly different ordering of 5 < 6 < 4 water molecules in the first coordination shell (Tsushima and Suzuki, 1999; Hay *et al.*, 2000). Additional structures are found with at least one water molecule displaced from the first shell into the second shell, where the molecule is hydrogen bonded to the uranyl oxygen atoms rather than directly coordinated to the uranium center.

As one proceeds across the actinide series, there is only a slight change in the experimental An–O bond length as measured in solution by EXAFS: 1.76 Å in $[UO_2(H_2O)_5]^{2+}$ (Allen *et al.*, 1997), 1.75 Å in $[NpO_2(H_2O)_5]^{2+}$ (Reich *et al.*, 2000; Den Auwer *et al.*, 2003), and 1.74 Å in $[PuO_2(H_2O)_5]^{2+}$ (Conradson, 1998). DFT (B3LYP) calculations using LC-RECPs predict a slight shortening of bond length of 1.756–1.742 Å across U(VI) to Pu(VI) (Hay *et al.*, 2000) (Fig. 17.7). In addition the calculations reasonably well describe the decrease in symmetric and antisymmetric O=An=O stretch frequencies across the series (Jones and Penneman, 1953; Basile *et al.*, 1974). It is somewhat curious that as the bond lengths are getting slightly shorter, the frequencies are actually decreasing – the reverse of the usual correlation. This trend is attributed to the decrease in An(5f)–O(2p) overlap going across the series as the 5f orbitals become more radially contracted.

The mechanisms for exchange of water (H_2O^*) with the aqua complex $[UO_2(H_2O)_5]^{2+}$ were investigated by Vallet *et al.* (2001). The possibilities of associative (via a six-coordinate intermediate), dissociative (via four-coordinate intermediate), and interchange (via a concerted symmetric transition state) pathways were probed using a combination of Hartree–Fock, MP2, and CPCM (conductor-like polarizable comtinuum model) solvent model (Fig. 17.8). The calculated activation energies were 74, 19, and 21 kJ mol^{-1}, respectively, for the D-, A- and I-mechanisms in the solvent. Comparison with the experimental value of 26 ± 1 kJ mol^{-1} eliminates the D mechanism, leaving it difficult to distinguish between the A- and I-mechanisms. A later study extended
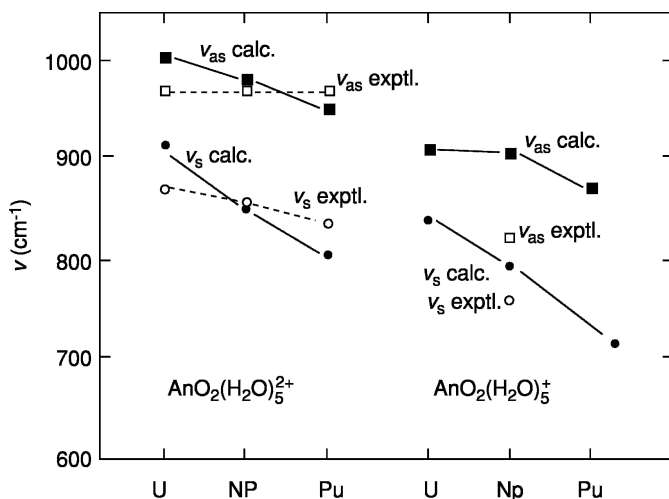
Fig. 17.7 *Plots of calculated and experimental vibrational frequencies for* $[AnO_2(H_2O)_5]^{2+}$ *and* $[AnO_2(H_2O)_5]^{+}$ *species (reproduced from Hay* et al.*, 2000).*
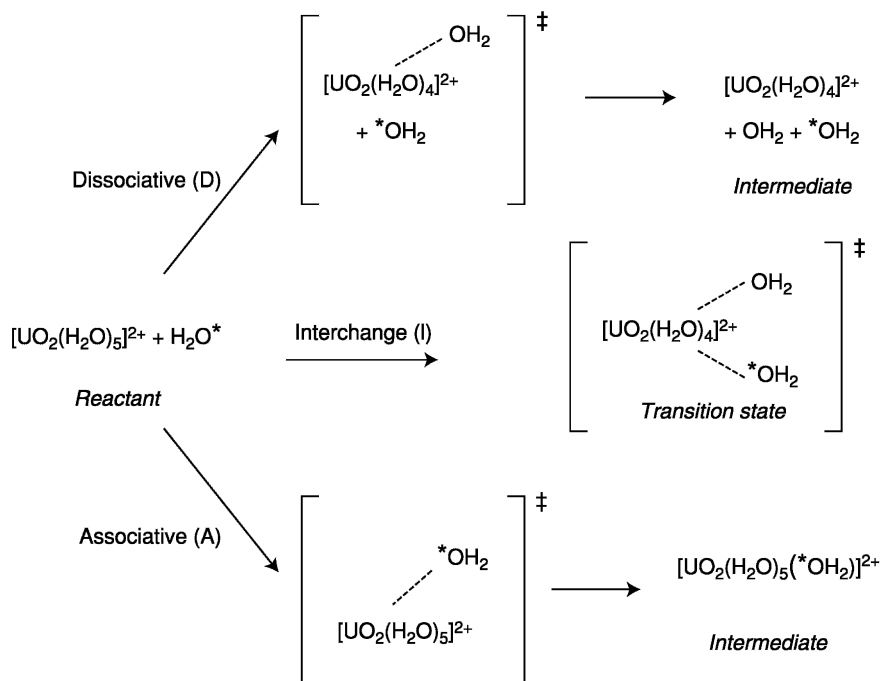
Fig. 17.8 *Intermediates for exchange of water molecules in* $[UO_2(H_2O)_5]^{2+}$ *by associative* (*A*)*, dissociative* (*D*)*, and interchange* (*I*) *mechanisms (adapted from Vallet* et al.*, 2001).*

these studies to exchange in aqua complexes of UO_2^+, NpO_2^{2+}, and AmO_2^{2+} with similar findings (Vallet *et al.*, 2004). This same group has modeled electron exchange between UO_2^+ and UO_2^{2+} in solution, examining potential intermediates in both outer-sphere and inner-sphere electron-exchange mechanisms (Privalov *et al.*, 2004). Other than this contribution, relatively little work has been done on dimeric and polymeric species that can be the dominant species in solution depending on the conditions. Schlosser *et al.* (2003) compared all-electron DFT results on one of the few dimeric complexes for which there is a crystal structure, $[(UO_2)_2(\mu^2\text{-}OH)_2Cl_2(H_2O)_4]$. In addition, the role of hydrogen bonding in the crystal was studied by adding a layer of water molecules.

(b)   Hydroxide complexes

At higher pH, one finds uranyl species with hydroxide ligands displacing water molecules coordinated to the metal. The first hydrolysis product formed is $[UO_2(H_2O)_4(OH)]^+$, which can also exist in dimeric form (Clark *et al.*, 1995). At much higher pH, the $[UO_2(OH)_4]^{2-}$ species has been observed and characterized in the solid state (Clark *et al.*, 1999). The structures of the tetrahydroxide species have been investigated using DFT techniques with RECPs (Schreckenbach *et al.*, 1998) and with model potentials with Douglas–Kroll corrections (AIMP-DK) (Wahlgren *et al.*, 1999). As shown in Table 17.6, the calculated U=O distances agree rather well with experiment while the U–OH bond lengths are overestimated somewhat by ∼0.1 Å compared to the crystal structure.

The U=O bonds in the hydroxide complexes are longer than those in the aqua complexes. This observation indicates weaker U=O interactions because of the competition with the equatorial OH⁻ ligands, which are acting as strong π-donors. The lone pair orbitals on the OH⁻ ligands have the proper symmetry to interact with the π_u and π_g U–O bonding orbitals of the UO_2^{2+} moiety (Schreckenbach *et al.*, 1998).

Solution EXAFS studies of uranyl hydroxide complexes in two different alkaline environments found relatively similar U–OH bond lengths (2.22–2.24 Å) that differ only slightly from the X-ray structure of $[UO_2(OH)_4]^{2-}$ (Clark *et al.*, 1999; Wahlgren *et al.*, 1999). The number of oxygen atoms in the equatorial plane was found to be 5 ± 0.5. Clark *et al.* interpret this result in terms of a $[UO_2(OH)_5]^{3-}$ structure. Calculations on the pentahydroxide structure by Wahlgren *et al.* gave U–OH bond lengths 0.3 Å longer, and hence they ruled out this form in favor of the tetrahydroxide. They also examined a third species with one water and four hydroxide ligands bound to the uranyl. More recently, Sonnenberg *et al.* (2005) found a stable pentahydroxide species with C_{5v} symmetry with no imaginary frequencies having U–OH bond lengths of 2.45 Å without incorporating solvent effects, which would be 0.2 Å longer than the derived value from the EXAFS analysis.

Table 17.6 *Theoretical and experimental geometries of hydroxyl complexes including* $[UO_2(OH)_4]^{2-}$ *and related complexes.*

Method	$R_{U=O}$ (Å)	$R_{U-O(H)}$ (Å)		References
$[UO_2(OH)_4]^{2-}$				
AIMD-DK	1.80	2.36–2.38		Wahlgren *et al.* (1999)
B3LYP LC-RECP	1.842	2.33		Schreckenbach *et al.* (1998)
	1.87	2.27–2.35	*cis*-O=U=O form	
B3LYP SC-RECP	1.84	2.31		Sonnenberg *et al.* (2005)
Expt (solid)	1.80–1.83	2.23–2.36		Clark *et al.* (1999)
$[UO_2(OH)_5]^{3-}$ and related species				
AIMD-DK	1.80	2.50	$[UO_2(OH)_4]^{2-}$	Wahlgren *et al.* (1999)
	1.80	2.36–2.38	$[UO_2(OH)_4(H_2O)]^{2-}$	
B3LYP SC-RECP	1.83	2.455	$[UO_2(OH)_5]^{3-}$	Sonnenberg *et al.* (2005)
EXAFS soln	1.79	2.22	$N_{eq} = 5.3 \pm 0.5$[a]	Clark *et al.* (1999)
EXAFS soln	1.82	2.24	$N_{eq} = 5.0 \pm 0.5$[a]	Wahlgren *et al.* (1999)

[a] Values for the coordination number from the EXAFS experiments.

Schreckenbach *et al.* (1998) investigated the possible isomerization of the tetrahydroxide in which protons are transferred from the equatorial hydroxides to the uranyl oxygen atoms to reconstitute the tetrahydroxide. Such a mechanism was suggested to account for the scrambling of ^{18}O in the complex in basic solution (Fig. 17.9). They found an unusual *cis*-oxo form with a bent O=U=O bond angle of 128° (Table 17.6) to be a local minimum with a calculated energy 18 kcal mol^{-1} above the more stable 'usual' *trans*-oxo form. The barrier between the two forms was calculated to be 38 kcal mol^{-1}, too high to account for rapid isomerization via a unimolecular mechanism.

(c) Complexes with bidentate ligands

Actinyl species can be found complexed to other inorganic ligands in a variety of conditions. Because waste treatments of actinides in solution use nitrates, actinyl complexes with coordinated nitrate ligands are common (Castellato *et al.*, 1981; Allen *et al.*, 1996). Actinyl complexes with carbonate ligands are also common and are especially relevant to studies of actinides in the environment with naturally occurring minerals, carbonate species are another important actinide complex (Clark *et al.*, 1995). Craw *et al.* examined prototypical nitrate complexes $UO_2(NO_3)_2(H_2O)_2$ at the Hartree–Fock level (Table 17.7) as well as a sulfate complex and their Pu(VI) analogs (Craw *et al.*, 1995). As shown
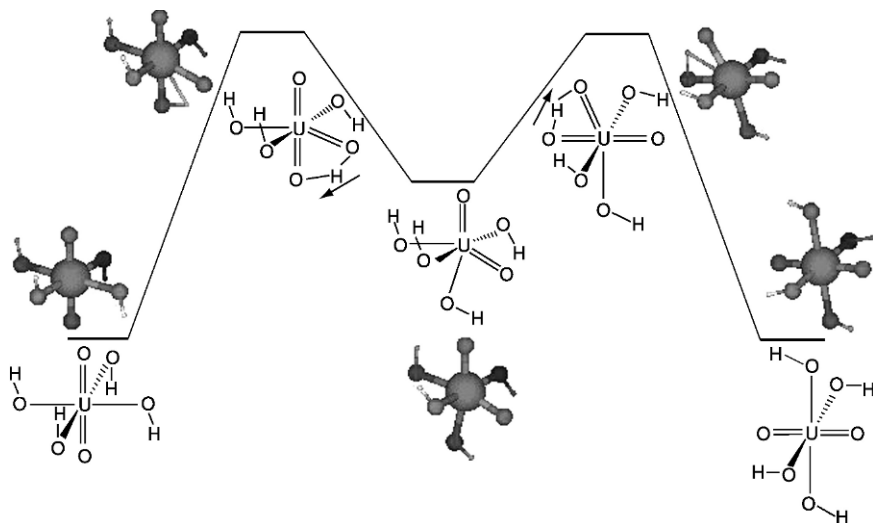
Fig. 17.9   *Isomers of* $[UO_2(OH)_4]^{2-}$ *involving conventional trans and unusual cis-O=U=O linkages (reproduced from Schreckenbach* et al., *1998).*

in Fig. 17.10, the nitrato complexes are coordinated in a bidentate mode. An analysis of the bonding in these complexes showed primarily ionic bonding dominated by electrostatic forces.

Gagliardi and Roos (Gagliardi *et al.*, 2001a; Gagliardi and Roos, 2002) have used complete active space self-consistent field (CASSCF)/CASPT2 calculations to examine carbonato complexes of the uranyl and neptunyl ions that have been the focus of several experimental studies (Clark *et al.*, 1995, 1996; Docrat *et al.*, 1999). Solid-state structures with both $[UO_2(CO_3)_3]^{4-}$ and $[UO_2(CO_3)_3]^{5-}$ are known. In both cases, three carbonates bind in the equatorial plane in a bidentate mode. Experimentally the U=O bond length increases from 1.80 to 1.90 Å when the extra electron is added in going from the U(VI) to the U(V) complex. The calculations also give an increase in the U=O bond length of 1.845 to 1.929 Å between the U(VI) and U(V) complexes. Similar increases in the U–O_{eq} bond length are also noted. For the Np(V) species $[NpO_2(CO_3)_2(H_2O)_2]^{3-}$, the calculated Np=O bond length, 1.854 Å, is between the U(VI)=O and U(V)=O values and is in excellent agreement with the experimental value of 1.85 Å.

Vázquez *et al.* (2003) studied tris-carbonato, tris-acetato, and related uranyl complexes using gradient-corrected DFT using the ADF code also employing a solvent continuum model. They also explored dimeric complexes with bridging hydroxide groups and examined the role of Ca^{2+} counter-ions and explicit water molecules. Coupez and Wipff (2003) reported Hartree–Fock and DFT calculations with diamide ligands (malonamide and succinamide) comparing the

Table 17.7 *Theoretical and experimental bond lengths* (Å) *of actinyl complexes with multidentate ligands.*

Complex	Method	R(U=O)	R(U–O)	R(U–O_H)	References
$UO_2(NO_3)_2$ $(H_2O)_2$	HF	1.72	2.56	2.40	Craw *et al.* (1995)
	expt	1.76		2.40	
$PuO_2(NO_3)_2$ $(H_2O)_2$	HF	1.68		2.45	Craw *et al.* (1995)
$UO_2(SO_4)(H_2O)_3$	HF	1.74	2.57	2.64	Craw *et al.* (1995)
	expt	1.75		2.40	
$PuO_2(SO_4)(H_2O)_3$	HF	1.70		2.47	Craw *et al.* (1995)
$[UO_2(CO_3)_3]^{4-}$	MBPT2	1.88	2.407		Gagliardi *et al.* (2001a)
	solv. PW91	1.86	2.44		Vazques *et al.* (2003)
	expt	1.80	2.43		Clark *et al.* (1996)
$[UO_2(CO_3)_3]^{5-}$	MBPT2	1.933	2.529		Gagliardi *et al.* (2001a)
	expt	1.90	2.50		Docrat *et al.* (1999)
$[NpO_2(CO_3)_2$ $(H_2O)_2]^{3-}$	CASPT2	1.854	2.548	2.585	Gagliardi *et al.* (2001a)
	expt	1.85	2.48		Clark *et al.* (1996)
$[UO_2(acetate)_3]^{1-}$	solv. PW91	1.81	2.50		Vazques *et al.* (2003)
	expt	1.76	2.48		Navaza *et al.* (1991)

relative stabilities of six- and seven-membered chelate rings in their bidentate coordination to the uranyl.

17.3.3 'Bare' actinyl species and actinyl ions in solids

While uranyl is the prototypical actinyl ion, with an oxidation state of +6, high-valent dioxo species are also well known for Np, Pu, and Am. For these actinides, the -yl name has also been applied to the +5 and +6 oxidation states (Katz *et al.*, 1986). In an overview of the electronic structure and spectra of these ions, Matsika *et al.* (2001) were able to characterize the strengths of different interactions found in actinyls. The strongest interaction is the antibonding one between the $5f\sigma_u$ and the $5f\pi_u$ and the ligand orbitals, resulting in high orbital energies for the molecular orbitals mostly derived from these 5f orbitals. Comparisons between the actinide electron repulsion parameters and the actinide spin–orbit parameter (ζ_{5f}) indicate that the electron repulsion is more

(a)

(b)
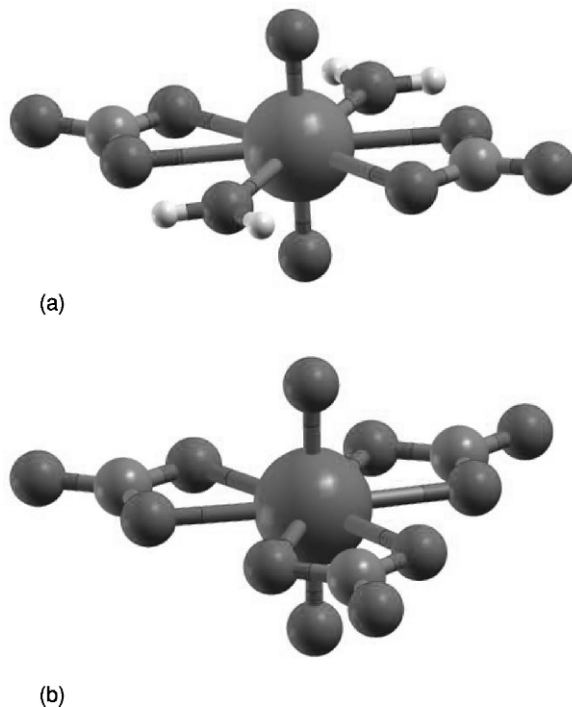
Fig. 17.10 *Calculated structures of bidentate complexes with* (*a*) *nitrate and* (*b*) *carbonate ligands* (*see Craw* et al., *1995; Gagliardi and Roos, 2002*).

significant, but that the spin–orbit splitting needs to be included. Lastly, the $5f\delta_u$ and the $5f\phi_u$ orbitals display weak-field coupling, i.e. the two-electron open-shell state is $\delta_u^1\phi_u^1$ rather than δ_u^2 or ϕ_u^2. The electron configurations for these ions can thus be characterized as $\sigma_u^2(\delta_u\phi_u)^n, \sigma_u^2(\delta_u\phi_u)^{n-1}\pi_u^1, \sigma_u^1(\delta_u\phi_u)^{n+1}$, with n ranging from zero to four, the ground states for these configurations for the various actinyl species are listed in Table 17.8. For example, for f^2 systems, the two actinyl ions studied were NpO_2^+ and PuO_2^{2+}. The lowest state for a given electron configuration is listed – for example, for the $\sigma_u^1(\delta_u\phi_u)$ ^3H configuration, that state would be $^5\Phi_{1g}$ for each of the two actinyl ions. Note that the occupation number for the δ_u and the ϕ_u orbitals are given together due to the strength of the electronic interactions listed above.

As mentioned previously, the COLUMBUS codes have recently enabled two-component multi-reference configuration interaction singles and doubles (SO-MRCISD) using CSF expansions on the order of millions. The great advantage of these calculations for linear molecules is that since the spin–orbit effects are incorporated in the variational calculation, the resultant states are eigenfunctions of the total z-component angular momentum, Ω. A survey of the computational uranyl literature referred to above reveals little information concerning

Table 17.8 *Lowest energy electronic states for various f^n actinyl electron configurations (see Matsika et al., 2001).*

Electronic configuration[a]	$n = 0$ UO_2^{2+} NpO_2^{3+}	$n = 1$ UO_2^+ NpO_2^{2+} PuO_2^{3+}	$n = 2$ NpO_2^+ PuO_2^{2+}	$n = 3$ PuO_2^+ AmO_2^{2+}	$n = 4$ AmO_2^+
$\sigma_u^2(\delta_u \phi_u)^n$	$^1\Sigma^+_{0^+g}$	$^2\Phi_{5/2u}$	$^3H_{4g}$	$^4\Phi_{3/2u}$	$^5\Sigma^+_{0^+g}$
$\sigma_u^2(\delta_u \phi_u)^{n-1}\pi_u^1$		$^2\Pi_{1/2u}$	$^3\Gamma_{3g}$	$^4I_{9/2u}$	$^5\Gamma_{2g}$
$\sigma_u^1(\delta_u \phi_u)^{n+1}$	$^3\Delta_{1g}$	$^4H_{7/2u}$	$^5\Phi_{1g}$	$^6\Sigma^+_{1/2u}$	$^5\Delta_{4g}$

[a] Note that the σ_u orbital refers to the highest ligand-based occupied orbital.

excited states. Experimentally, much of the spectroscopic work is based on actinyl ions in crystalline environments or in solutions. Computational modeling of the latter is discussed elsewhere in this review; as for the former, there are two well-known approaches: embedded potentials using AIMP, developed by Seijo and Barandiarán (1999), recently applied to Pa^{4+} and U^{4+} defects in chloride hosts (Barandiarn *et al.*, 2003) and to a study of Pa^{4+} defects in Cs_2ZrCl_6 (Seijo and Barandiarán, 2001), and a layered-cluster computational model developed by Winter and Pitzer (1985) and applied to actinyl systems by Matsika and Pitzer (2001). These authors have also examined the spectral intensities of actinyl ions (Matsika *et al.*, 2000).

The low-lying transitions of non-f^0 actinyl species are known to be f→f transitions, which are formally electric-dipole forbidden if the molecule has a center of symmetry based on group theory (Matsika *et al.*, 2001). By adding equatorial ligands to the actinyl complexes, the center of inversion can be removed. A study of intensities for $NpO_2^+ + nCl^-$ complexes reveals that, for the odd n cases (odd being required to remove the inversion point), the $n = 5$ case reproduces the experimental spectrum (Matsika *et al.*, 2000). Analysis of the crystal field shows that five-coordination allows for mixing between the 5fϕ and 6dδ orbitals, resulting in calculated oscillator strengths that can reproduce the experimental spectrum.

The excited states of the uranyl ion have been calculated for both gas-phase and crystalline environments by SO-MRCISD (Zhang and Pitzer, 1999; Matsika and Pitzer, 2001) and by CASPT2 [using Douglas–Kroll for scalar relativistic effects and RASSI (restricted active space state interaction) with atomic mean field integrals for spin–orbit effects] (Pierloot, 2003) methods. Both methods agree with the experimental results (Denning, 1992) as to the progression of the Ω values of the low-lying excited states: 1_g, 2_g, 3_g, 2_g, 3_g, and 4_g. The first three spin–orbit states are derived from the ΛS term $^3\Delta_g$ and the next three from $^3\Phi_g$–note that there is mixing between the two ΛS states in the $\Omega = 2_g$ and $\Omega = 3_g$ states. The latter method appears to have better quantitative agreement for transition energies (T_e) for the fluorescent transition, which is the $1_g \rightarrow 0_g^+$ transition: 20 363 cm^{-1} (for $Cs_2UO_2Cl_4^{2-}$) using

SO-MRCISD, 20 028 cm^{-1} (for the isolated $UO_2Cl_4^{2-}$ complex) using CASPT2, and 20 096 cm^{-1} from experiment.

There are far fewer experimental and computational studies for the neptunyl ions as compared to uranyl. For the NpO_2^{2+} ion, which is an f^1 system, the SO-MRCISD method gives a bond length of 1.66 Å and a symmetric stretching frequency of 1059 cm^{-1} for the gas phase (Matsika and Pitzer, 2000). All-electron scalar-relativistic DFT studies give values from 1.701 to 1.721 Å for the former and 1011 to 970 cm^{-1} for the latter, depending on the functional used (Garcia-Hernandez *et al.*, 2002). The experimental values (in solution and in the solid state) range from 1.75 (Clark, 1999; Tait, 1999) to 1.80 Å (Volkoy and Kapshuhof, 1976) and from 863 to 914 cm^{-1} (Basile *et al.*, 1974; Budantseva *et al.*, 2000). Matsika and Pitzer (2001) calculated a bond length of 1.70 Å and 950 cm^{-1} for NpO_2^{2+} doped into $Cs_2UO_2Cl_4$, values that are much closer to experiment and which emphasizes the need for comparing theory and experiment for the same phase of matter. The excited states show an interesting pattern: the ground state is an $\Omega = 5/2u$ state that is 86% $^2\Phi_{5/2u}$ and 14% $^2\Delta_{5/2u}$, the first excited state is an $\Omega = 3/2u$ that is predominantly $^2\Delta_{3/2u}$, followed by a 5/2u state (86% $^2\Delta_{5/2u}$ and 14% $^2\phi_{5/2u}$) and a 7/2u state ($^2\Phi_{7/2u}$). Although the 5fδ orbital is lower in energy than the 5fϕ orbital, the latter participates more in the ground state due to the greater spin–orbit splitting of the fϕ orbital. For NpO_2^{2+} doped into $Cs_2NpO_2Cl_4$, the calculated T_e values for the analogs of these states are 0, 1663, 5775, and 8463 cm^{-1} compared to the experimental 0, 1000, 6880, and 7990 cm^{-1} (Denning *et al.*, 1982a,b), which is good agreement for this level of theory (Matsika and Pitzer, 2001). Calculations on the energy of the first charge transfer state, a $^4H_{7/2u}$ state from a $\sigma_u^1\delta_u^1\phi_u^1$ configuration, are very dependent on the level of correlation. The experimental value is 13 264.9 cm^{-1} above the ground state, and the calculated values differ between 12 622 cm^{-1} (for 15 electrons correlated, in the isolated ion) and 18 236 cm^{-1} (for seven electrons correlated, in the crystal).

The Pu(VI) plutonyl ion, PuO_2^{2+}, is an f^2 system for which there are very little experimental data. The ground state has been determined by electron spin resonance (Bleaney, 1955) and spectroscopic methods (Denning, 1992) to be $^3H_{4g}$. Initial calculations on PuO_2^{2+} led to the proposal of a $^3\Sigma_g^-$ ground state derived from a δ_u^2 configuration (Craw *et al.*, 1995). However, as mentioned above, the δ_u and ϕ_u orbitals are weak-field-coupled and the ground state is proposed by several authors to be a ^3H_g state from a $\delta_u^1\phi_u^1$ configuration (Ismail *et al.*, 1999; Maron *et al.*, 1999; Hay *et al.*, 2000). The bond lengths for this ground state vary from 1.6770 Å using averaged quadratic coupled cluster (AQCC; Maron *et al.*, 1999) to 1.6883 Å using B3LYP (Ismail *et al.*, 1999). Examination of vertical excitations show the importance of spin–orbit splitting, as the ground state is more properly labeled as an $\Omega = 4_g$ state. The progression of states shows the interposition of states derived from different ΛS states, the total spin–orbit splitting between the $\Omega = 4_g$ and $\Omega = 6_g$ states is 7849 cm^{-1} from two-step quasi-degenerate perturbation theory calculations by Maron *et al.* (1999)

and 9613 cm^{-1} from a SO-MRCISD calculation (Blaudeau *et al.*, unpublished). Hay *et al.* (2000) also performed spin–orbit studies on plutonyl, as well as on the aqua complexes. Recently, an EPCISO calculation has been performed by Clavaguéra-Sarrio *et al.* (2004), which predicts the splitting between the $\Omega = 4_g$ and $\Omega = 6_g$ states to be 14 329 cm^{-1} (see Table 17.9 for the splittings of the ^3H_g and $^3\Sigma_g^-$ states; note that there are other states in the spectra that are not listed in the table). Their explanation of the discrepancy between this calculation and the previous ones are due to the inclusion of spin–orbit polarization effects in the EPCISO method. All of the calculations show the interspersing of the Ω states derived from different ΛS states, and thus the importance of incorporating spin–orbit methods in the calculations. A charge-transfer state, $^5\Phi_{1g}$ state from a $\sigma_u^1 \delta_u^2 \phi_u^1$ configuration, is found in the latter set of calculations at an adiabatic T_e of 20 279 cm^{-1}; the experimental value is 19 000 cm^{-1} (Jørgensen, 1970). Comparing the calculated excited states for the isoelectronic species NpO_2^+ and PuO_2^{2+}, the transition energies are lower for the monocation, e.g. the first excited state, with $\Omega = 0_g^+$, lies at 3366 cm^{-1}, compared to 3951 cm^{-1} for the plutonium species (Matsika and Pitzer, 2000; Blaudeau *et al.*, unpublished).

What is most significant for these results is that they illustrate the absolute need to include spin–orbit effects for open-shell actinide systems. Interestingly, the study by Clavaguéra-Sarrio *et al.* (2004) show that the geometries and frequencies of these states are very similar due to the atomic nature of the 5fδ and the 5fφ orbitals. Thus, single-reference methods, such as DFT, can still predict the structural properties of these molecules, although wavefunction techniques that include spin–orbit effects are required to predict the electronic spectra.

17.3.4 Other high oxidation state oxygen species

There has been much recent experimental and theoretical interest in actinide oxide species with formal metal oxidation states greater than +6. Domanov *et al.* report the formation of a volatile species they tentatively identify as a Pu(VIII) oxide, PuO_4 (Domanov *et al.*, 2002). They refer to previous work by

Table 17.9 *Vertical excitations* (cm^{-1}) *for the Ω states derived from the ^3H_g and $^3\Sigma_g^-$ states of PuO_2^{2+}, showing interspersing of the Ω states.*

Ω	Major ΛS state	CIPSO[a]	EPCISO[b]	Variational spin–orbit MRCISD[c]
6_g	^3H_g	7849	14 329	9613
1_g	$^3\Sigma_g^-$	7044	6068	5816
5_g	^3H_g	6593	8037	5158
0_g^+	$^3\Sigma_g^-$	4295	4194	3951
4_g	^3H_g	0	0	0

[a] Maron *et al.* (1999).
[b] Clavaguéra-Sarrio *et al.* (2004).
[c] Blaudeau *et al.* (unpublished).

Pershina and coworkers that had concluded that such a species in solution would be thermodynamically unstable (Ionova *et al.*, 1981; Pershina *et al.*, 1982). Pyykkö *et al.* speculated on the existence of neutral UO_6, with a formal oxidation state of $+12$ for the uranium atom (Pyykkö *et al.*, 2000). The octahedral structure of this hexaoxide is a minimum for several computational methods, including DFT and MRCI. However, it is found to have an imaginary frequency at the Dirac–Fock level. Some earlier studies included calculations on anionic U(VI) oxides, including UO_4^{2-} and UO_4^{6-}, with good agreement to experimental geometries (Ellis *et al.*, 1982; Pyykkö and Zhao, 1991).

Np(VII) species in solution have been studied by two groups. Williams *et al.* (2001) found a NpO_4^- complex, which, in agreement with DFT calculations, has D_{2d} symmetry. The deviation from planar geometry is slight (the *trans*-O–Np–O angle is 169.8°) but significant, as the planar form has an imaginary frequency. On the other hand, Bolvin *et al.* undertook calculations on the isoelectronic ions NpO_4^- and UO_4^{2-} and found the former to be square planar and the latter to be tetrahedral (Bolvin *et al.*, 2001a,b). Both studies agree that the increased contribution of the 5f orbitals destabilize the tetrahedral forms, and the different geometries for the Np and the U complexes are due to the lower energy of the 5f orbitals for Np(VII) compared to U(VI).

17.4 ACTINIDE HALIDE COMPLEXES

The actinide halides, particularly UF_6, have occupied a central role in actinide chemistry since the Manhattan Project. The high vapor pressure of UF_6 at room temperature made it the compound of choice to use in the gaseous diffusion cascade process for the separation of uranium isotopes. In addition, UF_6 is the most promising candidate for laser-induced isotope enrichment, in which the isotopic shifts of optical excitations are used to achieve isotope separation. The irradiation of UF_6 also generates the unsaturated photoproducts UF_5 and UF_4, which formally are f^1 U(V) and f^2 U(IV) complexes, respectively. Because of the dominant role these compounds play in actinide technology, the electronic structure of the ground and excited states of these highly symmetric (in the gas phase) uranium fluorides and related actinide halides has intrigued experimental and theoretical actinide chemists. In this section, some of the more recent theoretical calculations on the electronic structure of molecular actinide halides will be presented.

17.4.1 UF_6 and related complexes

The properties of actinide halides have been extensively studied both experimentally and theoretically. Much as the uranyl ion has been for oxo chemistry, the hexafluoride UF_6 has been the benchmark for theoretical studies of actinide halides over the past 25 years. Early electronic structure studies of UF_6 have

been extensively reviewed by Pepper and Bursten (1991) and included REX, nonrelativistic and relativistic MS-Xα calculations, and relativistic ECP calculations. The principal focus of these studies was on the energies of the occupied orbitals, the participation of the 5f orbitals in the bonding, and the nature of the excited states. The highest occupied valence orbitals, shown schematically in Fig. 17.11, arise naturally from the symmetry-adapted combination of six sets of fluorine 2p orbitals with admixture of 6d and 5f character on U. The two lowest
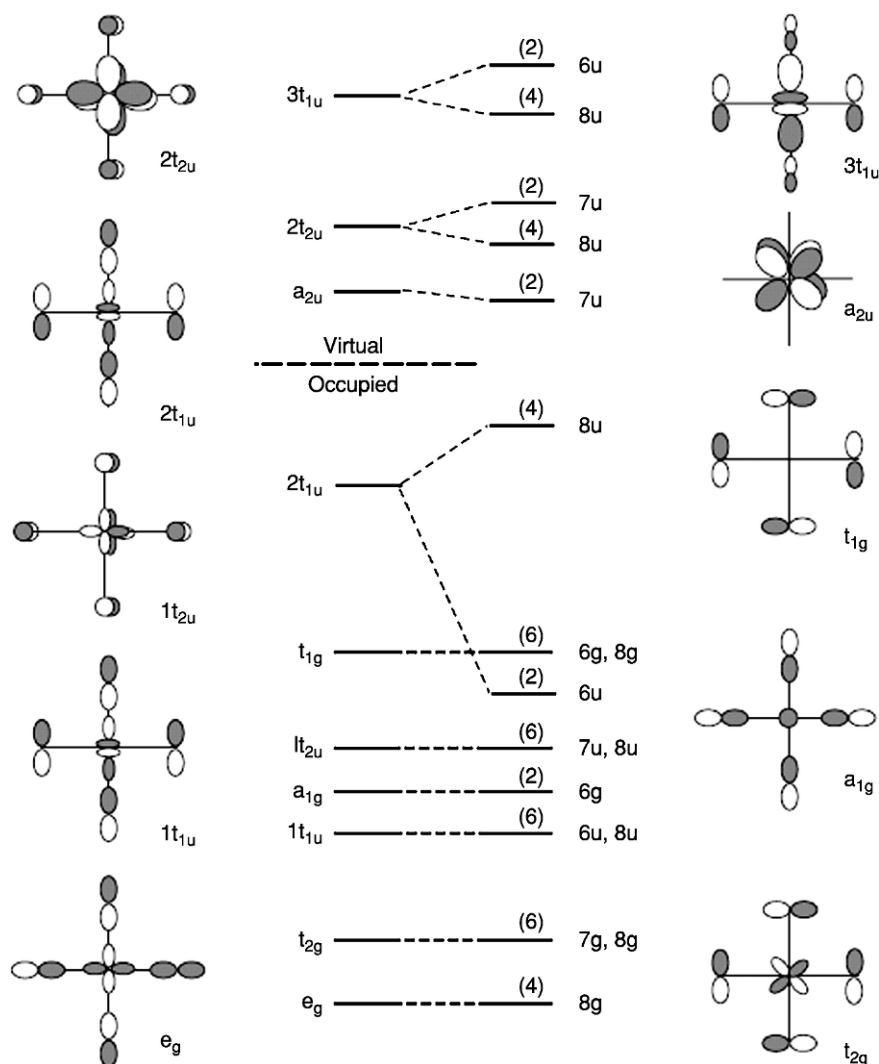
Fig. 17.11 *Schematic energy-level diagram for* UF_6 *without* (left) *and with* (right) *spin–orbit coupling* (adapted from Hay, 1983).

orbitals in this set, of e_g and t_{2g} symmetry, are of the proper symmetry for 6d mixing from the U, while the higher energy occupied orbitals of t_{1u} and t_{2u} symmetry can have 5f admixture. The lowest virtual orbitals having a_{2u}, t_{2u}, and t_{1u} symmetry essentially comprise the 5f set of orbitals. As one goes down the actinide series from UF_6, a formally $5f^0$ system, to NpF_6 ($5f^1$) and PuF_6 ($5f^2$), the additional electrons populate this manifold of orbitals that are unoccupied in UF_6. When spin–orbit effects are included, only modest splittings are observed with the exception of the highest occupied orbital ($2t_{1u}$), which, in addition to some 5f character, also has significant mixing with the occupied 6p orbital of U. This mixing leads to a large splitting ($\sim$1.2 eV) between the two spinor components γ_{8u} and γ_{6u}, where γ_{8u} and γ_{6u} are the double-group symmetries arising from the $2t_{1u}$ level when spin–orbit effects are included.

Several studies in recent years of UF_6 have been carried out using the modern approaches described in the earlier section. Hartree–Fock-based approaches include all-electron Hartree–Fock and Dirac HF calculations by de Jong and Nieuwpoort (1996) and RECP studies (Hay and Martin, 1998). Density functional approaches include DS-DV by Onoe *et al.* (1993), all-electron Douglas–Kroll local density (SVWN), and valence-electron SVWN by Garcia-Hernandez *et al.* (2002), and quasi-relativistic BLYP using ADF by Schreckenbach (2000). In Table 17.10, the energies of the occupied orbitals are shown from selected theoretical Hartree–Fock and DFT approaches. In general, we note that the predicted ionization potentials from Hartree–Fock-based methods using the orbital energies according Koopmans' theorem begin around 17 eV, which is considerably higher than the first observed peak at 14.1 eV in the photoelectron spectra. DFT methods give somewhat correspondingly lower predicted IPs ranging from 8 eV for a scalar (DV-DS), 11 eV for gradient-corrected (QR-PW91), and 12 eV for hybrid (B3LYP). Analysis of the bonding for the DHF wavefunctions showed a charge of +2.22 on U and populations 5f (1.82), 6d (1.31), 7s (0.06), while the DV-DS results showed a charge of 1.39 on U and populations 5f (2.51), 6d (1.83).

As mentioned in the earlier section on methods, one of the major developments over the past decade has been the capability to calculate geometries and frequencies using analytic derivative techniques. The geometries and frequencies of the AnF_6 hexafluorides have been determined using these capabilities, quasi-relativistic DFT by Schreckenbach *et al.* with ADF, and all-electron Douglas–Kroll DFT by Garcia-Hernandez *et al.* (Hay and Martin, 1998; Schreckenbach *et al.*, 1999; Garcia-Hernandez *et al.*, 2002) and with RECPs using Hartree–Fock and DFT approaches. The results are summarized in Table 17.11 and compared with experiment (Seip, 1965; Kimura *et al.*, 1968; McDowell *et al.*, 1974). Generally the experiences from these investigations have shown that methods that predict bond lengths accurately also typically calculate vibrational frequencies in good agreement with experiment. In this regard the LDA approaches (SWVN) either with RECPs or in all-electron DKH calculations are a good compromise in computational effort and

Table 17.10 *Calculated energy levels in UF$_6$ from various relativistic methods (in eV). Symmetries of MOs are labeled according to the O$_h$ group for the calculations without spin–orbit coupling, while the double-group labels of the O$_h^*$ group are used to label the MOs when spin–orbit effects are included.*

O$_h$ symmetry	O$_h^*$ double-group symmetry	Hartree–Fock methods			DFT methods	
		Dirac HF de Jong and Nieuwpoort (1996)	HF-SO[a] Hay (1983)	DV-DS Onoe et al. (1993)	QRPW91 Schreckenbach (2000)	B3LYP[b] Batista et al. (2004b)
2t$_{1u}$	γ8u	17.31	17.69	8.16	10.75	12.06
	γ6u	18.47	18.58	9.29		
t$_{1g}$	γ6g	18.45	18.59	9.14	11.16	12.47
	γ8g	18.51	18.49	9.12		
a$_{1g}$	γ6g	19.27	18.84	10.06	12.23	13.48
t$_{2u}$	γ8u	19.50	20.14	10.09	11.97	13.33
	γ7u	19.53	20.13	10.09		
1t$_{1u}$	γ8u	19.91	20.14	10.52	12.38	13.78
	γ6u	19.99	20.13	10.52		
t$_{2g}$	γ7g	20.65	20.67	10.99	12.71	14.17
	γ8g	20.67	20.70	10.99		
e$_g$	γ8g	21.18	20.84	11.10	13.30	14.76

[a] LC-RECP.
[b] SC-RECP.

Table 17.11 *Experimental and calculated bond lengths (Å) and vibrational frequencies (cm^{-1}) for UF$_6$.*

	Expt	VWN RECP (60e)	RECP (78e)	DK-VWN	QR-BLYP	B3LYP RECP (78e)
R(U–F)	1.996, 1.999	2.000	1.992	1.998	2.010	2.014
ν_1 (a$_{1g}$)	667	652	658	655	654	653
ν_2 (e$_g$)	534	565	552	547	541	552
ν_3 (t$_{1u}$)	626	657	630	626	618	647
ν_4 (t$_{1u}$)	186	174	175	167	185	191
ν_5 (t$_{2g}$)	200	169	147	142	183	178
ν_6 (t$_{2u}$)	143	141	110	104	141	150
|avg. error|	–	20	21	24	8	15
References	Seip (1965); Kimura et al. (1968)	Garcia-Hernandez et al. (2002)	Hay and Martin (1998)	Garcia-Hernandez et al. (2002)	Schreckenbach et al. (1999)	Hay and Martin (1998)

accuracy. Hartree–Fock approaches underestimate U–F bond lengths (and overestimate vibrational frequencies) whereas the opposite is true for gradient-corrected DFT methods. Hybrid approaches give predictions of bond lengths and frequencies similar to local density approaches.

The calculation of bond energies is a more difficult challenge for theoretical methods. Coupled with this is the relatively sparse database of thermochemical properties for actinide-containing molecules. For the uranium fluorides and chlorides, however, there is thermochemical data for most of these species, and the bond energy in UF$_6$ to form UF$_5$ + F is especially well known: 70 ± 2 kcal mol^{-1}, as measured by Hildenbrand and Lau (1991). Recently Batista *et al.* (2004b) carried out a systematic study of DFT approaches in their predictions of this bond energy. In addition the results of all-electron Douglas–Kroll–Hess results were compared using the same functionals. These results are summarized in Table 17.12. Among the main conclusions is that the SC-RECP (60-electron) potential of Küchle *et al.* is required to give agreement with the all-electron DKH results with a given functional. By contrast the results with the 78-electron LCRECP (not shown in the table) overestimates the bond energy for a particular method by 40–50 kcal mol^{-1} compared to the SC-RECP and DKH result. When corrected for zero-point and spin–orbit effects, the agreement between the hybrid DFT (B3LYP, PBE0), all-electron DKH and experiment is within the experimental uncertainties. These authors also presented an analysis of the effects on vibrational frequencies with variation of functionals and types of core potentials.

Table 17.12 *Comparison of calculated and experimental values of the bond dissociation energy of UF_6 (kcal mol^{-1}) (see Batista* et al.*, 2004b).*

Method	Scalar-relativistic		SO and ZPE corrections	
	SC-RECP	DKH	SC-RECP	DKH
HF	−5.7	7.7		
LSDA (scal)	124.4	123.7		
PBE (grad corr)	98.6	99.1		
PBE0 (hybrid)	73.8	74.4	68.3	68.9
B3LYP (hybrid)	75.0	75.8	69.6	70.4
Expt [a]			70 ± 2	

[a] Hildenbrand and Lau (1991).

The spectroscopy of the excited electronic states of UF_6 shows broad relatively unstructured bands in the ultraviolet region with the first strong peak occurring at 5.4–5.8 eV (C-band) and weaker peaks at lower energies 3.2–3.4 eV (A-band) and 3.8–4.6 eV (B-band) (Hay, 1983). Excited states were probed using earlier QR-MS (Boring and Wood, 1979), DS-DV (Koelling *et al.*, 1976), and RECP-SO (Hay, 1983) methods; there have been surprisingly few recent studies using newer techniques. Qualitatively the methods assign the weaker bands to 'u-to-u' dipole-forbidden excitations such as t_{1u} (8u) to the virtual 5f manifold while the strong C band is variously assigned to allowed 'g-to-u' excitations such as t_{1g}–t_{1u}, a_{1g}–t_{1u}, and t_{1g}–t_{2u}.

The structures and vibrational properties of UF_6, NpF_6, and PuF_6 were studied using DFT approaches with LC-RECPs (Hay and Martin, 1998) where the best agreement with available experimental data was obtained at the local density (SVWN) and hybrid (B3LYP) functionals. All-electron DKH calculations on NpF_6 had similar conclusions (Garcia-Hernandez *et al.*, 2002). The predicted Np–F bond lengths were 1.978 Å (VWN), 2.008 Å (BP), and 2.019 Å (PBEN) of which the local density VWN value agrees most closely with experiment (1.981 Å). By comparison the LC-RECP calculations with B3LYP hybrid functional and VWN functionals predicted a bond length of 2.013 and 1.998 Å, respectively.

Schreckenbach (2000) compared QR-PW91 and ECP-B3LYP calculations on the chlorine-substituted fluoride series $UF_{6-n}Cl_n$ and the related methoxide series $UF_{6-n}(OCH3)_n$. Batista *et al.* (2004a) computed the equilibrium structures of the UF_n and UCl_n series of halide species for $n = 1$–6 using ECP-B3LYP calculations. They found structures and corresponding symmetries as follows: UF_5 (C_{4v}), UF_4 (T_d), UF_3 (C_{3v}), and UF_2 (C_{2v}), as shown in Fig. 17.12, and similarly for the chloride analogs. Gagliardi *et al.* (2002) optimized the equilibrium geometries of ThX_4 (X = F, Cl, Br, and I) and computed the vibrational frequencies, of which only v_3 and v_4 had been measured for gas-phase ThF_4 and only v_3 had been measured for gas-phase $ThCl_4$. Mochizuki and Tatewaki (2003)

have reported DHF studies on CmF_n ($n = 1$–4). The bonding was found to be largely ionic in character, with some donation from the F 2p to the Cm 6d orbitals.

The electronic structure of the $5f^1$ actinide hexahalide complexes PaX_6^{2-} (X = F, Cl, Br, I), UX_6^- (X = F, Cl, Br), and NpF_6 were studied using relativistic DV-Xα approach (Kaltsoyannis and Bursten, 1995). Increased 5f participation was found in going from Pa to U to Np while the metal character remained relatively unchanged as one proceeds from F down to I. Electronic transition energies were calculated using the Slater's transition state method (Slater, 1974).

17.4.2 Actinide oxyhalides

Complexes containing halides and the actinyl AnO_2^{2+} unit represent another interesting class of species. The properties of uranyl halide species $[UO_2X_4]^{2-}$ are known in solid state structures for the chlorides but there are no known structures for the fluorides. While $[UO_2F_n]^{2-n}$ species exist in solution for $n = 0$–5, the solid state fluoride structures include dimers, neutral UO_2F_2 with six equatorial fluorine ligands around each U, and uranyl complexes with five or six equatorial F or H_2O ligands. In Table 17.13, the results of calculations on $[UO_2F_4]^{2-}$ and $[UO_2Cl_4]^{2-}$ are shown along with experimental values for various crystal structures of the chloride complexes. The bonding is analogous to the tetrahydroxide species discussed above except that the halides are much poorer π-donors than hydroxide ligands. The computational studies to date have focused primarily on the structures, vibrational frequencies, and to some extent on the thermodynamics with regard to overall stability with less emphasis on the nature of the bonding.

Recently, Straka *et al.* (2001) have examined all possible $[UO_2F_n]^{q+}$ species with f^0 configuration using DFT approaches. These include the known UO_2F_2 species and other reactive forms, some of which have been detected in mass spectra and matrix isolation studies. Some of these predictions are also given in Table 17.13. In addition, they examined other actinides from Pa through Am with f^0 configurations where the trends in bond lengths as a function of the actinide and the coordination number were examined (Fig. 17.13). Most recently, Straka (2005) has used DHF calculations to explore the bonding in later actinide AnO_2F_4 (An = Pu, Cm, Cf, Fm) complexes. These calculations suggest that the Pu and Cm species have D_{4h} symmetry and are stable with respect to decomposition to the elements. Infante and Visscher (2004a) investigated solvated forms of $[UO_2F_4]^{2-}$ complexes and especially on the relative stability of one vs two aqua equatorial groups in the first coordination shell in a study that combined quantum and classical (QM/MM) methods. In a related study, Wang and Pitzer (2001) studied the various structures arising from $UO_2F_2(H_2O)_n$, for $n = 2$–4 and the results for $n = 2$ are shown in Table 17.13. The possibilities of bonding in the series UF_4X_2 for a variety of pseudohalide ligands

Table 17.13 *Calculated structures of $[UO_2X_n]^q$ species.*

Species/Method	$R(U\text{–}O)$, Å	$R(U\text{–}X)$, Å	$\angle O\text{–}U\text{–}O$ (°)	$\angle X\text{–}U\text{–}X$ (°)	References
$[UO_2F_4]^{2-}$					
QR-BLYP	1.847	2.205	180	180	Schreckenbach et al. (1999)
RECP-B3LYP	1.823	2.259			Schreckenbach et al. (1999)
RECP B3LYP	1.819	2.233			Straka et al. (2001)
RECP MP2	1.839	2.223			Straka et al. (2001)
$[UO_2Cl_4]^{2-}$					
QR-BLYP	1.780	2.784	180	180	Schreckenbach et al. (1999)
RECP-B3LYP	1.799	2.730			Schreckenbach et al. (1999)
Expt (var.cryst.)	1.72–1.81	2.64–2.71			Schreckenbach et al. (1999)
$UO_2F_3^-$					
B3LYP RECP	1.790	2.161	180	120	Straka et al. (2001)
MP2 RECP	1.811	2.156			Straka et al. (2001)
UO_2F_2					
B3LYP RECP	1.768	2.075	168	114	Straka et al. (2001)
MP2 RECP	1.794	2.070	169	112	Straka et al. (2001)
UO_2F^+					
B3LYP RECP	1.731	2.000	120		Straka et al. (2001)
MP2 RECP	1.760	1.996	124		Straka et al. (2001)
$UO_2F_2(H_2O)_2$					
Cis LDA RECP	1.795	2.082	167	108	Wang and Pitzer (2001)
Trans LDA RECP	1.791	2.066	177	180	Wang and Pitzer (2001)
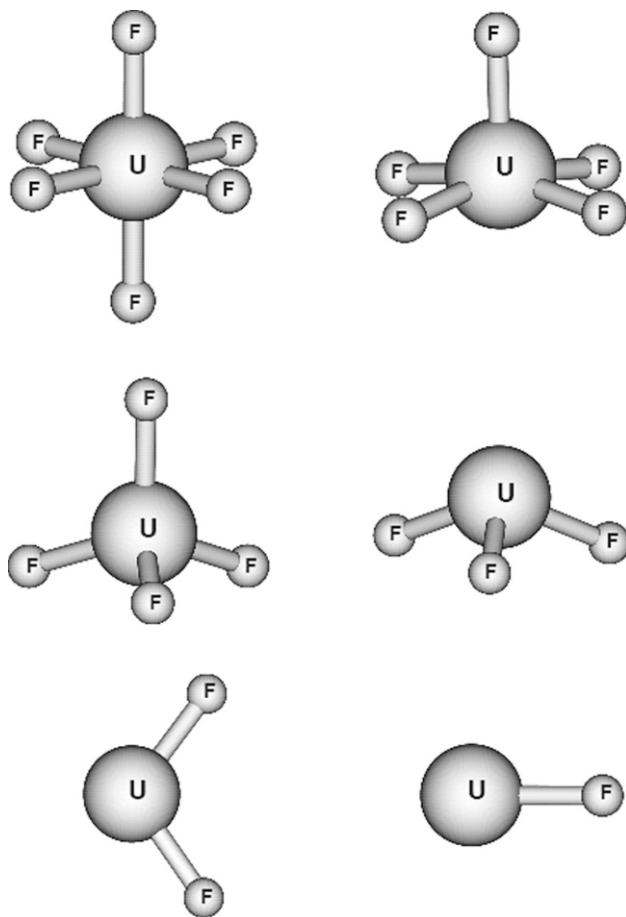
Fig. 17.12 *Calculated structures of UF$_n$ (n = 1–6) species (adapted from Batista et al., 2004a).*

X (H,Cl, CN, etc.) were probed by Straka *et al.* (2003) by computing the structures, frequencies, and thermochemistry with SC RECP calculations with the B3LYP functional. By examining substitution energies of 2X for 2F in UF$_6$, they were able to gauge relative stabilities. While none of the complexes was more stable than UF$_6$, they found relative stabilities NCO < Cl < NC < NCS < CN < OCN < SCN and related these trends to the poorer π-accepting ability of CN, for example, relative to NC and other ligands.

   Kovács *et al.* (2004) used the ZORA approach to determine the structures, vibrational analyses, and bonding of UX$_6$ and UO$_2$X$_2$ (X = F, Cl, Br, I) molecules. The UX$_6$ complexes maintained O$_h$ symmetry, while the UO$_2$X$_2$ complexes, which have C$_{2v}$ symmetry, showed structural variations with the heavier halides, with the O=U=O and X–U–X bond angles decreasing as the
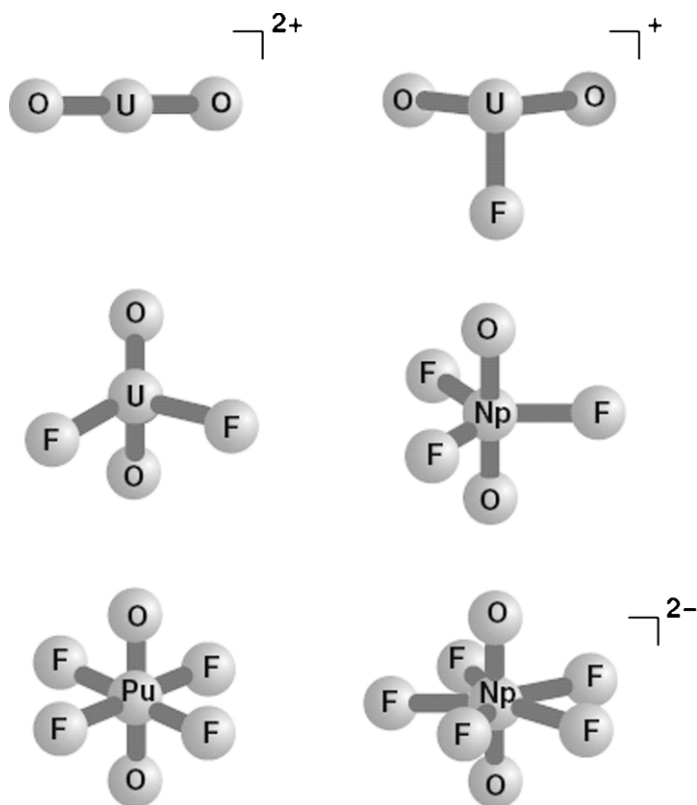
Fig. 17.13 *Calculated structures of* AnO_2F_n *(n = 1–5) species (adapted from Straka et al., 2001).*

halide ligands get heavier. For example, the X–U–X angle decreases from 110.6° for UO_2F_2 to 97.5° for UO_2I_2. They report the uranium 5f plays a predominant role in the orbital interactions, with increased contribution from the 6d in the heavier halide complexes.

17.5   ACTINIDE ORGANOMETALLICS

The growth in actinide chemistry following the Manhattan Project coincided with the birth of modern organometallic chemistry that followed the discovery of ferrocene in the early 1950s. It is therefore not surprising that actinide organometallic chemistry has developed into a thriving field. The growth in the chemistry and spectroscopy of actinide organometallics has been nicely reviewed in a series of articles by Marks (1976, 1979, 1982) and in Chapters 25 and 26. The study of organoactinide compounds benefits from some of the typical advantages of organometallic chemistry, including the use

of weakly coordinating nonaqueous solvents, the intrinsically molecular nature of organometallic compounds, and the well-developed arsenal of spectroscopic probes developed for organometallic systems. In this section, we will discuss theoretical aspects of the electronic structure of the major classes of organoactinide complexes, with an emphasis on systems in which an actinide atom is bonded to two or more cyclic hydrocarbyl ligands.

17.5.1 Actinocenes

The history of the actinocenes, $An(COT)_2$ ($COT = \eta^8$-C_8H_8), dates back to 1963, when R.D. Fischer first predicted that uranocene would be a stable compound, i.e. the actinide analog of the prototypical d-element sandwich molecule ferrocene (Fischer, 1963). Five years later, Streitwieser and Müller-Westerhoff (1968) reported the synthesis and characterization of $U(COT)_2$, thereby opening up a whole new area of organometallic chemistry. Subsequently several other actinocenes and actinocene anions were reported (Streitwieser, 1984; Streitwieser and Kinsley, 1985; Parry *et al.*, 1999), with An = Th, Pa, Np, Pu, and Am. Much of the chemistry of actinocenes has been the subject of recent reviews (see, for example, Roesky, 2001; Seyferth, 2004) and is detailed in Chapter 25.

The actinocenes have proved an irresistible challenge for many theoretical groups, due partly to the high molecular symmetry (which allows the relative roles of the 6d and 5f orbitals of the metal to be differentiated) and to the fact that $M(COT)_2$ compounds occur only in the f-block. These researchers have employed many different computational techniques, ranging from relativistic EHMO theory (Pyykkö and Lohr, 1981), to intermediate neglect of differential overlap (INDO; Cory *et al.*, 1994), to more sophisticated *ab initio* methods (Chang and Pitzer, 1989; Chang *et al.*, 1994; Dolg *et al.*, 1995; Liu *et al.*, 1997), as well as density functional approaches (Rösch and Streitwieser, 1983; Boerrigter *et al.*, 1988; Kaltsoyannis and Bursten, 1997; Li and Bursten, 1998). In this section, we shall review the issues that have been addressed by these studies, and summarize the key conclusions.

(a) Geometric structures of the actinocenes

The crystal structures of $Th(COT)_2$ and $U(COT)_2$ were reported in 1972 by Avdeef *et al.* (1972). Both molecules were found to have planar and parallel carbocyclic rings, sandwiching the metal center in an eclipsed (D_{8h}) orientation. It has been common practice for theoretical studies to assume the crystallographic geometry (e.g. Pyykkö and Lohr, 1981; Chang and Pitzer, 1989; Kaltsoyannis and Bursten, 1997), and there have been very few attempts to calculate the geometry of actinocenes. Most of these have focussed on optimizing the metal–ring distance while retaining both D_{8h} symmetry and planar rings. The results are summarized in Table 17.14, from which it can be seen that the metal–ring distance is generally overestimated.

Table 17.14 *Optimized metal–ring centroid distances (Å) in $An(COT)_2$ (M = Th to Pu).*

Metal	Method				
	HFS[a]	MP2[b]	MCSCF[c]	PW91[d]	Expt.[e]
Th	2.08	1.998			2.004
Pa	2.02			1.975	
U	1.98		2.047		1.923
Np	1.97				
Pu	1.96				

[a] Boerrigter *et al.* (1988).
[b] Dolg *et al.* (1995).
[c] Liu *et al.* (1997).
[d] Li and Bursten (1998).
[e] Avdeef *et al.* (1972).

In 1998, Li and Bursten reported fully optimized geometries for $Pa(COT)_2$ using relativistic DFT with a variety of different functionals (Li and Bursten, 1998). They found that the D_{8h} and D_{8d} (staggered) structures were essentially isoenergetic (providing some late-in-the-day computational justification of the ubiquitous assumption of D_{8h} symmetry in previous theoretical studies), and that the PW91 functional best reproduced the average of the experimental metal–ring distances in $Th(COT)_2$ and $U(COT)_2$. They also found that the hydrogen atoms are tilted toward the metal atom by as much $9°$, suggesting that the previous universal assumption of ring planarity in $Pa(COT)_2$ in particular and actinocenes in general may be a source of error and a possible reason for discrepancies between theoretical and experimental data. A ball-and-stick representation of the optimized PW91 geometry of $Pa(COT)_2$ under the constraint of D_{8h} symmetry is shown in Fig. 17.14.

(b)   Orbital interactions in the actinocenes

In 1998, Dolg and Fulde wrote: "any discussion of atomic or molecular electronic structure in terms of orbitals and single configurations....is a simplification, which works in many but not in all cases" (Dolg and Fulde, 1998). They were writing with reference to the lanthanocenes and actinocenes, and in particular to their finding that the ground state of the 4f systems are not well represented by a single configuration, a result which they predicted to also hold for the later actinocenes. Notwithstanding these observations, we will set out the basic electronic structure of the actinocenes within the usual orbital approach. This brings with it the conceptual advantages of the independent-particle description, and serves as a good starting point for discussion of the effects of relativity, the calculation of excited-state properties, and the introduction of multi-configurational character to the molecular wavefunctions.
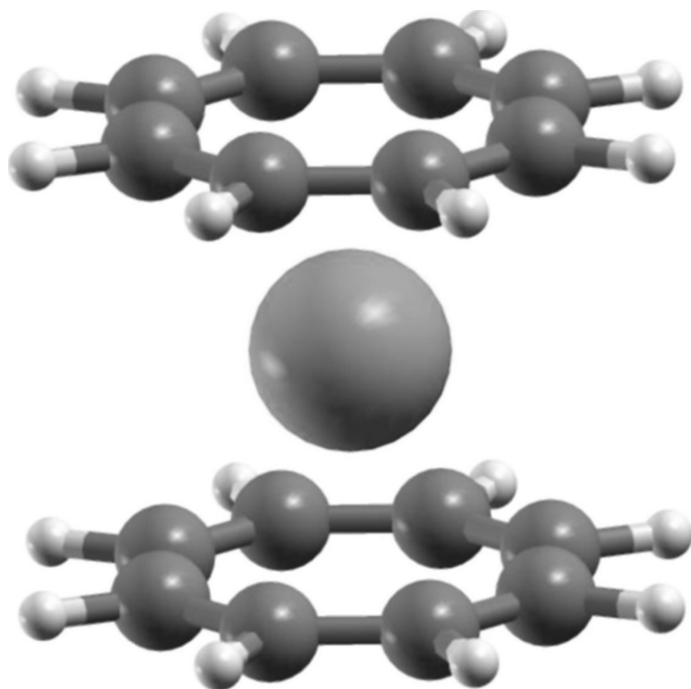
Fig. 17.14 *Representation of the optimized structure of protactinocene, Pa(η^8-C$_8$H$_8$)$_2$, from scalar-relativistic DFT (PW91) calculations (adapted from Li and Bursten, 1998).*

The generally accepted orbital interaction diagram for the actinocenes is given in Fig. 17.15. The eight-carbon $2p\pi$ atomic orbitals of a D_{8h} C_8H_8 ring give rise to eight molecular orbitals (MOs) transforming as a_{2u}, e_{1g}, e_{2u}, e_{3g}, and b_{1u} in order of increasing energy. These orbitals are commonly denoted π_n ($n = 0$–4), where n is the number of vertical nodes (i.e. nodes perpendicular to the plane of the ring). In a ligand field of two COT rings, these π MOs give rise to the combinations shown in the second column from the right in Fig. 17.15. The valence atomic orbitals (AOs) of the actinide elements that interact with the (COT)$_2$ ligands are primarily the 5f and the 6d. It is common practice to take advantage of the pseudoaxial nature of the D_{8h} (COT)$_2$ ligand-field and label the metal orbitals as σ, π, δ, and ϕ, corresponding to $m_l = 0, \pm 1, \pm 2$, or ± 3 respectively. In the absence of spin–orbit coupling, the 5f orbitals split in the (COT)$_2$ ligand field as e_{3u} (fϕ) $\approx$ a_{2u} (fσ) $<$ e_{1u} (fπ) $\ll$ e_{2u} (fδ), the strong destabilization of the latter resulting from their significant interaction with the highest occupied e_{2u} ring pπ levels. The 6d orbitals split as a_{1g} (dσ) $\ll$ e_{2g} (dδ) $<$ e_{1g} (dπ), and the total d-orbital splitting is larger than for the 5f on account of their greater radial extension and hence greater interaction with the ligand field.
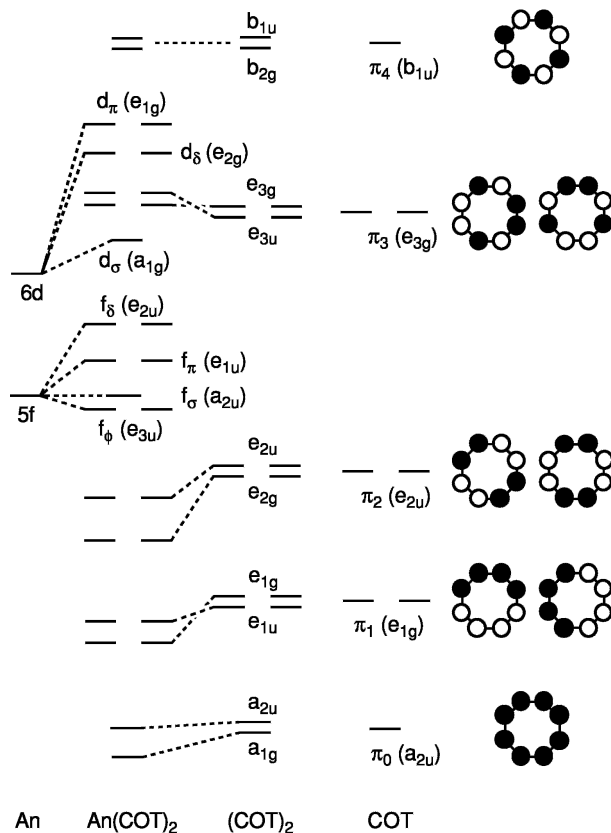
Fig. 17.15 *Principal interactions between the orbitals of two COT rings and the valence orbitals of an actinide atom in forming the frontier MOs of the actinocenes under D_{8h} single-group symmetry (reproduced from Li and Bursten, 1998).*

(c)   Electronic configurations, ground states, and oxidation states in the actinocenes

In their 1994 INDO study, Cory *et al.* found that the highest occupied MO (HOMO) of Th(COT)$_2$ was the ring e_{2u} orbital, and that the metal-based levels were empty (Cory *et al.*, 1994). Moving across the actinides increased the number of metal electrons from 1 for Pa(COT)$_2$ to 4 for plutonocene, and it was found that all of these electrons occupy the e_{3u} (fϕ) orbitals. These findings are consistent with the experimental observations that Th(COT)$_2$ and Pu(COT)$_2$ are diamagnetic (although the magnetic moment of Pu(COT)$_2$ exhibits unusual temperature dependence), that Pa(COT)$_2$ and Np(COT)$_2$ have doublet ground states, and that uranocene has a triplet ground state (Karraker *et al.*, 1970; Hayes and Edelstein, 1972; Karraker, 1973). Chang *et al.* (1994) also

concluded that $An(COT)_2$ (An = Pa to Pu) have the $5f^n$ (n = 1–4) ground state configuration.

Earlier *ab initio* (SOCI) work by Chang and Pitzer (1989) on $U(COT)_2$ also concluded that it has an f^2 ground state configuration. These authors reported that the best simple description of the ground state was weak-field $L–S$ $^3H_4$, with $|M_j| = 3$, where M_j is the magnetic quantum number. In the notation of the D^*_{8h} double point group, the spin–orbit-coupled ground state is E_{3g} (see below for more on spin–orbit coupling). Several configurations were found to contribute to this state, the leading one being $\pi(e_{2u})^4 e_{3u}^1 e_{1u}^1$, i.e. $f\phi^1 f\pi^1$. Several years later, Liu *et al.* (1997) also found that the ground configuration of uranocene is $5f^2$, although they calculated that the leading configuration to the ground state is $f\phi^1 f\sigma^1$.

In 1995 Dolg *et al.* used the MRCI and averaged coupled-pair functional (ACPF) *ab initio* methods to study $Th(COT)_2$ and its lanthanide analog $Ce(COT)_2$. They concluded that the ground state of $Th(COT)_2$ is $^1A_{1g}$, and that the dominant configuration to this state is $\pi(e_{2u})^4 f^0 d^0$, i.e. that there are no metal-based valence electrons (Dolg *et al.*, 1995). $Ce(COT)_2$ was also found to have a $^1A_{1g}$ ground state, but the $\pi(e_{2u})^4$ configuration was in this case found to contribute only $\approx 20\%$ to the ground state. The dominant contribution ($\approx 80\%$) comes from the $\pi(e_{2u})^3 f\delta^1$ configuration, in which the electrons are antiferromagnetically coupled in two MOs, and the direct product of their spatial symmetries is A_{1g}. Thus $Ce(COT)_2$ is best described as having a single metal-localized valence f-electron, i.e. as a Ce(III) compound containing two formally $COT^{1.5-}$ rings. This view, which was soon verified experimentally by Edelstein *et al.* (1996), is by contrast to that held historically, which saw both $Ce(COT)_2$ and $Th(COT)_2$ as M(IV) species.

Dolg and Fulde (1998) subsequently concluded that all of the lanthanocenes are Ln(III) compounds, and predicted that the later actinocenes should also be viewed in this way. By contrast, the early actinocenes are best described in the traditional manner, i.e. as An(IV) compounds with two COT^{2-} rings and a single dominant $\pi(e_{2u})^4 f^n$ configuration. It is perhaps rather fortunate then that the only actinocenes to have been studied by single-reference density functional methods are $Th(COT)_2$–$Pu(COT)_2$, precisely those that *ab initio* calculations suggest should be amenable to study by single-reference techniques.

Of those density functional studies, the most comprehensive remains the 1988 contribution from Boerrigter *et al.* (1988), which surveyed the first five actinocenes from $Th(COT)_2$ to $Pu(COT)_2$ using both nonrelativistic and relativistic HFS techniques. Their nonrelativistic calculations concluded that $Th(COT)_2$–$Pu(COT)_2$ have between 0 and 4 5f electrons, respectively, and that these electrons occupy the $f\phi$, $f\sigma$, and $f\pi$ levels equally. The relativistic spin–orbit-coupled calculations also find 0–4 5f electrons, occupying closely spaced $e_{5/2u}$ and $e_{1/2u}$ levels (D^*_{8h}). They concluded that both of these spin–orbit-coupled levels are composed primarily of atomic $5f_{5/2}$ character, and may be traced mainly to the $f\phi$ nonrelativistic molecular orbital. Two subsequent DFT studies of $Pa(COT)_2$

(Kaltsoyannis and Bursten, 1997; Li and Bursten, 1998) concur with the findings of Boerrigter *et al.*

(d) Metal–ring covalency

One of the most appealing features of actinocene electronic structure is the way in which the D_{8h} point group separates the metal's d- and f-orbitals into irreducible representations of g and u parity, thus preventing them from mixing with the same $(COT)_2^{4-}$ levels. There have been many estimates of covalency in the actinocenes, and in particular much has been made of its separation into d and f contributions. The metal content of the ring-based e_{2g} and e_{2u} levels has been a popular method for estimating the extent of covalency, and Table 17.15 collects the data from a range of studies. Uranocene is clearly the molecule for which most data are available, and it is notable that, while the exact numbers differ from study to study, all of the calculations show significant metal character to the e_{2g} and e_{2u} levels (or their spin–orbit-coupled equivalents). Boerrigter *et al.* (1988) find that the relative roles of the 6d and 5f orbitals alter from Th $(COT)_2$ to $Pu(COT)_2$, with the extent of 5f covalency significantly increasing with increasing actinide atomic number.

Other estimates of covalency have been made that do not explicitly involve the e_{2u}/e_{2g} composition. Chang and Pitzer (1989) calculated a metal charge of +0.98 in $U(COT)_2$, much reduced from the formal value of +4. They concluded

Table 17.15 *Metal 5f (e_{2u}) and 6d (e_{2g}) content (%) of the $(COT)_2$-based e_{2u} and e_{2g} molecular orbitals of $An(COT)_2$ (M = Th to Pu).*

| Metal | Orbital | Method | | | | |
		REX[a]	QR-SW-Xα[b]	HFS[c,f]	DV-Xα[d,f]	MRCI[e]
Th	e_{2u}			12		
	e_{2g}			19		
Pa	e_{2u}			16	17	
	e_{2g}			18	20	
U	e_{2u}	12	33	22		15
	e_{2g}	11	20	16		17
Np	e_{2u}			27		
	e_{2g}			15		
Pu	e_{2u}			33		
	e_{2g}			15		

[a] Pyykkö and Lohr (1981).
[b] Rösch and Streitweiser (1983).
[c] Boerrigter *et al.* (1988).
[d] Kaltsoyannis and Bursten (1997).
[e] Liu *et al.* (1997).
[f] Average of $f_{7/2}/f_{5/2}$ and $d_{5/2}/d_{3/2}$ contributions to spin–orbit-coupled components of e_{2u} and e_{2g}.

that there is extensive metal–ring covalency, and that this is mainly through the uranium 6d AOs as the total $(COT)_2^{4-} \rightarrow U^{4+}$ 6d donation is 1.98 electrons, significantly larger than the 0.5 electrons donated into the metal 5f orbitals. Dolg *et al.* (1995) found that the bonding in thoracene is also significantly covalent and is mainly 6d-based, using analysis methods similar to those employed by Chang and Pitzer. Cory *et al.* (1994) used the metal fδ and dδ populations to also conclude that 6d covalency is larger than 5f, although the fδ population increases from $Th(COT)_2$ to $Pu(COT)_2$ while the dδ remains approximately constant.

The consensus from all of these studies is that there is significant mixing of the metal AOs with the highest occupied pπ MOs of the COT rings and that, for the early actinocenes at least, 6d covalency is larger than that involving the 5f orbitals. Experimental estimates of covalency are not easy to obtain, and hence it can be difficult to assess the reliability of the computational results. However, a very important experimental contribution in this area came in 1989 from Brennan *et al.* (1989), who studied $U(COT)_2$ by variable photon energy photoelectron spectroscopy. They concluded that (a) the second and third ionization bands are due unequivocally to the ring e_{2u}^{-1} and e_{2g}^{-1} ionizations, respectively (providing good evidence for the MO ordering shown in Fig. 17.15), (b) there is direct evidence for significant U 5f orbital character to the ring e_{2u}-based MOs, and (c) that the position of the e_{2g} ionization band at higher energy than the e_{2u} band is strong indirect evidence for an even larger U 6d contribution to these MOs.

(e) Electronic transitions in the actinocenes

Thus far we have not considered in detail the effects of relativity on actinocene electronic structure. However, almost all of the data discussed to this point are taken from calculations in which some or all of the so-called scalar-relativistic corrections – e.g. the Darwin and mass–velocity terms – have been incorporated in one way or another. Such an approach is in many cases adequate, but is not really satisfactory when attempting to understand the electronic transitions of actinocenes, especially where comparisons with experiment are sought. This type of investigation requires that spin–orbit coupling effects are also taken into account. Indeed, non-spin–orbit-coupled calculations typically give poor agreement with experiment when excited states are involved.

(i) Pa(COT)₂

Barring f^0 thoracene, $Pa(COT)_2$, is in principle the simplest actinocene in terms of its electronic transitions, as it has only one metal-localized valence f-electron. It has proved a fertile testing ground for both *ab initio* (Chang *et al.*, 1994) and density functional studies (Kaltsoyannis and Bursten, 1997; Li and Bursten, 1998). The effect of spin–orbit coupling on a free f^1 atom or ion is to split the
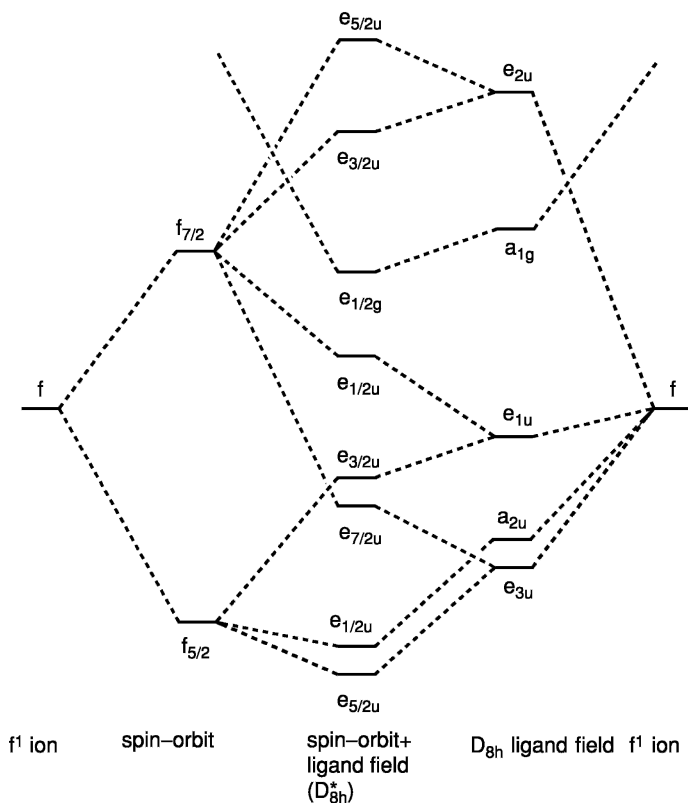
Fig. 17.16 *Correlation of the orbitals of an f1 Pa^{4+} ion split by spin–orbit coupling with the spin–orbit-coupled orbitals of Pa(COT)$_2$ under the D$^*_{8h}$ double group (adapted from Li and Bursten, 1998).*

f-orbitals into a lower energy f$_{5/2}$ level and a higher energy f$_{7/2}$ level, which are respectively six- and eight-fold spin–orbit degenerate. This splitting is indicated on the left-hand side of Fig. 17.16, which is a correlation diagram showing the effects of spin–orbit coupling and the D$_{8h}$ ligand field on an f^1 ion in a (COT)$_2^{4-}$ environment. In the absence of spin–orbit coupling but in the D$_{8h}$ field, the f-orbitals are split as shown on the right-hand side of the figure. This f-orbital ordering is as presented in Fig. 17.15.

One of the main reasons for the complexity of actinide molecular electronic spectra is that both the effects of the ligand field and spin–orbit coupling must be taken into account. This is in contrast to the situation in the d-block, where ligand-field effects dominate, and to the lanthanides where spin–orbit coupling is the principal perturbation. The central column of Fig. 17.16 shows the combined effects of spin–orbit coupling and the D$_{8h}$ ligand field on the f^1 ion.

All of the spin–orbitals now carry one of the labels of the D_{8h}^* double group, reflecting the fact that they are now properly characterized by non-integral total angular momentum, (i.e. spin + orbital). These arguments have been developed in greater detail (Kaltsoyannis and Bursten, 1997; Li and Bursten, 1998).

In Fig. 17.15, the metal d-based MOs are shown as being less stable than those arising from the 5f orbitals. While this is certainly the case for uranium/ neptunium onwards, for the very early actinides the $6d\sigma$ level is comparable in energy with the 5f manifold. Indeed, the DFT calculations of Boerrigter *et al.* (1988) predict the lowest unoccupied molecular orbital (LUMO) of $Th(COT)_2$ to be the $6d\sigma$ orbital, while for $Pa(COT)_2$ this level lies in amongst the f-manifold. This result has been confirmed by other studies (Chang *et al.*, 1994; Kaltsoyannis and Bursten, 1997; Li and Bursten, 1998) and is taken into account on Fig. 17.16 by the presence of the $e_{1/2g}$ (a_{1g}) orbital. It might be expected that the presence of a low-lying d-based orbital would have a significant effect on calculations of the electronic transitions of $Pa(COT)_2$, and this has indeed been found to be the case.

Although the optical spectrum of $Pa(COT)_2$ has not been reported, limited data are available for the octamethyl derivative $Pa(TMCOT)_2$ (Solar *et al.*, 1980). The latter has an absorption maximum at 380 nm, with a low-energy shoulder at 490 nm. Based on comparison with the bathochromic shifts induced by the replacement of COT by TMCOT in other actinocenes, Solar *et al.* estimated that the absorption maximum in $Pa(COT)_2$ would occur at ca. 365 nm. There have been three attempts to calculate the electronic transitions of $Pa(COT)_2$, and three different assignments of the proposed 365 nm band. All of the f $\rightarrow$ f and many of the f $\rightarrow$ d transitions are formally forbidden, and Chang *et al.* (1994) concluded that the 365 nm peak arises from a ligand-to-metal charge transfer (LMCT) transition from the highest occupied ring π_2 levels into the $e_{1/2g}$ (dσ) orbital, calculated at 341 nm. Later, Kaltsoyannis and Bursten (1997) suggested that the band arises from both f $\rightarrow$ π_3 metal-to-ligand charge transfer (MLCT) and π_2 $\rightarrow$ f LMCT transitions at 351 and 360 nm, respectively. Most recently, Li and Bursten (1998) concluded that the band is due to a 368 nm ligand-field transition from the (predominantly fϕ) $e_{5/2u}$ HOMO to one of the spin–orbit-coupled components of the dδ levels. This latter study, which is the most complete and convincing, also concluded that the experimental low-energy shoulder is due to the π_2 $\rightarrow$ dσ transition.

(ii) *Th(COT)₂ and U(COT)₂*

As noted above, $Th(COT)_2$ has no metal-localized valence electrons. Experimentally it has a strong absorption at ca. 450 nm (Streitwieser, 1979), which Rösch and Streitwieser assigned to an LMCT π_2 $\rightarrow$ fϕ transition (Rösch and Streitwieser, 1983). Subsequent calculations by Dolg *et al.* (1995) placed this transition at 230 nm, and assigned the experimental peak to an LMCT π_2 $\rightarrow$ dσ transition. This ties in well with the DFT calculations of Boerrigter *et al.* (1988)

which, as we saw previously, predict the LUMO of Th(COT)$_2$ to be the 6dσ level.

The actinocene for which the most extensive experimental transition energy data are available is U(COT)$_2$ (Dallinger *et al.*, 1978; Amberger, 1983). These electronic transitions have been studied computationally by two groups using SOCI *ab initio* techniques (Chang and Pitzer, 1989; Chang *et al.*, 1994; Liu *et al.*, 1997). The experimental and theoretical (allowed transitions only) data are collected in Table 17.16, from which it may be seen that the two studies concur as to the assignment of the lowest energy transition, but differ over the nature of the experimental transition at 0.290 eV. It should be noted that U(COT)$_2$ is computationally significantly more difficult to handle than either Th(COT)$_2$ or Pa(COT)$_2$, owing to the presence of two 5f-based electrons and their significant mutual repulsion. Such difficulties manifest themselves in the discrepancies between experimental and theoretical data.

17.5.2 Actinide–cyclopentadienyl complexes

It is now 50 years since the discovery of the first organometallic sandwich molecule, ferrocene [FeCp$_2$] (Cp = η^5-C$_5$H$_5$) (Wilkinson *et al.*, 1952; Wilkinson, 1975), and in the intervening period, the cyclopentadienyl ligand has become almost synonymous with organometallic chemistry. Indeed, the first organoactinide compound to be reported was the Cp derivative [UCp$_3$Cl] (Reynolds and Wilkinson, 1956), and there have been hundreds more subsequently. As with the actinocenes, Cp–actinide systems have been a target of many theoretical studies, and those up to 1990 have been reviewed by Bursten and Strittmatter (1991). In this section, we will summarize these efforts and set out their key conclusions.

Several structural motifs are commonly observed for Cp–actinide complexes. [AnCp$_4$] systems feature four η^5-bonded Cp rings, and are without parallel in transition metal chemistry. 'Base-free' tris-Cp complexes and their pseudotetrahedral derivatives [AnCp$_3$X] (X = wide variety of ligands) are common and

Table 17.16 *Experimental and calculated transition energies* (eV) *in U(COT)$_2$.*

Experimental energy[a]	Calculated energy[b]	Assignment[b]	Calculated energy[c]	Assignment[c]
0.058	0.109	E$_{3g}$ → E$_{2g}$ f^2 → f^2	0.062	E$_{3g}$ → E$_{2g}$ f^2 → f^2
0.290	0.360, 0.364	E$_{3g}$ → B$_{2g}$, B$_{1g}$ f^2 → f^2	0.411	E$_{3g}$ → E$_{1g}$ f^2 → f^2
1.881	2.728	E$_{2g}$ → E$_{2u}$ f^2 → f^{1}d^1		
1.939	2.837	E$_{3g}$ → E$_{2u}$ f^2 → f^{1}d^1		
2.017	2.905	E$_{3g}$ → E$_{3u}$ f^2 → f^{1}d^1		
	3.322	π_2 → f^{2}d^1 LMCT		

[a] Dallinger *et al.* (1978) and Streitwieser (1979).
[b] Chang and Pitzer (1989).
[c] Liu *et al.* (1997).

have been widely studied, as have the bis-Cp systems [AnCp$_2$] and [AnCp$_2$X$_2$]. The present review makes the somewhat arbitrary division of Cp–actinide chemistry into these three motifs, i.e. we group the compounds according to the number of carbocyclic rings bonded to the metal. The motifs are collected in Fig. 17.17.

(a) [AnCp$_4$] complexes

These compounds are known for Th, Pa, U, and Np, and the crystal structure of [UCp$_4$] shows it to contain four η^5-Cp ligands in a pseudotetrahedral arrangement (Burns, 1973). These systems were the subject of semiempirical and early DFT studies in the 1970s and 1980s, though they have not been subsequently probed by more modern methods. Quasi-relativistic Xα-SW (QR-Xα-SW) calculations on [ThCp$_4$] and [UCp$_4$] showed that, with the exception of a small An 7s contribution, the metal does not interact with the π_0 MOs of the Cp rings (i.e. those C 2pπ orbitals with no vertical nodes) (Bursten *et al.*, 1985). By contrast, the Cp π_1 levels interact significantly with the An, with donation into the 6d and, to a lesser extent, 5f orbitals. The 6d–Cp interaction was found to be more stabilizing than donation to the 5f levels (Bursten and Fang, 1985). The two metal-based electrons in the formally U(IV) [UCp$_4$] were found to
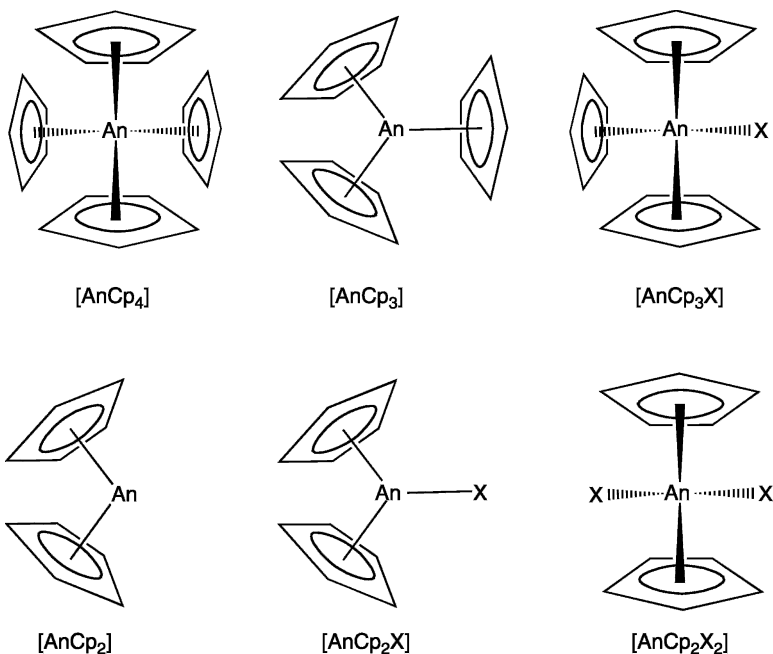
Fig. 17.17 *Structural motifs exhibited in complexes with actinide atoms and pentahapto-cyclopentadienyl ligands.*

occupy an essentially pure U 5f orbital of t_2 symmetry (T_d single-point group notation) with parallel spins.

Extended Hückel calculations on $[U(\eta^5\text{-Cp})_4]$ and $[U(\eta^5\text{-Cp})_3(\eta^1\text{-Cp})]$ probed the actinide preference for η^5 coordination (Tatsumi and Nakamura, 1984). The conclusion from these studies was that the all-η^5 system is indeed more stable than the $(\eta^5)_3/\eta^1$ arrangement, in agreement with experiment.

(b) 'Base-free' [AnCp$_3$] complexes

The [AnCp$_3$] complexes without an additional axial ligand are perhaps the most widely studied Cp–actinide system. The metal and the Cp centroids are coplanar, giving rise to a virtually D_{3h} molecular symmetry. The interactions of a Cp$_3$ ligand field with a central metal are now well established, based on the results of extended Hückel, QR-Xα-SW, and DV-Xα studies (Lauher and Hoffmann, 1976; Bursten *et al.*, 1989a; Strittmatter and Bursten, 1991; Kaltsoyannis and Bursten, 1997), and we now set out the key features. The principal metal–ring bonding occurs between the valence AOs of the central atom and the highest occupied π_1 MOs of the Cp rings ($e_1^{''}$ in the D_{5h} symmetry of a Cp ring), with a lesser interaction between the metal AOs and the Cp $\pi_0(a_2^{''})$ level (as was found for the [AnCp$_4$] systems). In a C_{3v} ligand field, the Cp π_0 orbitals give rise to $a_1 + e$ symmetry combinations, while the π_1 orbitals result in $a_1 + a_2 + 2e$ levels. Ligand–ligand interactions result in the $a_2 \pi_1$ combination being destabilized above the others. This a_2 combination is important in that its interaction (or lack thereof) with the central metal elegantly rationalizes the paucity of the [MCp$_3$] unit when M is a transition metal and the abundance of this unit for the actinides. There is no d AO that transforms as a_2 symmetry in C_{3v}. By contrast, the $f_{y(3x^2-y^2)}$ orbital can stabilize the ligand a_2 combination and provide significant metal–ligand bonding in the process.

A qualitative energy level diagram for the interaction of an actinide atom with the Cp π_1 MOs in a C_{3v} [AnCp$_3$] complex is shown in Fig. 17.18. The 5f/π_1 a_2 interaction is shown as being the most important involving the 5f orbitals; the other six 5f-based levels span a very narrow energy range, reflecting their largely actinide nature. The relative position of the 5f manifold and the 6d$_{z^2}$ level has been extensively studied, due in part to the experimental observation that $[ThCp_3^{''}](Cp_3^{''} = \eta^5 - C_5H_3(SiMe_3)_2)$ possesses a 6d^1 ground configuration (Kot *et al.*, 1988). The evidence from both Xα-SW (Bursten *et al.*, 1989a) and DV-Xα (Kaltsoyannis and Bursten, 1997) calculations is that at the start of the actinide series, the 6d$_{z^2}$ orbital lies below the 5f manifold in [AnCp$_3$] complexes. Furthermore, the d-below-f ordering is found to be a relativistic effect, as nonrelativistic DV-Xα calculations predict a 5f^1 ground configuration for [ThCp$_3$] (Kaltsoyannis and Bursten, 1997). Xα-SW studies predict that as the actinide series is crossed the 5f manifold is stabilized with respect to the 6d$_{z^2}$ level, and hence that the later [AnCp$_3$] compounds have a 5f$^n >$ ground state configuration (Bursten *et al.*, 1989a).
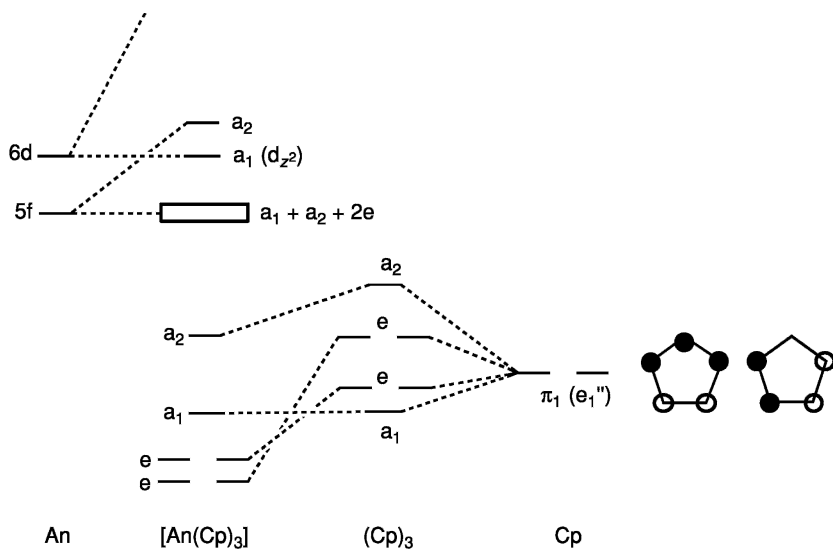
Fig. 17.18 *Qualitative energy-level diagram for the interaction of an actinide atom with the Cp π_1 MOs in a C_{3v} [AnCp$_3$] complex.*

The discrepancy between the nonrelativistic and relativistic results for the ground state configuration of [ThCp$_3$] is an excellent example of the need to incorporate relativity when calculating actinide electronic structure. More specifically, the calculated electronic absorption spectrum of $6d^1$ [ThCp$_3$] is very different from that from a $5f^1$ ground state configuration, with intense d $\rightarrow$ f transitions as opposed to weak Laporte-forbidden f $\rightarrow$ f transitions. The experimental spectrum of [ThCp$_3''$] indeed displays intense peaks, consistent with the $6d^1$ ground state configuration (Kot *et al.*, 1988).

As ever, the nature and extent of metal–ligand covalency has been the subject of extensive research and discussion (Burns and Bursten, 1989; Jensen and Bond, 2002). In particular, the relative contributions of the An 6d and 5f AOs to the two Cp π_1-based e symmetry MOs has come under scrutiny, as these are the two π_1-based MOs to which both An 6d and 5f AOs can contribute (the a_2 level can only have metal 5f character by symmetry, and the a_1 orbital is found to contain almost no metal contribution). Xα-SW calculations find that the 6dδ and 6dπ contributions to these orbitals are much larger than those of the 5f for the early An, with increasing 5f character to one of the levels (6dπ) with increasing An atomic number (Strittmatter and Bursten, 1991). The total metal involvement is in the 15–25% range, depending upon the orbital and compound in question. These results were later corroborated for [ThCp$_3$] by DV-Xα calculations (Kaltsoyannis and Bursten, 1997). The An 5f content of the a_2 level was found by Xα-SW to increase very significantly across the actinides,

to as high as 55% in [CfCp$_3$]. By contrast, the DV-Xα studies of [ThCp$_3$] find only 10% metal 5f content in this level.

(c) [AnCp$_3$X] complexes

When a fourth ligand X binds to a [AnCp$_3$] fragment, the Cp ligands pyramidalize to open up a coordination site for the X moiety. Several groups have investigated the nature of the An–X interaction, with much attention being paid to the An orbitals involved in the An–X bond. Early extended Hückel work on [UCp$_3$]$^+$ indicated that pyramidalization causes a stabilization and hybridization of the metal $6d_{z^2}$ and $7p_z$ AOs, resulting in a low-lying σ orbital that can accept charge from the X ligand (Tatsumi and Nakamura, 1984). A similar conclusion was drawn from Xα-SW calculations on [UCp$_3$] and [ThCp$_3$] (Bursten *et al.*, 1989a), although these studies suggested that the vacant hybrid is approximately isoenergetic with the 5f levels, in contrast to the extended Hückel calculations, which place the σ acceptor level well above the 5f manifold.

Xα-SW studies of the U–H bonding in [UCp$_3$H] support the results of the pyramidal base-free calculations in concluding that the U–H bond is indeed dominated by the U $6d_{z^2}$ AO (Bursten *et al.*, 1989b). Subsequent nonrelativistic DV-Xα calculations on [UCp$_3$X] (X = Me, NH$_2$, BH$_4$, NCS) suggest that the situation may be more complex, however, in that the U AO involved in the U–X σ bond depends upon the energies of the X orbitals (Gulino *et al.*, 1992). Thus, when X = NH$_2$ or NCS, the σ-bond is dominated by U $6d_{z^2}$, while for X = Me the U $5f_{z^3}$ plays a much larger role in σ-bonding. By contrast, RECP *ab initio* studies by the same workers on [AnCp$_3$Me] (An = Th, U) concluded that the An–Me σ bond is dominated by the metal $6d_{z^2}$ AO (Di Bella *et al.*, 1993).

The bonding of X to the An center is not necessarily restricted to purely σ interactions; π-donor and even π-acceptor ligands can also bind to the [AnCp$_3$] moiety as well. Quasi-relativistic Xα-SW calculations on [UCp$_3$CO], a model for the experimentally characterized [UC$_3^\dagger$CO](Cp† = η^5-C$_5$H$_4$SiMe$_3$) (Brennan *et al.*, 1986), found a U–C σ-bond similar in nature to those discussed above (i.e. a CO $5\sigma \rightarrow$ U $6d_{z^2}$ donation) (Bursten and Strittmatter, 1987). However, in addition, there is significant π-backbonding from the U $5f\pi$ AOs into the vacant CO π^* orbitals. Thus, the overall U–CO interaction is an excellent example of the classic Dewar–Chatt–Duncanson model of synergic bonding, more usually associated with transition metal carbonyl complexes. Furthermore, the computational evidence for U $\rightarrow$ CO π-backbonding provides solid rationalization of the experimental observation that the CO stretching vibration in [UCp$_3^\dagger$CO] is about 170 cm^{-1} lower than in free CO. Since that initial synthesis, a number of other UCp$_3$CO complexes with different substituents on the Cp rings have been synthesized and characterized (Parry *et al.*, 1995; Del Mar Conejo *et al.*, 1999; Evans *et al.*, 2003). The observed C–O stretching frequencies of these complexes show some surprising trends that will stimulate further theoretical studies (Kaltsoyannis, 2003). Recent experimental and theoretical studies

by Andersen, Eisenstein and coworkers have addressed the bonding of CO to organolanthanide complexes of the type Cp_2^*Ln, and propose significant differences between the binding of CO to 4f metals relative to 5f metals (Maron *et al.*, 2002).

Compounds in which there is π donation from ligand to metal have also been investigated computationally. Cramer *et al.* (1988) conducted extended Hückel calculations on N-based π-donor [UCp_3X] complexes where X = NH_2, NPH_3, $NHCHCHPH_3$, and NPh. They concluded that, for the latter three complexes, there is significant N $2p\pi \rightarrow U$ π donation, mainly into the U 6dπ levels. Subsequent DV-Xα calculations on similar complexes where X = NH_2 and NCS also found π character to the U–N bond, although they indicated that the donation is from N $2p\pi \rightarrow U$ 5fπ (Gulino *et al.*, 1992). Interestingly, this study found that alterations in X produced almost no change in the metal's charge ($+1.8 \pm 0.06$) or configuration ($5f^{3.4}6d^{0.7}$). The conclusion was that this electronic 'buffering' of the U is facilitated by changes in the U–Cp bonding; as the donation from X, and hence U–X covalency, increases, the U–Cp bonding becomes more ionic.

In addition to N-donor ligands, complexes containing alkoxide groups have also been studied, using extended Hückel (Gulino *et al.*, 1992), Xα-SW (Bursten *et al.*, 1989b), DV-Xα and fully relativistic local density Dirac–Slater (Gulino *et al.*, 1993) approaches. The conclusions from all studies are broadly similar; the An–O bond has both σ and π character, with significant O $2p\pi \rightarrow$ An 6d and (lesser) 5f π donation. A comparison of [$ThCp_3OMe$] with the U analog found that $1.895 \ e^-$ are transferred to the Th center (along the Me→O→AnCp$_3$ direction), increasing to $2.185 \ e^-$ in [UCp_3OMe], i.e. the U compound was found to be more covalent (Gulino *et al.*, 1993). These workers noted, as have others (Bursten and Strittmatter, 1991), that the partial π character of the An–O bond may account for the prevalence of linear (or nearly linear) An–O–R vectors in actinide alkoxide systems.

(d)   [AnCp$_2$X$_2$], [AnCp$_2$X], and [AnCp$_2$] complexes

The metallocene structures MCp_2X_2 are common structures for the transition metal, lanthanide, and actinide elements, and thus provide an opportunity to compare and contrast the electronic structure of d- and f-block metals. Many of the f-element complexes of formulation MCp_2X_2 contain the sterically bulky and electron-rich pentamethylcyclopentadienyl (η^5-C_5Me_5, denoted Cp^*) ligand; the steric bulk of the Cp^* ligand is often needed to avoid the coordination of more than two Cp ligands about the large f-element centers (Janiak and Schumann, 1991).

The 1980s saw a number of extended Hückel calculations on compounds of the general formula [AnCp$_2$X$_2$], in which unsubstituted Cp rings were used to model the much bulkier Cp^* groups used in synthetic investigations (Tatsumi *et al.*, 1985; Smith *et al.*, 1986; Tatsumi and Nakamura, 1987). These extended

Hückel calculations are well summarized in the 1991 review by Bursten and Strittmatter (1991), and space does not allow us to go into detail here. Topics covered include (a) rationalization of the existence of both 'O inside' and 'O outside' structures in [UCp$_2$Cl(η^2-COR)], by contrast to the transition metal preference for O inside (Tatsumi *et al.*, 1985), (b) rationalization of the preference for the butadiene *s-cis* geometry in [AnCp$_2$(C$_4$H$_6$)] (An = Th, U) (Smith *et al.*, 1986), (c) determination that the actinacyclopentadiene complex is ca. 250 kJ mol^{-1} more stable than the corresponding cyclobutadiene structure in [UCp$_2$(C$_4$H$_4$)] (Tatsumi and Nakamura, 1987), and (d) studies of CO insertion pathways in [UCp$_2$Me$_2$]$^{2+}$ (Tatsumi *et al.*, 1985). Slightly earlier, quasi-relativistic Xα-SW calculations on [UCp$_2$X$_2$] (X = Cl, Me) were used to show that Me$^-$ is a stronger σ donor than Cl$^-$ to the actinide center, and concluded that there no significant Cl$^- \rightarrow$ U π donation (Bursten and Fang, 1983). Hay has recently reported DFT calculations on models of the formally U(VI) bis-imido complexes Cp$_2^*$U(= NR)$_2$ and related N-ligand systems (Hay, 2003). These systems demonstrate some of the complex chemical transformations that can occur at a uranium center (Arney *et al.*, 1992; Warner *et al.*, 1998; Kiplinger *et al.*, 2002), and an understanding of their behavior challenges the ability of calculations to determine reaction pathways for large actinide-containing systems.

In 1996, Di Bella *et al.* used configuration interaction *ab initio* methods to study the formally U(III) [UCp$_2$CH(SiH$_3$)$_2$] (Di Bella *et al.*, 1996). The U center was found to have a 5f^3 ground state configuration, and it was argued that the stability of this configuration vs 5f^{2}6d^1 correlates well with the inherent chemical stability of U(III) organometallics in comparison with 6d^1 Th(III) analogs. In agreement with previous studies, the U–Cp bonding was found to be primarily U 6d/Cp π_1, with the metal 5f electrons being only marginally involved in bonding. The U–CH(SiH$_3$)$_2$ bond is σ only.

More recently, Kaltsoyannis and Russo (2002) have used ZORA relativistic gradient-corrected DFT to show that the equilibrium geometry of [NoCp$_2^*$] is bent by 26° (i.e. the angle subtended by the centroids of the Cp* rings and the No atom is 154°), this structure being ca. 9 kJ mol^{-1} more stable than the linear arrangement. This study also examined the lanthanide analog, [YbCp$_2^*$], and also found it to be bent, in excellent agreement with gas-phase electron diffraction data (Andersen *et al.*, 1986). The bent structure of [NoCp$_2^*$] was traced to a combination of valence orbital and electrostatic factors. The involvement of the No 5f AOs in bonding to the Cp* rings is minimal, although ca. 10% metal d content is found in the Cp* ring pπ e$_{1g}$ levels.

(e) Bis(cyclopentadienyl) actinide complexes with metal–metal bonds

Despite extensive efforts, no organometallic (or nonorganometallic!) compound has been synthesized containing a direct An–An bond. Nevertheless, organometallic systems do exist that contain a bond between an actinide metal and a

transition metal (both direct and bridged), and some have been investigated computationally. Xα-SW calculations have been performed on [MCp$_2$(I)–RuCp(CO)$_2$] (M = Zr, Th) (Bursten and Novo-Gradac, 1987), a model for the first ever compound with a direct actinide–transition metal bond (Sternal *et al.*, 1985). The M–Ru bonding was found to be very similar in the transition metal and actinide systems, consisting of donation from the filled 4d$_{z^2}$ orbital of Ru to the empty d$_{z^2}$ valence function of Zr or Th. The bond is highly polarized toward the Ru, and is best described as a dative donor–acceptor bond from [RuCp(CO)$_2$]$^-$ to the d^0 Zr(IV) or d^{0}f^0 Th(IV) center.

Extended Hückel (Ortiz, 1986), Xα-SW (Makhyoun *et al.*, 1987), and *ab initio* (HF + generalized valence bond [GVB]) calculations (Hay *et al.*, 1986) have been performed on bis-Cp systems containing bridged bonds between Th and a late transition metal (Ni or Pt). The latter study took [Th(Cl)$_2$(μ-PH$_2$)$_2$Pt(PH$_3$)] as a model for the experimental Cp$_2^*$ system (the replacement of Cp by Cl is a computational simplification often made in early calculations on large systems, justified on the grounds that both ligands possess one filled σ and two filled π orbitals with respect to the ligand–metal axis), and concluded that there is direct M–M bonding between the 5d$_{x^2-y^2}$ orbital of Pt and the 6d$_{x^2-y^2}$ orbital of Th, with the larger fraction of the electron density on the Pt. The bond is best described as dative, from the formally filled 5d^{10} shell of the Pt into the formally empty 6d shell of Th.

17.5.3 Sandwich complexes with six- and seven-membered rings: An(η^6-C$_6$H$_6$)$_2$ and An(η^7-C$_7$H$_7$)$_2$

In 1999, Hong *et al.* published the results of an in-depth *ab initio* study of the energetics and bonding in [MBz$_2$] (M = Th, U, variety of lanthanide elements; Bz = η^6-C$_6$H$_6$) (Hong *et al.*, 1999). These calculations employed extensive electron correlation techniques (e.g. state-averaged CASSCF, MRCI, and CCSD(T)) in conjunction with large pseudopotential basis sets, and assumed D$_{6h}$ molecular symmetry (i.e. the Bz rings were fixed to be parallel to one another). It was found that both [ThBz$_2$] and [UBz$_2$] are stable with respect to dissociation into two benzene rings plus the metal, but that the An–ring bonding is weaker than in analogous bis-COT systems due to the lack of ionic contributions to the bonding (Bz is, of course, formally neutral and closed shell).

In a conclusion reminiscent of their earlier work on the lanthanocenes and actinocenes (Dolg *et al.*, 1995; Dolg and Fulde, 1998), these workers found that the ground state of both [ThBz$_2$] and [UBz$_2$] is not completely described by a single configuration. Thus, while the leading configuration to the ground state of the Th and U compounds is e$_{2g}^4$5f^0 and e$_{2g}^4$5f^2, respectively (the e$_{2g}$ level being a mixture of An 6d$_{\pm2}$ and ring π$_2$), the ground state wavefunctions have a contribution from the e$_{2g}^2$a$_{1g}^2$5f^0 (Th) and e$_{2g}^2$a$_{1g}^2$5f^2 (U) configurations (the a$_{1g}$ orbital is a mixture of An 7s and 6d$_0$). The principal source of metal–ring

covalency is a backbonding interaction from the An $6d_{\pm 2}$ levels to the ring π_2 orbitals, although there is some evidence for weak $5f_{\pm 2}$ involvement in this process.

Hong *et al.*'s assumption of D_{6h} symmetry for [MBz$_2$] was called into question by the work of Li and Bursten (1999), published in the same year. These workers used gradient-corrected DFT to probe the geometric structures of [AnBz$_2$] (An = Th to Am) and [An(η^6-C$_6$H$_3$R$_3$)$_2$] (An = Th, U, Pu; R = Me, ^{t}Bu). They found that the equilibrium geometry of [AnBz$_2$] is significantly bent, with the angle subtended by vectors connecting the ring centroids and the metal ranging from 135 to 142°, depending on the metal. This bending is electronically driven, with greater covalency in the bent geometry arising from greater Bz → An 6d and 5f donation. Fig. 17.19 shows the calculated energy curves for the TiBz$_2$ and ThBz$_2$ as a function of the centroid–metal–centroid angle, showing that the former is 'linear' whereas the latter is predicted to prefer a 'bent' geometry.

Replacement of three H atoms on each ring by Me groups also results in bent equilibrium geometries. However, when the Me groups are replaced by the much bulkier ^{t}Bu units the equilibrium geometry reverts to linear, i.e. for very bulky R substituents, the steric repulsion between the rings overcomes the electronic preference for bending. These conclusions are summarized in Fig. 17.20, which shows the calculated structures of U(η^6-C$_6$H$_3$Me$_3$)$_2$ and U(η^6-C$_6$H$_3$^{t}Bu$_3$)$_2$. The former is found to have a bent geometry with a centroid–U–centroid angle of 139.8° whereas the latter is found to be linear. It is notable that the experimental crystal structure of Gd(η^6-C$_6$H$_3$^{t}Bu$_3$)$_2$ is indeed linear (Brennan *et al.*, 1987).

Shortly after Li and Bursten's work was published, Hong *et al.* (2000) revisited [ThBz$_2$] and [UBz$_2$] using both *ab initio* and ZORA DFT methods. They found that neither molecule is bent at the *ab initio* SCF level. Inclusion of electron correlation, however, using MP2 and CCSD(T) methods, results in significantly bent structures (ca. 140–145°), although the energy differences between the linear and bent geometries is so small that the equilibrium geometry cannot be unequivocally established using these *ab initio* techniques, probably because of the use of an unrelaxed structure for the rings. Hong *et al.* then went on to conduct ZORA DFT studies which also indicated that the bent structures are the most stable, and hence they concluded that "qualitatively...we confirm their [Li and Bursten] result that the bis benzene complexes of Th and U have bent structures", and that bending enhances the metal–ring bonding. Dolg (2001) has also reported additional calculations on these systems at the scalar-relativistic level using a combination of energy-consistent *ab initio* pseudopotentials and gradient-corrected density functionals.

A number of recent investigations have focused on actinide sandwich molecules involving the cycloheptatrienyl ligand (Cht = η^7-C$_7$H$_7$). In 1995, Ephritikhine and coworkers isolated a salt of the [U(Cht)$_2$]$^-$ anion, which is the first and, to date, only experimental example of a sandwich complex involving two Cht ligands (Arliguie *et al.*, 1995). The [U(Cht)$_2$]$^-$ anion was characterized
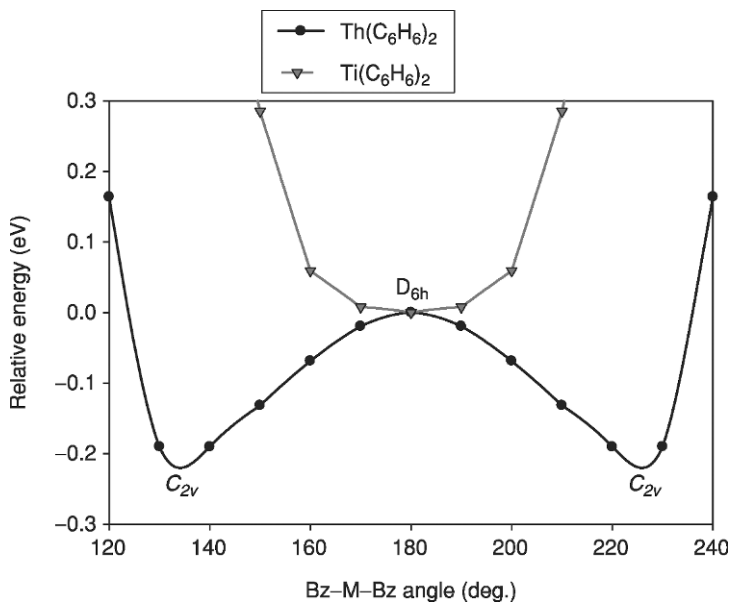
Fig. 17.19 *DFT-calculated potential energy curves for Ti(η^6-C_6H_6)$_2$ and Th(η^6-C_6H_6)$_2$ as a function of centroid–metal–centroid angle (reproduced from Li and Bursten, 1999).*
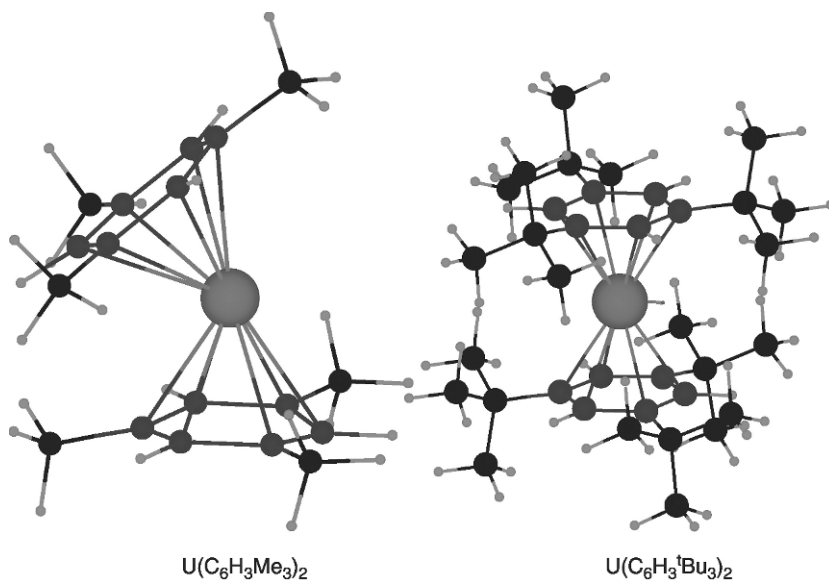
Fig. 17.20 *DFT-calculated structures of U(η^6-$C_6H_3Me_3$)$_2$ and U(η^6-$C_6H_3{}^tBu_3$)$_2$ as a function of centroid–metal–centroid angle (reproduced from Li and Bursten, 1999).*

crystallographically and was found to be a 'parallel' sandwich complex, i.e. the two Cht ligands are parallel to one another with a centroid–U–centroid angle of 180°.

Li and Bursten (1997) reported relativistic DFT calculations at both the LDA and Becke–Perdew86 (BP86) levels on $[An(Cht)_2]^q$ (An = Th to Am; $q = 2-$, $1-$, 0, 1+) complexes. The geometries were optimized in both D_{7h} and D_{7d} symmetries, with the latter (staggered rings) arrangement being found to be 2–4 kJ mol^{-1} more stable. The H atoms were found to be canted in toward the metal atom (e.g. by 4° in $[UCht_2]^-$), reminiscent of the results of similar calculations by the same researchers on protactinocene (Section 17.5.1) (Li and Bursten, 1998).

The metal–ring bonding was found to involve both the An 5fδ and 6dδ levels. The former interact with the $e_2'' \pi_2$ levels of the Cht ligands, and are as important as the 6dδ in stabilizing the frontier pπ orbitals of the rings. As the actinide atomic number increases, the An 5f and ring frontier pπ orbitals come into closer energetic proximity, resulting in an increase in the 5f contribution to the ring e_2'' levels and a decrease in the 6d content.

One of the most interesting aspects of this study concerns the formal oxidation states of the Cht rings and hence the metal centers. Formal charges of 1+ and 3– for a Cht ring satisfy the Hückel $4n+2$ rule for aromaticity. When reporting the experimental characterization of $[U(Cht)_2]^-$, Ephritikhine *et al.* suggested that the complex is a U(v) f^1 system with two 3– rings (Arliguie *et al.*, 1995). Li and Bursten, however, suggest that this is not the best description on the grounds that the $3e_2''$ level of $[U(Cht)_2]$ (HOMO) and $[U(Cht)_2]^-$ (HOMO–1) is an approximately equal mixture of U 5f and Cht π_2. They argued that two of the four electrons in this level should be associated with the metal and two with the rings, resulting in an f^2 U(IV)/2 × Cht^{2-} description for $[U(Cht)_2]$, with $[U(Cht)_2]^-$ being a U(III) f^3 system. That the formal description of the oxidation state of the Cht ligand is intermediate between the +1 and –3 limits is in agreement with previous experimental and theoretical studies of mixed ring transition metal Cht/Cp complexes (Green *et al.*, 1992, 1994; Kaltsoyannis, 1995). Gourier *et al.* (1998) performed an EPR and angle-selected ENDOR study of the $[U(Cht)_2]^-$ anion to determine the ordering of the electronic energy levels and the metal–ligand interaction. They indeed find that the single electron is localized in the U 5f-orbital, a spin–orbit-coupled mixture of fσ and fπ orbitals, and there exists strong participation of the fδ orbitals in the covalent bonding.

17.5.4 π-Backbonding in U(III) complexes containing N-based ligands

In our discussion of $[AnCp_3X]$ complexes, we came across Xα-SW calculations on $[UCp_3CO]$ (Bursten and Strittmatter, 1987), which found a significant π-backbonding interaction between the 5f AOs of the U(III) center and the CO π^* levels. Slightly over a decade after these calculations were published, Roussel and Scott (1998) reported the synthesis and
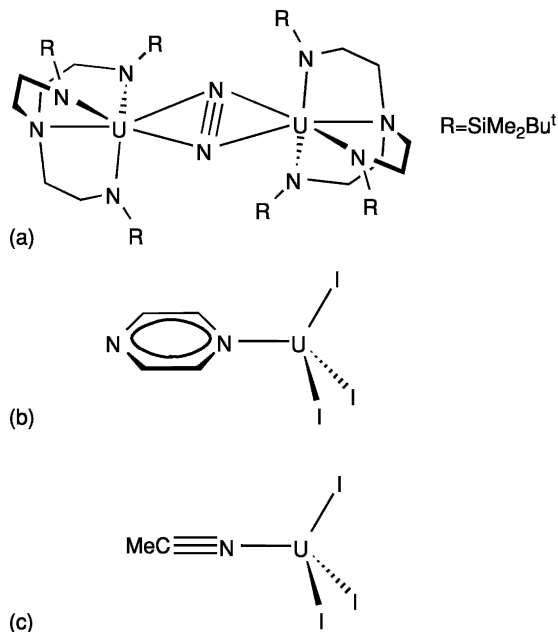
Fig. 17.21 *Molecular structures of three uranium compounds featuring metal→ligand π-backbonding (see Roussel and Scott, 1998; Mazzanti et al., 2002).*

characterization of the first dinitrogen compound of an actinide element, $[\{(NN_3)U\}_2(\mu^2 + \eta^2:\eta^2 + N_2)]$ $[NN_3 = N(CH_2CH_2NSiBu^tMe_2)_3]$ (Fig. 17.21a). The fact that the N–N distance in this compound is essentially the same as in free dinitrogen prompted these workers to conclude that the interaction between the N_2 and U centers is σ-donation from ligand to metal. Subsequent quasi-relativistic gradient-corrected DFT calculations on the model complex $[\{(NH_2)_3(NH_3)U\}_2(\mu^2-\eta^2:\eta^2-N_2)]$ (Kaltsoyannis and Scott, 1998), however, found that the only significant metal–N_2 interaction is π-backbonding from the 5f AOs of the formally U(III) centers into the N_2 π_g N–N antibonding MOs, very reminiscent of the earlier Xα-SW calculations on $[UCp_3CO]$. A three-dimensional representation of one of the two such π-backbonding MOs is shown in Fig. 17.22.

One of the more curious aspects of the work on $[\{(NH_2)_3(NH_3)U\}_2(\mu^2-\eta^2:\eta^2-N_2)]$ is the N–N bond length. Significant population of the N_2 π_g level should result in an increase in the N–N distance, and geometry optimizations of $[\{(NH_2)_3(NH_3)U\}_2(\mu^2-\eta^2:\eta^2-N_2)]$ indeed lead to a shortening of the U–N (N_2) distance and a lengthening of the N–N distance in comparison with experiment. These conclusions were reinforced by analogous DFT studies of UN_2 (Brown and Kaltsoyannis, 1999) and U_2N_2 (Roussel *et al.*, 2001).
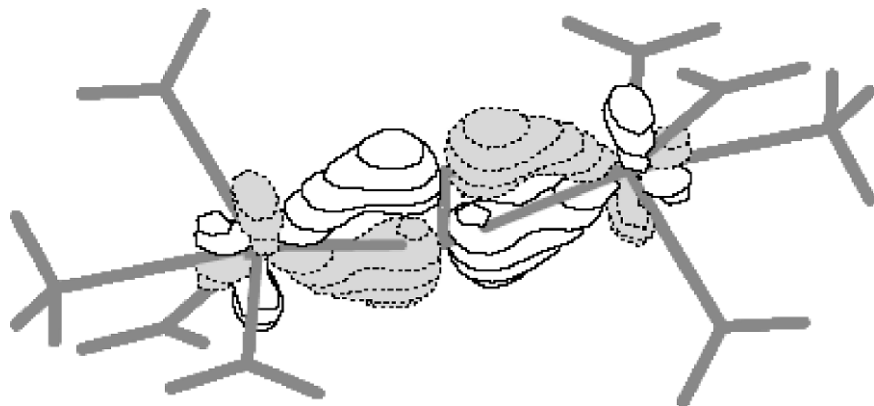
Fig. 17.22 *Three-dimensional representation of one of the two $U_2 \rightarrow N_2$ π-backbonding MOs in* $[\{(NH_2)_3(NH_3)U\}_2(\mu^2\text{-}\mu^2{:}\eta^2\text{-}N_2)]$, *a computational model for* $[\{(NH_2)_3(NH_3)U\}_2$ $(\mu^2\text{-}\eta^2{:}\eta^2\text{-}N_2)]$ *(see Fig. 17.21(a) and Kaltsoyannis and Scott, 1998).*

A possible explanation for the discrepancy between theory and experiment is that the NN_3 ligands are so bulky that they prevent the two ends of the molecule from coming any closer together, as would accompany a reduction in the U–N (N_2) distance. The conclusion was therefore that there is an electronic driving force toward U–N(N_2) shortening and N–N lengthening, but that this is opposed (and overcome) by the highly sterically demanding NN_3 ligands.

Recent experimental work by Cloke and Hitchcock (2002) has, however, called this conclusion into question. These workers have synthesized and characterized a bimetallic dinitrogen uranium complex with $CpCp^*$ and pentalene ancillary ligands, $[(U(\eta^5\text{-}C_5Me_5)(\eta^8\text{-}C_8H_4\{Si^iPr_3\text{-}1,4\}_2))_2(\mu\text{-}\eta^2{:}\eta^2\text{-}N_2)]$. By contrast to triamidoamine system of Roussel and Scott, the N–N distance in the Cloke complex is significantly longer than in free N_2, consistent with the presence of an N=N double bond. Intriguingly, however, the U–N distances are essentially the same as in $[\{(NN_3)U\}_2$ $(\mu^2\eta^2{:}\eta^2\text{-}N_2)]$, and Cloke has suggested that the difference between $[\{(NN_3)U\}_2$ $(\mu^2\text{-}\eta^2{:}\eta^2\text{-}N_2)]$ and $[(U(\eta^5\text{-}C_5Me_5)(\eta^8\text{-}C_8H_4\{Si^iPr_3\text{-}1,4\}_2))_2(\mu\text{-}\eta^2{:}\eta^2\text{-}N_2)]$ may be a consequence of different frontier orbital geometries in the two ligand environments.

A model for the Cloke pentalene system has been studied computationally by Cloke *et al.* (2004). These relativistic, gradient-corrected DFT studies reinforce the conclusions from the previous work on $[\{(NH_2)_3(NH_3)U\}_2(\mu^2\text{-}\eta^2{:}\eta^2\text{-}N_2)]$, i.e. both complexes contain two $5f^2$ U(IV) centers, with substantial covalent interaction between the U 5f atomic orbitals and one component of the N_2 π_g orbitals. The interaction may be characterized as reduction of the N_2 to N_2^{2-}, and geometry optimizations of the Cloke model concur with experiment in finding an N–N distance appreciably longer than in free N_2. However, this agreement between theory and experiment is only achieved at the expense of a

non-Aufbau electronic occupation. The origin of the short N–N distance in $[(N_3N')U)_2(\mu\text{-}\eta^2{:}\eta^2\text{-}N_2)]$ is therefore still not unambiguously resolved.

Mazzanti *et al.* (2002) have recently reinforced previous conclusions that U(III) can function as a π basic center. These workers have conducted quasi-relativistic gradient-corrected DFT calculations on [M(pyrazine)I$_3$] (Fig. 17.21b), [M(acetonitrile)I$_3$] (Fig. 17.21c), and [M(pyrazine)$_3$I$_3$] (M = La, Nd, U), models for experimentally characterized tris[(2-pyrazinyl)methyl]amine systems. Geometry optimizations of these compounds reproduce experimental trends, i.e. there is a reduction in M–N from La to U even though the ionic radii of La^{3+} and U^{3+} are very similar. The calculations reveal that there is essentially no orbital interaction between Ln^{3+} and the N-donor ligands, in contrast to the actinide system in which there is π-backdonation from the 5f AOs of U^{3+} into the π^* levels of both acetonitrile and pyrazine. This interaction leads to a larger total bonding energy for the U(III) species compared with the Ln systems (even though the shorter U–N distances produce larger Pauli repulsion energies).

Meyer *et al.* have also encountered π effects in uranium–nitrogen chemistry (Castro-Rodrigues *et al.*, 2003b). These researchers have conducted DFT calculations on uranium tris-aryloxide derivatives supported by triazacyclononane, in which the metal center is also bonded to NCCH$_3$, NSi(CH$_3$)$_3$, or N$_3$. In the NCCH$_3$ and NSi(CH$_3$)$_3$ systems, the acetonitrile– and imido–uranium bonds display strong covalent π interactions; interestingly, the azide derivative features an essentially electrostatic U–N$_3$ interaction. The uranium tris-aryloxide moiety has also been employed by the same researchers in the synthesis of an alkane-coordinated system (Castro-Rodrigues *et al.*, 2003a). Preliminary DFT calculations of this complex indicate a weak σ-type orbital interaction between the $(\eta^2\text{-}H,C)$-coordinated alkane and U-based fragments.

17.5.5 Miscellaneous organometallic systems

In 1989, Van der Sluys *et al.* reported the synthesis and structure of U[CH(SiMe$_3$)$_2$]$_3$, a U(III) complex that was the first homoleptic alkyl complex of an actinide element (Van der Sluys *et al.*, 1989). The molecule exhibits a somewhat nonintuitive pyramidal structure that could have been motivated for electronic or steric reasons. Ortiz *et al.* (1992) used *ab initio* CASSCF methods to study the electronic and geometric structures of [AnMe$_3$] (An = U, Np, Pu) as models of the isolated complex. They found that the pyramidal structure was more stable than the planar for the ground state of each molecule. The driving force toward pyramidalization is increased An 6d orbital participation in the An–C bonding orbitals. For example, the U 6d$_{xz}$ and 6d$_{yz}$ atomic populations increase from 0.04 to 0.34 electrons as [UMe$_3$] pyramidalizes from 0 to 23° out of plane. Further evidence for the key role of the 6d AOs come from the observation that if these functions are removed from the basis set, the planar geometry is the most stable for each molecule. Later scalar-relativistic DFT calculations by

Joubert and Maldivi (2001) lead to similar conclusions. Schneider *et al.* (1991) used Dirac–Fock–Slater calculations based on the discrete-variational Xα method to investigate the effects of spin–orbit and ligand-field effects on UH_3 and $U(NH_2)_3$. They found that the metal–ligand σ-bonding predominantly involves the U 6d orbitals and that the trigonal ligand field effectively quenches the spin–orbit coupling in the 6d manifold.

Nash and Bursten (1995) used relativistic DV-Xα calculations to study the electronic structure of octahedral $[M(CO)_6]$ (M = Cr, W, U, Sg). Population analyses and electron density plots indicate that there is more extensive π-backbonding in the actinide system than in the transition metal molecules. However, while $[Cr(CO)_6]$ and $[W(CO)_6]$ are stable species, $[U(CO)_6]$ cannot be isolated outside of a cold matrix, perhaps at odds with the electronic structure results. The rationalization of theory and experiment is that for the U species only there is a high density of 5f-based dissociative states close in energy to the ground state. Indeed, the calculations on $[U(CO)_6]$ required a thermal spreading factor (a Boltzmann weighting of orbital populations around the HOMO) to achieve SCF convergence. The authors conclude that "the 'clean' MO description of the transition metal systems is lost in $[U(CO)_6]$ owing to the energetic closeness of the U 5f and 6d AOs". The same authors also performed higher-level (MP2, CCSD(T)) calculations on $Sg(CO)_6$ (Nash and Bursten, 1999). These calculations affirm that $Sg(CO)_6$ is predicted to be a d^6 transition-metal carbonyl complex analogous to $Mo(CO)_6$ and $W(CO)_6$.

Recently, Korobkov *et al.* (2001) reported the results of hybrid DFT (B3LYP) studies on a model binuclear tetrapyrrole system $[(TP)U_2I_4]^{2-}$, in which the bridging $C(CH_2)_5$ units of the experimentally characterized molecule are replaced by CH_2 groups. Both high- and low-spin calculations were performed, essentially corresponding to ferromagnetic and antiferromagnetic coupling of the two U(III) $5f^3$ centers. The results, in agreement with experimental magnetic measurements, indicate that the ground state is low spin, but only by a very small energy (ca. 1 kJ mol^{-1}). The unpaired electrons are found in all spin cases to be nearly pure U 5f in character.

As we have seen, there has been a great deal of interest in organoactinide sandwich molecules and, more recently, in bimetallic uranium complexes involving π-backbonding from the U centers. Cummins *et al.* have synthesized and studied computationally inverted sandwich molecules of the form $[\{L_nU\}_2(\mu\text{-R})]$, where L is a nitrogen-based ligand and R is toluene, naphthalene, or COT (Diaconescu *et al.*, 2000; Diaconescu and Cummins, 2002). The ORTEP of $[\{(N[Ad]Ar)_2U\}_2(\mu\text{-}C_7H_8)]$ is shown in Fig. 17.23, and it can clearly be seen how the carbocyclic toluene ligand bridges the two U centers. DFT calculations reveal that the primary bonding interaction between the metals and the bridging ligand in $[\{(NH_2)_2U\}_2(\mu\text{-}C_6H_6)]$, a model for $[\{(N[Ad]Ar)_2U\}_2(\mu\text{-}C_7H_8)]$, is δ-backbonding from the U 5f atomic orbitals into the free arene LUMO. Fig. 17.24 presents three-dimensional representations of the two near-degenerate δ-backbonding levels. It is noticeable that the computed arene ring
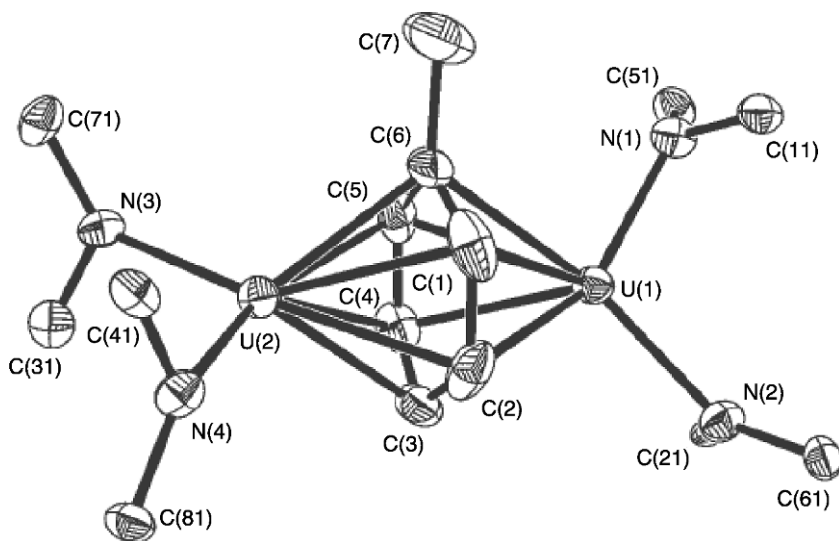
Fig. 17.23 *Structural drawing of* [{(N[Ad]Ar)$_2$U}$_2$(μ-C$_7$H$_8$)] (*reproduced from Diaconescu* et al., 2000).
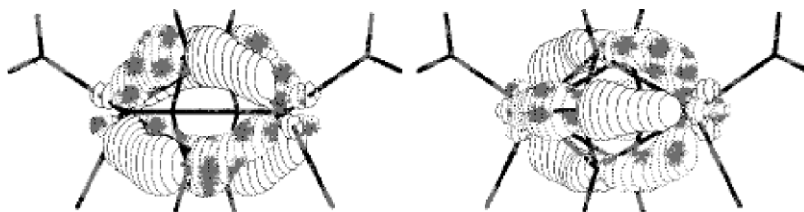
Fig. 17.24 *Two near-degenerate δsymmetry U→Bz backbonding orbitals in* [{(NH$_2$)$_2$U}$_2$ (μ-C$_6$H$_6$)], *a model for* [{(N[Ad]Ar)$_2$U}$_2$(μ-C$_7$H$_8$)] (*reproduced from Diaconescu* et al., 2000).

C–C distance is 1.461 Å, significantly longer than in free benzene (1.39 Å), as expected for partial population of the e$_2$ symmetry-free benzene LUMO. Similar conclusions concerning the nature of the bonding between the U centers and the arene bridge in [(C$_5$Me$_5$)$_2$U]$_2$(η-μ^6:μ^6-C$_6$H$_6$) were drawn by Evans *et al.* (2004).

17.6 MATRIX-ISOLATED ACTINIDE MOLECULES

In previous sections of this chapter, we have examined the electronic structure of some very small and some very large actinide-containing molecules and ions. Part of the appeal of the actinyl ions discussed in Section 17.3 is their small size

and their high symmetry, both of which facilitate high-level electronic structural studies. In contrast, the large organometallic complexes discussed in Section 17.5 present a much larger challenge to computational methods. One difficulty in comparing calculated electronic structural properties of the AnO_2^{q+} actinyl ions with experimental data is the fact that actinyl ions are generally found experimentally with equatorial ligands. Indeed, the experimental properties of isolated AnO_2^{q+} ions are largely unknown.

In this section, we will discuss another class of small actinide-containing species, namely those that can be isolated and detected in low-temperature matrices. Matrix isolation has been proven to be an effective way to stabilize reactive or transient species so that spectroscopic characterizations can be performed on otherwise thermodynamically unstable molecules (Bondybey *et al.*, 1996; Himmel *et al.*, 2002). Inert gas (e.g. noble-gas, N_2, H_2) matrices are frequently used because they usually protect (or prevent) the newly formed gas-phase products from undertaking further reactions. For several decades, matrix isolation techniques have helped scientists to identify and characterize thousands of new compounds, including many species that are unexpected from the traditional point of view of chemistry (Jacox, 2003). The first studies of matrix-isolated transient actinide molecules occurred in the early 1970s. These early studies reported the first data on matrix-isolated UO, UO_2, and UO_3 (Abramowitz *et al.*, 1971; Leary *et al.*, 1971; Abramowitz and Acquista, 1972; Carstens *et al.*, 1972), as well as the first uranium carbonyl complexes (Slater *et al.*, 1971), and the generation of UF_5 in matrices (Paine *et al.*, 1976; Jones and Ekberg, 1977). Reedy and coworkers performed a series of matrix-isolation experiments in the 1970s that led to a number of new species that will be discussed below. In the last decade, Andrews and coworkers have extensively explored the chemistry of Th and U in noble-gas (Ng) matrices, and these more recent studies will be much of the focus of the remainder of this section.

The generation of isolated small actinide transients is a very fertile area for electronic structure calculations, especially given some of the potential difficulties in characterizing transient molecules using only experimental methods (Beattie, 1999). Many of the new actinide molecules that have been detected in solid matrices are formed from the reaction of electronically excited actinide atoms, typically generated via laser ablation, with small substrate molecules, such as O_2, CO, NO, N_2, H_2O, and CO_2. Vibrational spectroscopy has been the most common and sensitive experimental probe of the products trapped within the low-temperature matrices. In addition, the use of isotopomers of the substrate molecules has allowed the vibrational studies to determine the stoichiometries of the reactions as well as the isotope shifts in the vibrational frequencies. Thus, the experimental studies typically can determine the reaction stoichiometries between the actinide atoms and the substrate molecules, and provide the vibrational frequencies of multiple isotopomers of the actinide-containing products. Theoretical studies of the matrix-isolated species can provide predictions of the geometric structures, relative isomer energies, and

electronic structures of the proposed products. In recent years, the ability to determine vibrational frequencies and normal modes directly from the electronic structure calculations has provided an important benchmark for the quality of the theoretical methods. Indeed, the understanding of matrix-isolated actinide molecules has greatly benefited from the synergy between experimental and theoretical studies, and the combination of experiments and theory has led to much more progress than either would in isolation.

Here we will provide a brief summary of recent developments in this fruitful field of actinide chemistry, with particular focus on the actinide oxides, nitrides, nitride–oxides, and carbide–oxides. The analogous transition-metal species characterized using the same technique have been reviewed recently (Zhou *et al.*, 2001; Andrews and Citra, 2002). The geometries, electronic structures, and vibrational frequencies of UO_2^{2+}, UO_2, UN_2, PuO_2^{2+}, and PuN_2 were recently investigated (Clavaguéra-Sarrio *et al.*, 2004). We will proceed by discussing the molecular and electronic structures of the actinide molecules formed upon the reactions of laser-ablated actinide atoms with various small molecules. Typically, the reaction of laser-ablated actinide atoms with small molecules leads to the formation of many products because of the excess energy of the laser-ablated atoms and the existence of multiple reaction channels. We will focus on some selected matrix-isolated actinide molecules that have been definitively characterized via experiment and are of fundamental importance in actinide chemistry. Also, we will limit our discussion primarily to molecules with three atoms or more that result from the addition of actinide atoms to diatomic or larger substrate molecules.

Many of the species that we will discuss in this section are triatomic molecules of the type XAnY involving a variety of actinide atoms in different oxidation states. This chemistry becomes closely linked to that of the actinyl ions, AnO_2^{q+}, that were discussed in Section 17.3. Not surprisingly, the majority of actinide matrix-isolation experiments have involved uranium because of the availability of the element and the relative ease with which it can be handled. Thus, many of the matrix-isolated species will be closely related to the uranyl ion, UO_2^{2+}, which, as we have pointed out, is probably the most prevalent species in uranium chemistry. In order to give a sense of the electronic structural diversity even among formally U(VI) species isoelectronic to UO_2^{2+}, we will present first a comparison of the energy-level diagrams for the isoelectronic series UO_2^{2+}, NUO^+, and CUO. The electronic structure of this series was first considered by Pyykkö *et al.* (1994) via Hartree–Fock calculations with quasi-relativistic pseudopotentials. The relative MO energies of UO_2^{2+}, NUO^+, and CUO from recent scalar-relativistic DFT calculations (Bursten *et al.*, 2003) are presented in Fig. 17.25. The electronic structures of these U(VI) f^0 species are qualitatively similar inasmuch as the highest occupied MOs form the familiar $(\sigma)^2(\pi)^4(\pi)^4(\sigma)^2$ manifold that is derived from the formally filled 2p orbitals of the $(O\cdots O)^{4-}$, $(N\cdots O)^{5-}$, and $(C\cdots O)^{6-}$ ligand sets. Quantitatively, however, the relative positions of the MOs vary substantially across the series because of
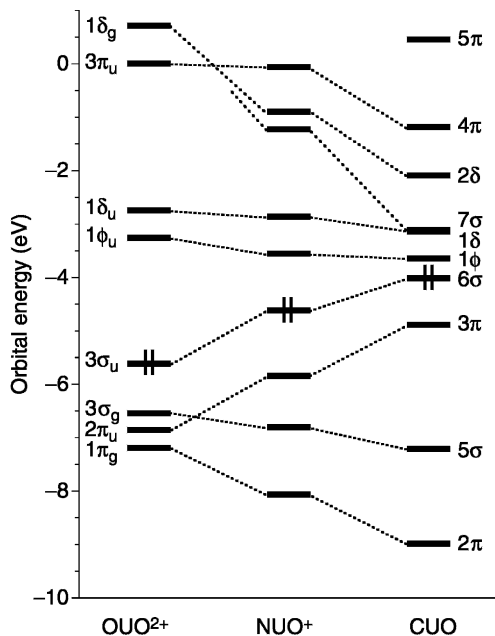
Fig. 17.25 *MO energies of the isoelectronic series* UO_2^{2+}, NUO^+, *and CUO from scalar-relativistic DFT calculations. The orbitals are labeled under* $D_{\infty h}$ *symmetry for* UO_2^{2+} *and* $C_{\infty v}$ *symmetry for* NUO^+ *and CUO (reproduced from Bursten* et al., *2003).*

the changes in the relative energies of the 2p orbitals for O, N, and C atoms. In particular, the rise of the HOMO across the series places it closer to the LUMO, which is a U-localized 5fϕ orbital in each case. We will find the energetic ordering of the MOs in this figure and the trends in orbital energies to be useful in this section.

17.6.1 Matrix-isolated actinide dioxides

The oxides occupy a central place in the natural, environmental, and technological aspects of actinide chemistry (Matthews, 1987). A variety of actinide oxides exist as solids or aqueous solutions in nature and in human-made reservoirs, such as nuclear fuel rods, nuclear waste repositories, and actinide storage tanks. We will focus our discussion here on the electronic structure of molecular actinide oxides, and particularly some of the actinide dioxides, that have been isolated in low-temperature matrices. As noted above, the largest body of research in this area has involved uranium chemistry. In addition to the ubiquitous chemistry of the uranyl ion, gas-phase reactions of uranium and other actinide atoms with atmospheric components are of great interest because

actinide metals experience oxidation when exposed to the atmosphere. Reactions of actinide atoms with oxygen, and the products thereof, thus represent one of the most important aspects of actinide chemistry.

Matrix-isolated uranium oxides were first explored in the early 1970s and the infrared (IR) spectra of UO, UO_2, and UO_3 were observed and assigned in several laboratories (Abramowitz *et al.*, 1971; Leary *et al.*, 1971; Abramowitz and Acquista, 1972; Carstens *et al.*, 1972). The IR spectra and assignments reported by Reedy and coworkers for UO, UO_2, and UO_3 (Gabelnick *et al.*, 1973a,b,c) and for ThO and ThO_2 (Green *et al.*, 1980) are generally accepted and has led to the interesting observation that UO_2 is linear (like UO_2^{2+}) whereas molecular ThO_2 has a bent structure (Pepper and Bursten, 1991). Green and Reedy (1978a) also reported the IR spectra of PuO and PuO_2 in Ar and Kr matrices. Because of the difficulty in handling the radioactive Pu systems, there are comparatively few experimental data available for them, although Green (1980) has also reported the gas-phase enthalpies of formation of PuO and PuO_2, and Capone *et al.* (1999) have reported an ionization energy for gaseous PuO_2.

In 1993, Andrews and coworkers generated UO_n species in an argon matrix via the reaction of laser-ablated U atoms with O_2 molecules in an argon carrier followed by condensation of a solid matrix at low temperature, and were able to obtain more accurate IR frequencies for UO, UO_2, and UO_3 (Hunt and Andrews, 1993). These species are also formed upon the reaction of laser-ablated U atoms with other substrates that can provide O atoms (e.g. NO, CO, CO_2) as will be discussed later. Interestingly, despite its stability and ubiquitous presence in solution and coordination chemistry, the UO_2^{2+} dication has not yet been observed in noble-gas matrices. The 'bare' UO_2^{2+} ion was first observed in the gas phase in 1996 (Cornehl *et al.*, 1996), although the vibrational properties of the bare ion are still unknown experimentally. Because the uranyl ion is highly charged, it is expected to have strong electrostatic or even covalent interactions with the matrix atoms or other residue counter-anions in the reactions. To date, the best known matrix-isolated species containing the UO_2^{2+} ion are those with various counter-ions, such as $UO_2^{2+}(NO^-)$, $UO_2^{2+}(NO_2^-)$, and $UO_2^{2+}(O_2^-)$ (Green *et al.*, 1976; Hunt and Andrews, 1993).

As shown in Section 17.3, there have been a great number of theoretical calculations on the free uranyl dication and other actinyl cations, and those results will not be repeated here. In order to relate the neutral uranium oxides detected via matrix isolation to the UO_2^{2+} ion, however, it is relevant to discuss briefly here the electronic structures of the UO_2^q ($q = +2, +1, 0, -1$) series. With reference to Fig. 17.25, the UO_2^{2+} ion has a closed-shell $^1\Sigma_g^+$ ground state with a $(3\sigma_u)^2(f\phi_u)^0(f\delta_u)^0$ electron configuration, consistent with the notion that uranyl is a U(VI) complex with an f^0 configuration. The UO_2^+ cation, which has one more electron than UO_2^{2+}, has a $^2\Phi_u$ ground state corresponding to the $(3\sigma_u)^2(f\phi_u)^1(f\delta_u)^0$ configuration. Although the $^2\Delta_u$ state, from the $(3\sigma_u)^2(f\phi_u)^0(f\delta_u)^1$ configuration, is only slightly higher in energy, the first-order

spin–orbit splitting of $^2\Phi_u$ is much larger than that of $^2\Delta_u$, which renders the $^2\Phi_u$ as the ground state. Upon adding two electrons to UO_2^{2+} to form neutral UO_2, we see the effect that changing the oxidation state of U has upon the relevant atomic orbital energies and, hence, the ground state of the molecule. At first glance one might expect that UO_2 would have a ^3H_g state derived from the $(3\sigma_u)^2(f\phi_u)^1(f\delta_u)^1$ configuration, which is the case for the isoelectronic PuO_2^{2+} ion. However, because of the increase in the U–O bond lengths and the decrease in the formal oxidation state to U(IV), the U 7s orbital is energetically very close to the $(f\phi_u f\delta_u)$ manifold in UO_2. As we will discuss in detail below, the free UO_2 molecule has a 'nonintuitive' $^3\Phi_u$ state derived from the $(3\sigma_u)^2(f\phi_u)^1(f\delta_u)^0(7s)^1$ configuration. Similarly, the UO_2^- anion has a $^2\Phi_u$ ground state from the $(3\sigma_u)^2(f\phi_u)^1(f\delta_u)^0(7s)^2$ configuration.

The nonintuitive ground state of UO_2 is a problem of great current interest and serves as a paradigm of the challenges in determining the electronic structures of even small actinide molecules. Part of the current interest in the electronic structure of matrix-isolated UO_2 is due to some current experimental anomalies that, at the time of this writing, are not resolved. UO_2 has very different IR-active U–O stretching frequencies in solid argon than in solid neon. In 1993, Hunt and Andrews reported that UO_2 in solid argon has an antisymmetric stretching mode at 776.0 cm^{-1} (Hunt and Andrews, 1993), a value that is in close agreement with earlier Knudsen effusion studies (Gabelnick *et al.*, 1973a). In 2000, Zhou *et al.* reported that UO_2 in solid neon exhibits a stretch at 914.8 cm^{-1}, ca. 139 cm^{-1} higher than in solid argon (Zhou *et al.*, 2000). The large shift in frequency from an argon to a neon matrix is unlikely to be due to typical polarizability-based matrix effects, which tend to cause shifts on the order of 5–20 cm^{-1} in vibrational frequencies (Jacox, 1994). As will be discussed in detail below, similar large frequency shifts were seen for matrix-isolated CUO and were ultimately shown to be the result of a noble-gas induced change in the electronic state of that molecule due to direct U–Ng bonds.

Calculations on the isolated UO_2 molecule have been carried out at several different levels of theory over the past few years, starting with some early Hartree–Fock–Slater work by Baerends *et al.* (Allen *et al.*, 1988; van Wezenbeek *et al.*, 1991). Zhou *et al.* (2000) reported DFT calculations on UO, UO_2^q ($q = 1+, 0, 1-$), and UO_3, including the calculation of vibrational frequencies and were the first to propose that neutral UO_2 has a $^3\Phi_u$ ground state arising from a $5f^1 7s^1$ configuration for the U(IV) center. Their calculated antisymmetric stretching frequency for UO_2 was 931 cm^{-1}, which is in good agreement with the experimental value observed in solid neon. Gagliardi and Roos with coworkers carried out CASSCF/CASPT2 and CASPT2/SO calculations on the geometries, electronic states, and vibrational frequencies of UO_2^{2+}, UO_2^+, and UO_2 (Gagliardi and Roos, 2000; Gagliardi *et al.*, 2001b). They also concluded that UO_2 has a $^3\Phi_u$ ($\Omega = 2$) ground state and found that the lowest state

derived from the $5f^2$ configuration was the ^3H_g ($\Omega = 4$) state, which was 0.52 eV above the ground state. Chang and Pitzer performed SOCI calculations on neutral UO_2 (Chang, 2002). They also found a $^3\Phi_u$ ($\Omega = 2$) ground state, with the ^3H_g ($\Omega = 4$) state only 0.20 eV above the ground state. Majumdar *et al.* (2002) also calculated the geometries and frequencies of the UO_2^q ($q = 2+, 1+, 0, 1-$) series using CASSCF and MRCI methods. A summary of the calculated geometric parameters and vibrational frequencies of the various uranium oxide species is presented in Table 17.17.

The theoretical results on isolated UO_2 could not be used to reconcile the difference in the experimentally observed IR stretching frequencies of UO_2 in argon and neon. Li *et al.* (2004) have performed scalar-relativistic DFT and CCSD(T) calculations on a series of UO_2 and $UO_2(Ar)_n$ complexes to explore the possibility that the electronic state of UO_2 is different in Ar than in Ne. Their calculated geometries and vibrational frequencies for UO_2, $UO_2(Ar)$, and $UO_2(Ar)_5$ are listed in Table 17.18, and Fig. 17.26 shows their linear transit potential energy curves for the interaction between five Ar atoms and UO_2 in two different electronic states of the model complex $UO_2(Ar)_5$. On the basis of these calculations, Li *et al.* proposed that UO_2 forms direct U–Ar bonds in the argon matrix, and that these bonds lead to stabilization of the $5f^2$-derived ^3H_g state below the $5f^1 7s^1$-derived $^3\Phi_u$ state that is the apparent ground state for UO_2 in solid neon. The significantly lower U–O antisymmetric stretching frequency for the ^3H_g state of UO_2 relative to the $^3\Phi_u$ state was proposed to explain the different IR frequencies of UO_2 in argon and neon matrices.

Recent experiments by Heaven *et al.* suggest that UO_2 is in the same electronic state in the gas phase and in an argon matrix (Han *et al.*, 2003). By using resonance-enhanced multiphoton ionization (REMPI) spectroscopy, they obtained a new value of 6.13 eV for the first ionization energy of UO_2, which was in good agreement with the calculated values of Zhou *et al.* (2000) and Gagliardi *et al.* (2001b). Their results were consistent with a $^3\Phi_u$ ground state for UO_2. They have also obtained dispersed fluorescence spectra for molecular UO_2 in solid argon, which suggest that UO_2 has the same ground state in the matrix as in the gas phase (Lue *et al.*, 2004), although these results cannot reconcile the different stretching frequencies of UO_2 in solid neon relative to solid argon. There are clearly still some unanswered questions with regard to the electronic state of UO_2 in noble-gas matrices. The recent calculation of the electronic spectra of isolated UO_2 by Gagliardi *et al.* (2005) represents one of such efforts. Nevertheless, the mystery of the different results from the two experiments will likely persist until it is possible to perform accurate theoretical calculations on the electronic spectra of UO_2 with the Ar matrix environment included.

The proposal of direct U–Ar bonds when UO_2 is in an argon matrix followed shortly after the proposal of the first uranium-to-noble-gas bonds, which involved the CUO molecule that will be discussed in the next section. Other recent discoveries in the interactions of noble-gas atoms with metal

Table 17.17 *Selected calculated bond lengths, bond angles, and vibrational frequencies of UO, UO_2^q (q = +2, +1, 0, −1), and UO_3.*[a]

Species	Method	State	U–O	∠O–U–O	ν_b[b]	$\nu_s(U–O)$[b]	$\nu_{as}(U–O)$[b]	References
UO	B3LYP	$^5\Gamma$	1.850	–			846	c
UO_2^{2+}	B3LYP	$^1\Sigma_g^+$	1.705	180°	161×2	1041	1140	c
	CASPT2	$^1\Sigma_g^+$	1.705	180°	–	959	1066	d
	MP2	$^1\Sigma_g^+$	1.728	180°	126×2	923	1024	e
	CCD	$^1\Sigma_g^+$	1.678	180°	194×2	1100	1179	e
UO_2^+	B3LYP	$^2\Phi_u$	1.764	180°	148×2	936	1010	c
	CASPT2	$^2\Phi_u$	1.773	180°	–	858	942	d
	MP2	$^2\Phi_u$	1.780	180°	101×2	901	955	e
	CCD	$^2\Phi_u$	1.744	180°	146×2	971	1031	e
UO_2	B3LYP	$^3\Phi_u$	1.800	180°	138×2	874	931	c
	CASPT2	$^3\Phi_u$	1.806	180°	–	809	932	f
	CASPT2/SO	$^3\Phi_u(\Omega = 2)$	1.766	180°	–	948	923	f
	MP2	$^3\Phi_u$	1.795	180°	149×2	896	913	e
	CCD	$^3\Phi_u$	1.766	180°	168×2	927	958	e
UO_2^-	B3LYP	$^2\Phi_u$	1.828	180°	136×2	825	874	c
	MP2	$^2\Phi_u$	1.825	180°	150×2	869	856	e
	CCD	$^2\Phi_u$	1.797	180°	160×2	872	895	e
UO_3	B3LYP	$^1A_1$	1.810, 1.853	100.6°, 158.8°	887 (a$_1$)	885 (b$_2$)	782 (a$_1$)	c

[a] Bond lengths in Å, bond angles in degrees, and frequencies in cm^{-1}.
[b] ν_b, $\nu_s(U–O)$, and $\nu_{as}(U–O)$ are the bending, symmetric stretching, and antisymmetric stretching frequencies of the UO_2^q species. For UO and UO_3, these categories do not apply.
[c] Zhou et al. (2000).
[d] Gagliardi and Roos (2000).
[e] Majumdar et al. (2002).
[f] Gagliardi et al. (2001b).

Table 17.18 *Calculated DFT and CCSD(T)[a] bond lengths (Å) and U–O stretching frequencies (cm^{-1}) for the $^3\Phi_u$- and ^3H_g-derived states of UO$_2$ ($D_{\infty h}$), UO$_2$(Ar) (C_{2v}), and UO$_2$(Ar)$_5$ (D_{5h}) (see Li et al., 2004).*

Molecule	State	U–O	U–Ar	ν_s(U–O)	ν_{as}(U–O)[b]
UO$_2$	$^3\Phi_u$	1.807 (1.835)	–	856	919
	^3H_g	1.851 (1.893)	–	779	824
UO$_2$(Ar)	"$^3\Phi_u$"	1.808 (1.834)	4.30 (4.006)	855	918
	"^3H_g"	1.851 (1.895)	3.28 (3.192)	765	806
UO$_2$(Ar)$_5$	"$^3\Phi_u$"	1.808 (1.833)	4.31 (4.097)	851	917
	"^3H_g"	1.856 (1.901)	3.37 (3.216)	755	805

[a] CCSD(T) values are listed in parenthesis when available.
[b] Only the antisymmetric stretches (ν_{as}) are infrared active.
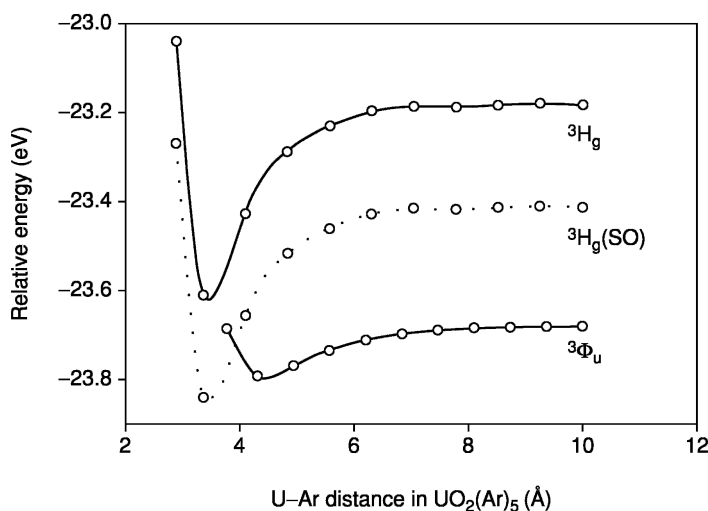
Fig. 17.26 *Calculated linear-transit potential energy curves for D_{5h} (UO$_2$)(Ar)$_5$ for the $^3\Phi_u$ and ^3H_g electronic states of UO$_2$. The dotted line represents a lowering of the curve for the ^3H_g state by 0.23 eV, the differential stabilization due to spin–orbit effects found by Gagliardi et al. (2001b) (reproduced from Li et al., 2004).*

centers, notably the remarkable stability of the [AuXe$_4$]$^{2+}$ complex (Seidel and Seppelt, 2000), suggest that the interaction of Ng atoms will be stronger with cationic centers because of electrostatic stabilization. Consistent with this notion, recent experimental and theoretical results suggest U–Ng interactions in a series of UO$_2^+$(Ng)$_n$(Ng = Ne, Ar, Kr, Xe) complexes in low-temperature matrices that are stronger than those for neutral UO$_2$ (Wang *et al.*, 2004).

A recent combined experimental and computational study also provides evidence for the formation of Ar atom binding to the simplest neutral uranyl complex, i.e. $H_2UO_2(Ar)_n$ (Liang *et al.*, 2005).

There have been other neutral actinide oxide molecules that have been studied by matrix-isolation techniques. As noted earlier, the bent structure of ThO_2 was indicated by the IR spectra of the matrix-isolated molecule. The interesting observation that ThO_2 is bent whereas the isoelectronic UO_2^{2+} ion is linear has stimulated a number of theoretical investigations. Much of the early work in this area was covered in detail by Pepper and Bursten (1991). Since that review was written, there have been applications of higher-level methods by Dyall (1999) and by Straka *et al.* (2001). The bent structure of ThO_2 is attributed to the favorable mixing of the Th 5f and 6d orbitals that can occur upon bending. Liang and Andrews (2002) recently generated ThS and ThS_2 in an argon matrix and investigated these molecules using scalar-relativistic DFT calculations. The IR spectrum of matrix-isolated ThS_2 indicates that it is also a bent molecule, and the DFT calculations predict a S–Th–S bond angle of $112°$.

As noted earlier, Green and Reedy (1978a) reported the matrix isolation of PuO_2 in 1978, formed from the sputtering of a plutonium cathode with Ar/O or Kr/O mixtures. Isotopic labeling of the O atoms allowed them to conclude that PuO_2 was a linear molecule. PuO_2 is formally a Pu(IV) complex with four metal-based electrons, and based on our discussion this far it is anticipated to have a complex electronic structure. To date, the only detailed electronic structure calculations on PuO_2 have been carried out by Archibong and Ray (2000), who used coupled-cluster and CAS calculations with RECPs. They found that the two lowest-energy states of PuO_2 are nearly degenerate, namely a $^5\Sigma_g^+$ state derived from the $(f\delta_u)^2(f\phi_u)^2$ electron configuration and a $^5\Phi_u$ state from the $(f\delta_u)^2(f\phi_u)^1(7s\sigma)^1$ configuration. Because these states are derived from different configurations (f^4 vs f^3s^1), they have significantly different calculated properties, as has been proposed for UO_2 and CUO. The calculated Pu–O bond lengths in the $^5\Sigma_g^+$ state range from 1.85 to 1.88 Å, depending on the method, and from 1.78 to 1.80 Å in the $^5\Phi_u$ state. The shorter An–O bonds in the states derived from the $f^{n-1}s^1$ configuration relative to those from the f^n configuration is consistent with what was observed for UO_2 (Table 17.18). Based on a comparison of the calculated antisymmetric stretching frequencies and $^{16}O/^{18}O$ isotopic ratios, Archibong and Ray propose that the $^5\Sigma_g^+$ state is the likely ground state of PuO_2.

17.6.2 Matrix-isolated actinide carbide oxides

One of the most interesting aspects of the chemistry of matrix-isolated actinide atoms has involved their reactions with CO and CO_2 as matrix substrates. The activation and sequestration of these two important molecules are and will continue to be fundamental areas of research. As we will see in this section,

actinide atoms, and particularly laser-ablated actinide atoms, have a remark-able ability to react with CO and CO_2. We will also see that some atypical species have been formed as well as some unusual types of bonds, providing many challenges to electronic structure calculations. To date, the experimental studies have been limited to reactions of Th and U with CO and CO_2, and we will limit our discussion here to some of the carbide–oxide products that form from these reactions. A discussion of some of the carbonyl species formed in these reactions will be presented later in this section.

The reaction of laser-ablated U atoms with CO produces a number of interesting products corresponding to the addition of one or more CO molecules to a U atom (Tague *et al.*, 1993; Zhou *et al.*, 1999a; Andrews *et al.*, 2000b). The 1:1 stoichiometry products are UCO and CUO, and the 2:1 products are $U(CO)_2$, OUCCO, and $(\eta^2\text{-}C_2)UO_2$. Evidence has also been found for the higher binary carbonyl complexes $U(CO)_n$ (n = 3–6). Table 17.19 presents the calculated scalar-relativistic DFT relative energies, geometric parameters, and some of the calculated vibrational frequencies of the 1:1 and 2:1 adducts of CO to U (Zhou *et al.*, 1999a). In both the isomers of UCO and $U(CO)_2$, the calculated lowest energy isomer is the one that involves the maximum number of U–O bonds, consistent with the high oxophilicity of uranium.

Table 17.19 *Relative energies, geometric parameters, and vibrational frequencies for the isomers of UCO and $U(CO)_2$ from scalar-relativistic DFT calculations, along with the experimental frequencies of the matrix-isolated species in solid neon (see Zhou* et al., *1999a).*

Species	Structure	Relative energy (eV)	Geometry	Frequencies (cm^{-1}) Calculated	Ne matrix
UCO	linear, $C_{\infty v}$	+2.29	U–C = 2.236 Å C–O = 1.178 Å	1818	1918[a]
CUO ($^1\Sigma^+$)	linear, $C_{\infty v}$	0	U–C = 1.764 Å U–O = 1.808 Å	874 1049	872 1047
$U(CO)_2$	bent, C_{2v}	+4.44	U–C = 2.236 Å ∠U–C–O = 179.4° ∠C–U–C = 76.2°	1810 1861	1791 1840
OUCCO	linear, $C_{\infty v}$	+1.42	U–O = 1.795 Å U–C = 2.026 Å C–C = 1.298 Å C–O = 1.176 Å	897 1393 2125	841 1362 2052
$(\eta^2\text{-}C_2)UO_2$	C_2	0	U–C = 2.289 Å U–O = 1.796 Å C–C = 1.271 Å ∠O–U–O = 155.8° CUC/OUO dihedral = 55°	849 910	843 922

[a] This value is uncertain.

Of the species formed in these reactions, the CUO molecule is especially interesting from an electronic structural viewpoint for several reasons. CUO is isoelectronic with UO_2^{2+} and can be considered as an f^0 U(VI) complex like the uranyl ion. Fig. 17.27 shows a qualitative interaction diagram that compares the valence MOs of CUO to those of UO_2^{2+}. This diagram is constructed by allowing the MOs of the f^0 fragment UO^{4+} to interact with the AOs of either O^{2-} or C^{4-}. As expected for isoelectronic systems, there is a one-to-one correspondence of the filled MOs of UO_2^{2+} (labeled under $D_{\infty h}$ symmetry) and CUO ($C_{\infty v}$ symmetry). The energies of the MOs in CUO differ from those of UO_2^{2+} because of the higher energy of the C 2s and 2p orbitals relative to the O 2s and 2p orbitals. In particular, the C 2p-based 4σ HOMO of CUO is much closer in energy to the empty 5f-based MOs than is the corresponding $2\sigma_u$ HOMO of UO_2^{2+}. As shown, the CUO molecule has a closed-shell $^1\Sigma^+$ ground state analogous to the $^1\Sigma_g^+$ ground state of UO_2^{2+}.

The CUO molecule was first isolated in 1993 by Andrews and coworkers (Tague *et al.*, 1993) in solid argon, where it exhibits stretching modes at 804.4 and 852.6 cm^{-1}. Later studies of CUO in solid neon led to very different frequencies, 1047.3 and 872.2 cm^{-1}, which isotopic substitution showed predominantly U–C and U–O stretching modes, respectively (Zhou *et al.*, 1999a). These large frequency shifts upon changing the matrix are greater than would be expected for normal polarizability-based matrix effects. As shown in Fig. 17.27, CUO is expected to have a $^1\Sigma^+$ ground state with a $(4\sigma)^2(5f\phi)^0$ configuration. However, the U–C-based 4σ orbital is so close in energy to the U $5f\phi$ orbital that the open-shell $^3\Phi$ excited state corresponding to the $(4\sigma)^1(5f\phi)^1$ configuration is very close in energy to the $^1\Sigma^+$ ground state. Initial scalar-relativistic DFT calculations predicted that the $^3\Phi$ excited state is only about 1 kcal mol^{-1} higher in energy than the singlet 'ground state' of free CUO and that the two states would have very different vibrational frequencies because they arise from different electronic configurations. The experimentally observed large vibrational frequency shifts were thus preliminarily explained in terms of a matrix-induced ground state reversal (Andrews *et al.*, 2000a).

To understand the ground-state reversal of CUO in the Ne and Ar matrices, further detailed theoretical calculations were performed to model the interaction between CUO and the noble-gas matrix. It was discovered that the CUO molecule tends to form direct albeit weak bonds to the Ar atoms in the matrix, leading to the proposal of a CUO(Ar)$_n$ complex that has a U–Ar bond (Li *et al.*, 2002). The formation of the U–Ar bond stabilizes the $^3\Phi$ ($^3A''$ under C_s symmetry) state of the molecule to such an extent that it drops below the $^1\Sigma^+$ ($^1A'$ under C_s) ground state of the isolated CUO molecule, as shown by the DFT energy curves shown in Fig. 17.28. This proposal of the first U–Ar bonding was affirmed by matrix experiments that showed that the U–Ar interactions occur even in a matrix of 1% Ar in neon (Fig. 17.29). The discovery of direct actinide-to-noble-gas bonding adds to the recent renaissance in noble-gas chemistry (Pyykkö, 2000a; Christe, 2001).
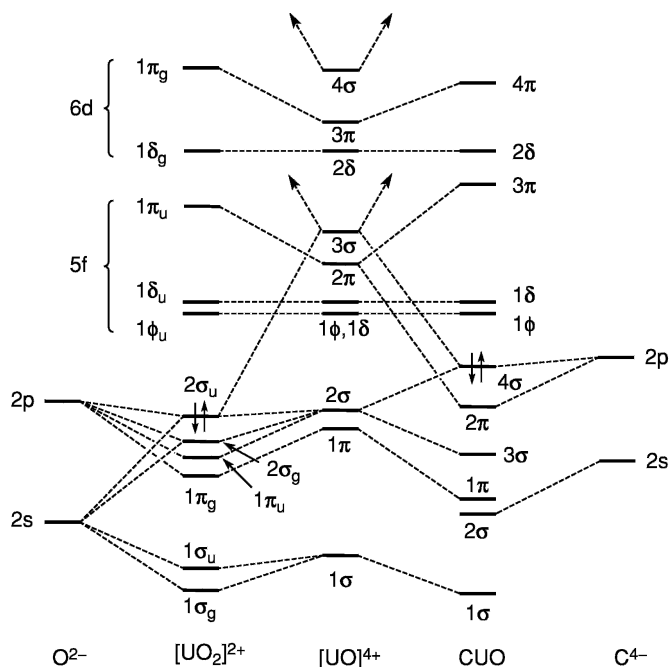
Fig. 17.27 *Qualitative interaction diagram showing the formation of the molecular orbitals of UO_2^{2+} and CUO by the interaction of O^{2-} and C^{4-} with UO^{4+}. Only the 5f and 6d orbitals of U are shown, although the U 7s and 7p AOs contribute non-negligibly to the bonding (reproduced from Zhou et al., 1999a).*

As noted above, the very small energetic separation (1 kcal mol^{-1}) between the $^1\Sigma^+$ ground state and the $^3\Phi$ excited state of CUO was first found using scalar-relativistic DFT calculations. The validity of this small gap was questioned because of concerns about the ability of DFT to calculate excited-state energies reliably and the lack of inclusion of spin–orbit effects, which are expected to affect the two states to a different extent. Recent CCSD(T) calculations with geometry optimizations on CUO and CUO(Ng) (Ng = Ne, Ar, Kr, Xe) confirm that the previous DFT triplet–singlet energy difference is underestimated and that the coordination of one (or more) heavier Ng atom indeed stabilizes the $^3\Phi$ excited state more than the $^1\Sigma^+$ ground state of CUO (Bursten et al., 2003). This energy difference is found to be around 16 kcal mol^{-1} from CCSD(T) calculations without including spin–orbit effects. Roos et al. (2003) performed CASPT2/SO calculations with spin–orbit effects included and found that the $^3\Phi$ state is stabilized by spin–orbit coupling by about 8–10 kcal mol^{-1} relative to the $^1\Sigma^+$ state. The additional differential stabilization of the $^3\Phi$ state upon multiple coordination of heavier Ng atoms would therefore seem to make the proposed ground-state reversal of CUO quite feasible. A recent study by
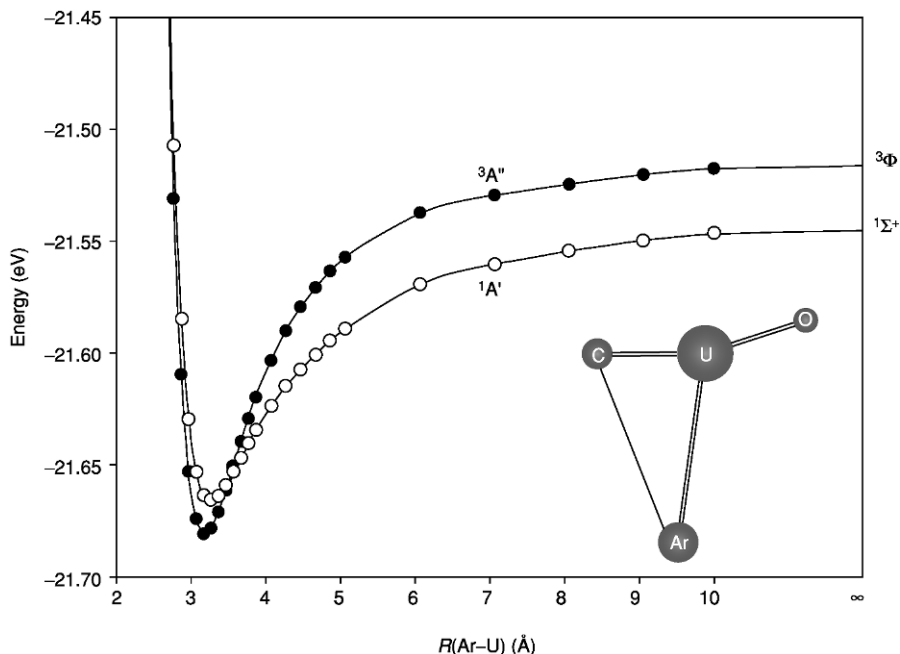
Fig. 17.28 *Potential energy curves for the $^1A'$ and $^3A''$ states of CUO(Ar) as a function of the U–Ar distance. The U–Ar bond length in this complex is 3.16 Å (reproduced from Li et al., 2002).*

Infante and Visscher (2004b) at the fully relativistic CCSD(T) level has confirmed that with inclusion of the high-level electron correlation and spin–orbit effects the $^3\Phi$ triplet state lies $\sim$14 kcal mol^{-1} above the $^1\Sigma^+$ ground state for isolated CUO. They concluded that "our result gives further justification to the interpretation of the measured frequency shifts of this species (CUO) in various noble gas matrices as being caused by significant interaction between the uranium and the heavier noble gas atoms."

Binding energy calculations on CUO(Ng)$_n$ (Ng = Ar, Kr, Xe; n = 1–6) predicted that CUO prefers five-coordination for Ar and Kr, and four-coordination for Xe. Experimental efforts indeed uncovered the coordination of CUO by multiple noble-gas atoms (Liang *et al.*, 2002; Andrews *et al.*, 2003). Recent experiments further confirm that the multiple coordination of CUO is necessary for the ground state reversal, with the experimentally determined singlet-to-triplet crossover points as CUO(Ar)$_3$, CUO(Kr)$_3$, and CUO(Xe)$_4$ (Liang *et al.*, 2003, 2004; Andrews *et al.*, 2004).

The only other CAnO species that has been detected thus far experimentally is the CThO molecule, which is formed upon the reaction of laser-ablated Th atoms with CO in excess neon (Zhou *et al.*, 1999b; Li *et al.*, 2001). The properties of the CThO molecule differ markedly from those of CUO because of the
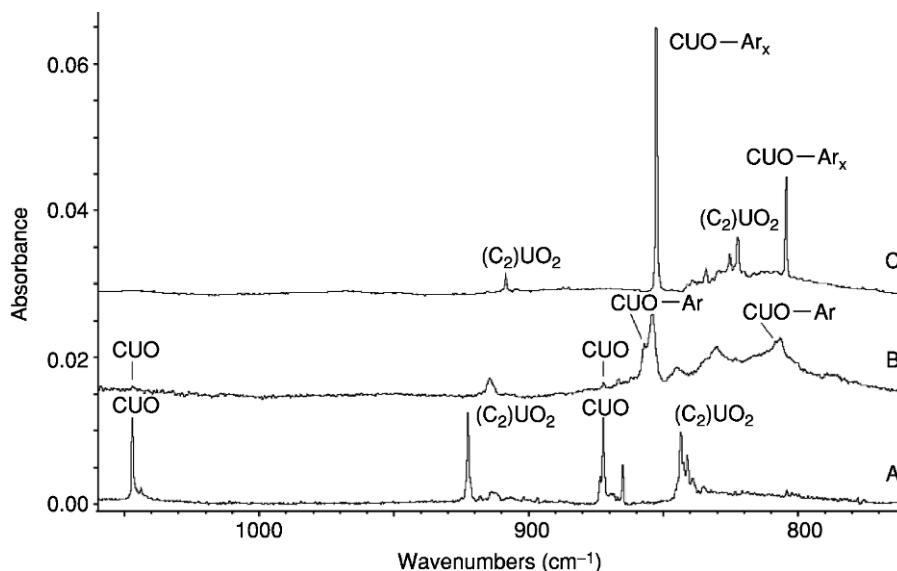
Fig. 17.29 *Infrared spectra in the* 1060–760 cm^{-1} *region for laser-ablated U atoms co-deposited with CO in excess noble gas.* (*A*) *Spectrum obtained when U atoms and* 0.1% *CO in Ne are deposited for* 30 min, *followed by full-arc photolysis and annealing at* 10 K. (*B*) *Spectrum obtained when U atoms,* 0.1% *CO, and* 1% *Ar in Ne are deposited for* 30 min, *followed by full-arc photolysis and annealing at* 10 K. (*C*) *Spectrum obtained when U atoms and* 0.3% *CO in Ar are deposited for* 15 min, *followed by full-arc photolysis and annealing at* 35 K (*reproduced from Li* et al., 2002).

difference in the number of valence electrons for Th and U. As discussed earlier, the $^1\Sigma^+$ state of CUO is isoelectronic with UO_2^{2+} and is best considered as a U(VI) complex. Because Th has only four valence electrons, the maximum oxidation state of Th is +4. The most obvious Lewis structure of CThO is the carbene :C=Th=Ö:, which is the actinide analog of the organic carbene ketenylidene, (:C=C=Ö:). Ketenylidene, which has been detected in interstellar space (Ohishi *et al.*, 1991), is a linear radical with a triplet ground state (Devillers and Ramsay, 1971). It was not apparent *a priori* whether CThO is linear or bent, and whether its ground state is a singlet or a triplet. Fig. 17.30 shows linear-transit potential energy curves from scalar-relativistic DFT calculations for the lowest singlet and triplet states of CThO (Li *et al.*, 2001). These studies predict that CThO prefers a highly bent structure ($\angle$CThO = 108.9°) with a triplet ground state. The bending of CThO is caused by factors similar to those used to explain the bent structure of ThO_2. From the CUO energy level in Fig. 17.25, linear CThO is expected to be a closed-shell molecule with a $(3\pi)^4(6\sigma)^0$ configuration. Because the 6dσ orbital participates strongly in the 6σ orbital, the unoccupied 6σ and occupied 3π MOs are very close in energy in linear structure; thus, a bending distortion via a second-order Jahn–Teller
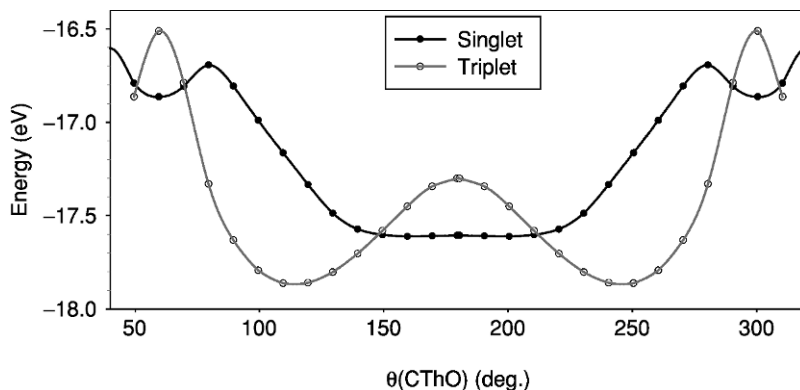
Fig. 17.30 *Linear-transit energy curves for the lowest singlet and triplet states of CThO (reproduced from Li et al., 2001).*

interaction is energetically favorable. The degenerate 3π orbital splits into a' + a'' upon bending, and the ground state of bent CThO corresponds to an $(a'')^2(a')^1(a')^1$ configuration that correlates with the $(3\pi)^3(6\sigma)^1$ configuration of the linear molecule.

The difference in the valence electronic structures of CUO and CThO has a remarkable effect on the observed stretching frequencies of the molecules. CThO in solid neon exhibits stretches at 617.7 and 812.2 cm^{-1}, and isotopic substitution demonstrates that these are predominantly Th–C and Th–O modes, respectively. The scalar-relativistic DFT calculations on isolated CThO model these vibrations extremely well, with calculated frequencies of 621 and 811 cm^{-1} and excellent calculated values for the isotopic ratios. Some of the properties of $^1\Sigma^+$ CUO and $^3A'$ CThO are compared in Table 17.20. Particularly notable are the changes in the calculated An–C bond lengths and the calculated and experimental An–C stretching frequencies. The Th–C bond length in CThO is more than 0.35 Å longer than the U–C bond length in CUO, and the predominantly Th–C stretching frequency is more than 400 cm^{-1} lower than the predominantly U–C stretching frequency. Both of these changes are consistent with a significantly lower bond order for the Th–C bond in CThO relative to the U–C bond in CUO, which is consistent with the simple Lewis structures of the molecules. The Th–O bond in CThO is slightly longer and weaker than the U–O bond in CUO, although the difference of the An–O bonding is not nearly as great as for the An–C bonds.

We will briefly discuss here the electronic structural aspects of some of the other products of the reactions of laser-ablated U and Th atoms with CO (Zhou *et al.*, 1999a; Li *et al.*, 2001). The most stable product from the addition of two CO molecules to a U atom is the unusual molecule $(\eta^2\text{-}C_2)UO_2$. This molecule results from the insertion of a U atom into two CO molecules, and its stability

Table 17.20 *Comparison of the properties of* $^1\Sigma^+$ *CUO and* $^3A'$ *CThO calculated from scalar-relativistic DFT calculations, along with the experimental frequencies of the matrix-isolated species in solid neon (see Zhou et al., 1999a; Li et al., 2001).*

	CUO	CThO
ground state	$^1\Sigma^+$	$^3A'$
An–C (Å)	1.764	2.124
An–O (Å)	1.808	1.889
∠C–An–O (°)	180	108.9
ν(An–C)[a] (cm^{-1}), calc	1049	621
ν(An–C) (cm^{-1}), expt	1047.3	617.7
ν(An–O) (cm^{-1}), calc	874	811
ν(An–O) (cm^{-1}), expt	872.2	812.2

[a] The vibrations are labeled 'An–C' and 'An–O' based on the predominant component of the normal mode.

relative to the other isomers [U(CO)$_2$ and OUCCO] is a consequence of the high oxophilicity of uranium and its preference for the +6 oxidation state. (η^2-C$_2$) UO$_2$ can be viewed as a closed-shell organometallic complex of the uranyl ion with a C$_2^{2-}$ ligand that is obtained by deprotonating acetylene. Experimentally, (η^2-C$_2$)UO$_2$ shows two vibrational frequencies in the U–O stretching region at 843.2 and 922.1 cm^{-1}. Scalar-relativistic DFT calculations found a minimum structure with calculated symmetric and antisymmetric U–O stretching frequencies at 849 and 910 cm^{-1}, respectively, in good agreement with the experimental values. The calculated structure of (η^2-C$_2$)UO$_2$ is unusual in two respects. First, the UO$_2$ moiety is bent (∠O–U–O = 155.8°), which is highly unusual for uranyl complexes. Second, the dihedral angle between the C–U–C and O–U–O planes is 55°, nearly halfway between a pseudotetrahedral (C$_{2v}$) structure with a dihedral angle of 90° and a completely planar structure. It is proposed that the 'twisted' C$_2$ structure allows for the maximum donation from the filled π orbitals of the C$_2^{2-}$ ligand to the f^{0}d^0 UO$_2^{2+}$ fragment (Zhou *et al.*, 1999a). There is no experimental evidence for the formation of the analogous (η^2-C$_2$)ThO$_2$ molecule. Because Th cannot achieve a +6 oxidation state, this isomer is calculated to be considerably higher in energy than OTh(η^3-CCO), which is a lower oxidation state complex of Th (Li *et al.*, 2001). The OUCCO and OTh (η^3-CCO) molecules are highly unusual inasmuch as they are the first examples of mononuclear ketenylidene complexes (Geoffrey and Bassner, 1988).

The major products of the reaction of laser-ablated Th or U atoms with CO$_2$ are the OThCO and OUCO molecules (Tague *et al.*, 1993; Andrews *et al.*, 2000b). These oxocarbonyl complexes were the first reported complexes of Th(II) and U(II). They provide an interesting contrast in structure and bonding because of the presence of a π-basic oxo ligand, which typically favors high oxidation states, and a π-acidic CO ligand, which generally favors lower oxidation states. Scalar-relativistic DFT calculations on these products lead to the prediction that they are high-spin complexes with linear CO ligands and

severely bent O–U–C linkages. The calculated electronic states, geometries, and vibrational frequencies, along with the experimental frequencies in solid neon, are presented in Table 17.21.

The OUCO molecule is predicted to be a planar, bent molecule with four unpaired electrons that correspond to a $(7s)^1(5f)^3$ configuration at the U(II) center. The bending of the molecule is a consequence of a Renner–Teller distortion that splits the 5fϕ orbitals, which are degenerate in the linear geometry. The bent geometry allows the U atom to serve as an efficient conduit of electron density from the strongly donating oxo ligand to the CO ligand, thus helping to explain the ca. 300 cm^{-1} reduction of the C–O stretching frequency in OUCO relative to free CO.

The bonding in OThCO differs substantially from that in OUCO because Th(II) has only two metal-localized valence electrons. Further, because the 6d orbitals of Th are lower in energy than the 5f orbitals, the two metal-based electrons are predicted to adopt a $(7s)^1(6d)^1$ electron configuration. Linear OThCO is predicted to have a Renner–Teller-active $^3\Pi$ state. Distortion causes OThCO to bend even more severely than OUCO, and it has a quite remarkable 90° O–Th–C angle. The greater radial extension of the 6d orbitals relative to the 5f orbitals allows the former to interact more strongly with the 2π orbitals of the CO ligand. As a result, the calculated and observed C–O stretching frequencies in OThCO are lower than those for OUCO even though the Th–C bond is predicted to be longer than the U–C bond.

17.6.3 Matrix-isolated actinide binary carbonyls

Binary zero-valent carbonyl complexes of the actinides have been a long-sought goal of actinide chemists because of their potential attractiveness in isotope-separation processes. In 1971, Slater *et al.* reported the isolation of

Table 17.21 *Predicted properties of OThCO and OUCO from scalar-relativistic DFT calculations, along with the experimental frequencies of the matrix-isolated species in solid neon (see Andrews et al., 2000b).*

	OThCO	OUCO
ground state	$^3A''$	$^5A''$
An–O (Å)	1.871	1.828
An–C (Å)	2.488	2.259
C–O (Å)	1.161	1.174
∠O–An–C (°)	90.8	113.8
∠An–C–O (°)	176.8	179.1
ν (C–O) (cm^{-1}), calc.	1789	1842
ν (C–O) (cm^{-1}), expt.	1778.4	1806.9
ν (An–O) (cm^{-1}), calc.	850	859
ν (An–O) (cm^{-1}), expt.	[a]	823.2

[a] Not observed.

U(CO)$_n$ ($n = 1$–6) in solid argon (Slater *et al.*, 1971). Since then there have been some reports of isolable carbonyl complexes of uranium, most notably the U(III) cyclopentadienyl carbonyl complexes discussed in Section 17.5.2. To date, however, the only reports of binary actinide carbonyls have involved matrix-isolated species. In this section, we will discuss the electronic structures of some actinide mono- and dicarbonyls. The higher carbonyls tend to be harder to characterize experimentally and there has been only one theoretical study of one of these species (Nash and Bursten, 1995).

The binary uranium carbonyls U(CO)$_n$ ($n = 1$–6) were reinvestigated by Zhou *et al.* (1999a) in a neon matrix. The monocarbonyl UCO was difficult to identify experimentally and a vibrational band at 1917.8 cm^{-1} was tentatively assigned to this species. The dicarbonyl U(CO)$_2$ exhibited absorptions at 1840.2 and 1790.8 cm^{-1}, which were assigned to the symmetric and antisymmetric C–O stretching modes, respectively, of a bent (C$_{2v}$) molecule. It is to be noted that the stretches assigned to U(CO)$_2$ are both at significantly lower frequencies than that for UCO, which is counter-intuitive. ThCO and Th(CO)$_2$ have both been identified in a neon matrix, along with the first report of the higher binary carbonyls of Th (Li *et al.*, 2001). The C–O stretch for ThCO is observed at 1817.5 cm^{-1} and the symmetric and antisymmetric stretches of Th(CO)$_2$ are assigned at 1827.7 and 1775.6 cm^{-1}, respectively. The reduction of the C–O stretching frequencies in these complexes by more than 300 cm^{-1} below that of free CO is quite striking given that Th is considered an early metal with only four electrons for potential backbonding.

Theoretical studies of even these simple mono- and dicarbonyl complexes are extremely challenging because of the presence of four (Th) or six (U) metal-based valence electrons at the An(0) center. The coordinative unsaturation of these complexes combined with the energetic closeness of the An 7s, 5f, and 6d orbitals leads to a large number of low-lying states that will almost certainly demand multiconfigurational approaches to discern. To date, the only computational studies of these molecules have used scalar-relativistic DFT, which is intrinsically a single-configuration approach. Nevertheless, the results reported do provide useful information about the bonding in these complexes and we will discuss them briefly here. We will focus on ThCO and Th(CO)$_2$, which are somewhat cleaner systems than the uranium complexes because of the smaller number of metal-based electrons.

Scalar-relativistic DFT calculations on ThCO predict that it is a linear molecule with Th–C = 2.261 Å and C–O = 1.181 Å, and a $^3\Sigma^-$ ground state that corresponds to a $(7s)^2(6d\pi)^2$ electron configuration at Th. Two other states, namely a $^5\Delta$ [$(7s)^1(6d\pi)^2(5f\delta)^1$] and a $^3\Pi$ [$(7s)^1(6d\pi)^3$] are found at 3.2 and 11.1 kcal mol^{-1} above the ground state, respectively. The calculated C–O stretching frequency of ThCO is 1790 cm^{-1}, in good agreement with the experimental neon-matrix value, and the calculated ^{12}C/^{13}C and ^{16}O/^{18}O isotopic vibrational ratios are also in excellent agreement with the experimental values.

An energy level diagram for ThCO is presented in Fig. 17.31 (Li *et al.*, 2001). This diagram illustrates some of the important features of the bonding within actinide carbonyl complexes. The relativistic destabilization of the Th 5f orbitals and stabilization of the Th 7s orbital are shown in the first two columns, which compare atomic results on Th at the nonrelativistic and scalar-relativistic levels. The dominant interactions involve the Th 6d orbitals. The Th 6dσ orbital is strongly destabilized by interaction with the filled 5σ orbital of CO whereas the 6dπ orbitals are stabilized by a backbonding interaction with the CO 2π orbitals. In contrast, the Th 7s and 5f orbitals are minimally affected by the CO ligand. The $^3\Sigma^-$ ground state of ThCO corresponds to the $(3\pi)^2(6\sigma)^2$ MO configuration in which only two of the four Th-based electrons are involved in Th-to-CO π-backbonding. The large reduction in the C–O stretching frequency with only two π-electrons involved is attributed to the highly electropositive nature of Th, which leads to very effective charge transfer from Th to CO. The authors also reported a calculation on the hypothetical $^1\Sigma^+$ excited state that arises from the $(3\pi)^4(6\sigma)^0$ configuration in which all four of the Th-based electrons are involved in π-backbonding. This excited state is found ca. 36 kcal mol^{-1} above the $^3\Sigma^-$ ground state, and leads to a predicted C–O stretching frequency of 1630 cm^{-1}, a value considerably lower than the lowest known CO-stretching frequency of any terminal metal carbonyl.

Scalar-relativistic DFT calculations on Th(CO)$_2$ also led to some interesting and unusual results. Three relatively low-lying states were found, each with different spin multiplicities. The ground state is predicted to be a closed-shell $^1A_1$ state in which two MOs that each involve strong Th 6d $\rightarrow$ CO 2π-backbonding are doubly occupied. The two occupied MOs are sketched in Fig. 17.32. By doubly occupying these MOs, all four of the metal-based electrons are involved in metal-to-ligand backbonding. The calculated geometry of ground state Th(CO)$_2$ is highly unusual inasmuch as it has two terminal CO ligands with $\angle$C–Th–C = 49.6°. This very acute angle is a consequence of the strong desire of electropositive Th to transfer its electrons to the ligands. At this small angle, the CO ligands are brought into close enough proximity (1.89 Å) to produce a significant C–C bonding interaction, which lowers the energies of the 2π orbitals and facilitates even better Th-to-CO donation. In essence, the strong Th 6d $\rightarrow$ CO 2π-backbonding has led to partial reductive coupling of the two carbon atoms. The low-lying triplet and quintet excited states depopulate the MOs in Fig. 17.32, leading to longer C–C interactions and correspondingly larger C–Th–C angles.

The calculated symmetric and antisymmetric C–O stretching frequencies for $^1A_1$ Th(CO)$_2$ are 1766 and 1734 cm^{-1}, respectively, which are slightly lower than the neon-matrix experimental values. Both the experimental and calculated mean C–O stretching frequencies of Th(CO)$_2$ are lower than the corresponding values for ThCO, which seems consistent with (i) the fact that two electrons are involved in backbonding in ThCO whereas four electrons are involved in Th(CO)$_2$ and (ii) the acute C–Th–C angle in Th(CO)$_2$ allows for
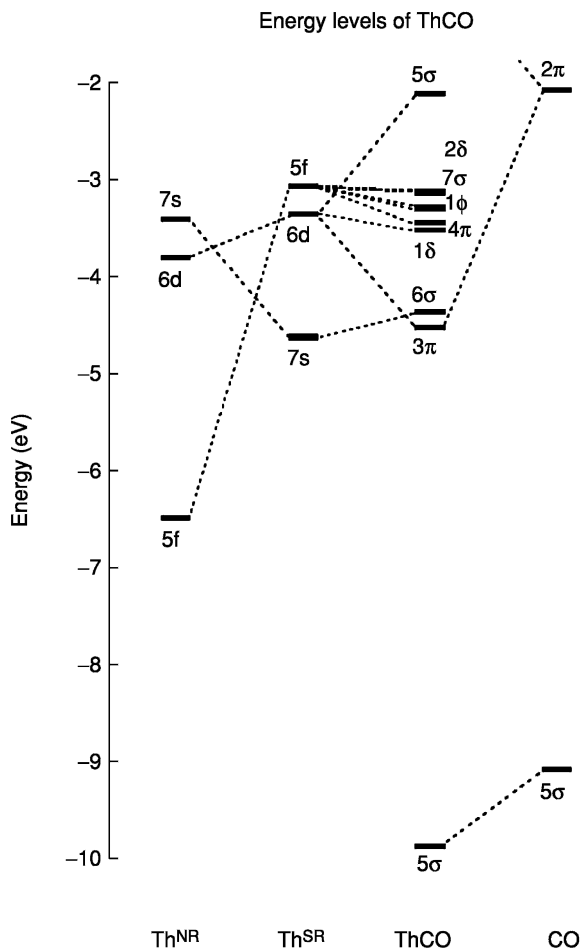
Fig. 17.31 *Energy-level diagram showing the interaction of a CO ligand with a Th atom to form ThCO. The atomic energy levels of Th^{NR} and Th^{SR} are for nonrelativistic and scalar-relativistic calculations on Th, respectively* (*reproduced from Li* et al., 2001).

better backbonding than can occur for a single CO ligand. The extreme ability of Th(0) to transfer electron density to CO is remarkable and is unprecedented among the transition metals.

17.6.4 Matrix-isolated actinide nitrides

The dinitrogen molecule is one of the most stable molecules with the N≡N bond energy of 225 kcal mol^{-1} (9.76 eV) (Gingerich, 1967). As a result, significant activation energy is needed to activate the N$_2$ molecule, as is the case for
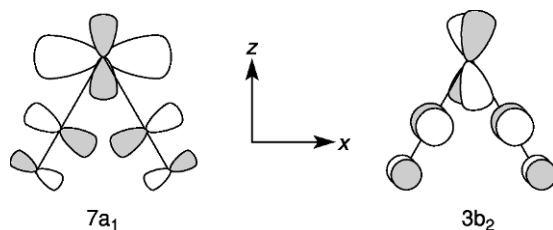
Fig. 17.32 *Sketches of the two highest occupied MOs of the calculated ground state of Th(CO)$_2$. Both MOs are doubly occupied in the ground state* (*reproduced from Li et al., 2001*).

activating the CO molecule. In the preceding sections we have seen that laser-ablated actinide atoms have sufficient activity to insert into the CO molecule, and the dinitrogen molecule can analogously be activated by energetic actinide atoms. Green and Reedy first generated the mono- and dinitrides of Th, U, and Pu via reactions of cathode-sputtered actinides with N$_2$ in a solid argon matrix (Green and Reedy, 1976, 1978b, 1979). By reacting laser-ablated Th and U atoms with N$_2$, N$_2$/O$_2$ mixtures, NO, NO$_2$, and N$_2$O, the Andrews group isolated the actinide mononitrides (AnN), dinitrides (NAnN), and some dinuclear actinide species in noble-gas matrices (Hunt *et al.*, 1993; Kushto *et al.*, 1997, 1998). Sankaran *et al.* (2001) also reported the matrix IR spectra of the UN and NUN molecules.

DFT calculations have been carried out on the matrix-isolated AnN and NAnN molecules using the ADF program with the PW91 and BP86 functional (Kushto *et al.*, 1997, 1998). It is predicted that without spin–orbit coupling the ThN, UN, and PuN are in $^2\Sigma$, $^4\Sigma$, and $^6\Pi$ electronic states, respectively, and the optimized bond lengths are consistent with triple bonds for these diatomic actinide molecules. All the NAnN (An = Th, U, Pu) molecules are predicted to be linear, consistent with the experimental IR spectra. Because the NUN molecule is isoelectronic to the uranyl ion, the electronic structures of these NAnN molecules can be qualitatively deduced from Fig. 17.27. Specifically, NUN is expected to have a $^1\Sigma_g^+$ ground state corresponding to the $(3\sigma_u)^2(f\phi_u)^0(f\delta_u)^0$ configuration, and NThN and NPuN should have the $(3\sigma_u)^0(f\phi_u)^0(f\delta_u)^0$ and $(3\sigma_u)^2(f\phi_u)^1(f\delta_u)^1$ configuration, respectively. The DFT calculations on the Th, U, and Pu dinitrides confirm these expectations: the Th and U dinitrides are found to have singlet states, while the NPuN molecule is in triplet state. Note instead of the $^3\Pi_g$ state assigned originally, the ground state of NPuN should be a ^3H_g state with a $(5f\phi)^1(5f\delta)^1$ configuration, as is confirmed in later calculations (Clavaguéra-Sarrio *et al.*, 2004).

The DFT-optimized An–N bond lengths and calculated vibrational frequencies of AnN and NAnN complexes are listed in Table 17.22, together with the experimentally measured data in Ar and N$_2$ matrixes. In agreement with the predicted linear structure of the NAnN molecules, only one IR absorption,

Table 17.22 *Predicted bond lengths* (Å) *and vibrational frequencies* (cm^{-1}) *of the AnN and NAnN molecules from scalar-relativistic DFT calculations, along with the experimental frequencies of the matrix-isolated species in solid argon and dinitrogen matrices (see Kushto et al., 1997, 1998).*

	An–N	ν_{bend}	ν_{sym} (An–N) Calculated	$\nu_{antisym}$(An–N) Calculated	Experimental
ThN	1.795			999	934.3 (Ar), 835.6 (N$_2$)
UN	1.746			1045	1000.9 (Ar), 890.5 (N$_2$)
PuN	1.756			863	855.73 (Ar)
NThN	1.864	64 × 2	828	830	756.6 (Ar), 716.4 (N$_2$)
NUN	1.717	53 × 2	1087	1123	1050.8 (Ar), 1010.3 (N$_2$)
NpuN	1.703	143 × 2	1012	1091	1029.74 (Ar)

corresponding to the antisymmetric stretching mode, was observed for each NAnN species in the matrices. By using the Ar matrix frequencies for different isotopomers, the NUN symmetric stretching frequency is estimated to be 1008.3 cm^{-1} via an F–G matrix approach (Hunt *et al.*, 1993). The large differences of the calculated 'gas-phase' antisymmetric frequencies and those measured in the Ar and N$_2$ matrices imply that, like the CUO and UO$_2$ molecules, these highly unsaturated species have significant chemical and physical interactions with the micro-solvating atoms in the Ar matrix, and even stronger interactions with those in the N$_2$ matrix. A recent CCSD(T) calculation on the $(f\phi_u)^1(f\delta_u)^1$ electron configuration of NPuN by Archibong and Ray (2000) leads to an optimized Pu–N bond length of 1.719 Å and the antisymmetric stretching frequency at 1117 cm^{-1}, in good agreement with the predictions from the DFT calculations. Gagliardi *et al.* (2003) also performed a CASPT2/SO calculation to explore the reaction energetics of U inserting to N$_2$ molecule.

The NThN molecule offers some interesting questions with respect to bonding. Terminal nitride ligands are generally formulated as N^{3-} and thus NUN and NPuN are considered complexes of U(VI) and Pu(VI) that have An≡N triple bonds. Because the maximum oxidation state of Th is +4, the bonds in NThN must be considered double bonds and the nitride ligands in this complex are formally N^{2-}. The calculated bond length for NThN is considerably longer than that in NUN and NPuN, consistent with these expected differences in the bonding.

17.6.5 Matrix-isolated actinide nitride–oxides

The NO$^+$ ion is another member of the isoelectronic series that includes N$_2$ and CO. Andrews and coworkers have examined the reactions of laser-ablated U and Th atoms with N$_2$/O$_2$ mixtures or NO. They have determined the

vibrational spectra and molecular structures of a series of actinide molecules of formula NAnO and NAnO$^+$ (An = Th, U) and have also performed DFT calculations on some of these species (Kushto *et al.*, 1997; Kushto and Andrews, 1999; Zhou and Andrews, 1999). The NUO$^+$ ion was also observed by Heinemann and Schwarz (1995) in gas-phase ion–molecule reactions. Inasmuch as the NUO$^+$ molecule is isoelectronic with UO$_2^{2+}$ and CUO, and the NUO molecule is isoelectronic with the UO$_2^+$ ion, it is not unexpected that both NUO and NUO$^+$ are predicted to be linear. In contrast, the NThO molecule is bent, with an optimized N–Th–O angle of 127.5°, similar to the OThO and CThO molecules. From Fig. 17.27, the NUO$^+$ ion is expected to have an electron configuration of $(6\sigma)^2(f\phi)^0(f\delta)^0$. However, because the N 2p orbitals are lower in energy than the C 2p orbitals, the HOMO–LUMO gap of NUO$^+$ is larger than that of CUO. As a result, a ground-state reversal such as that observed for CUO is unlikely to occur. The NUO molecule has a $^2\Phi$ ground state with the $(6\sigma)^2(f\phi)^1(f\delta)^0$ configuration. The geometric parameters and vibrational frequencies of the actinide nitride–oxides from the DFT calculations reported by Zhou and Andrews (1999) are summarized in Table 17.23. Gagliardi and Roos (2000) also have reported CASPT2 calculations on the geometric structures and vibrational frequencies of NUO and the NUO$^+$ ion.

In this section, we have summarized the geometric structures, electronic structures, and vibrational frequencies of some of the small molecules and ions that have been detected experimentally via matrix isolation. The combined efforts of low-temperature matrix-isolation experiments with state-of-the-art computational chemistry methods have greatly helped to rationalize and understand the chemistry of these unique actinide species. Further experimental and theoretical studies on these and other actinide species will greatly advance our

Table 17.23 *Predicted bond lengths* (Å) *and vibrational frequencies* (cm^{-1}) *of NUO, NUO$^+$, and NThO from B3LYP DFT calculations, along with the experimental frequencies of the matrix-isolated species in solid neon and argon matrices (see Zhou and Andrews, 1999).*

		N–An	An–O	∠NAnO	ν_{bend}	ν(An–O)	ν(N–An)
NUO	calc.	1.735	1.811	180°	125, 139	856	1063
	expt. (Ne)					833.5	1004.9
	expt. (Ar)					818.9	983.6
NUO$^+$	calc.	1.685	1.746	180°	129 × 2	1005	1191
	expt. (Ne)					969.8	1118.6
	expt. (Ar)					(882.5)	(1035.8)
NThO	calc.	1.957	1.901	127.5°	117 × 2	785	708
	expt. (Ne)					784.2	709.8
	expt. (Ar)					760.3	697.3

understanding of the structure and bonding of actinide complexes. In particular, the presumably innocent noble-gas matrices have been shown to play sometimes significant roles in the geometries, electronic structures, and spectroscopy of actinide compounds. The existence of the noble-gas actinide bonding indicates that the long overlooked role of noble gas atoms will have to be considered in future matrix-isolation experiments and in reinterpreting previous experimental results.

17.7   SPECIATED ACTINIDE IONS

In contrast to the high-valent actinyl series, An(III) and An(IV) ions exist in solution as bare ions (surrounded, of course, with solvent molecules and counter-ions). As with the actinyl ions, the characterization of their behavior in aqueous solution, i.e. their speciation, is of great interest in order to obtain a better understanding of their structures, stabilities, reactivities, and solution chemistry and of their environmental implications.

Recently, a hydration (electrostatic) model to describe monoatomic ions has been developed by David and Vokhmin (2001). They predict experimental An–O distances of 2.56, 2.52, 2.51, 2.51, and 2.44 Å for U^{3+}, Np^{3+}, Pu^{3+}, Am^{3+}, and Cf^{3+}, respectively. Their coordination numbers for the first solvation shell are between 9 and 10 for the first four ions and 8.5 for Cf^{3+}. Blaudeau and coworkers performed DFT (PW91) calculations on the hydrated Pu^{3+} ion and predicted a coordination number of eight or nine in the complex (Blaudeau *et al.*, 1999). Their calculated bond lengths were 2.508 Å for the eight-coordinate complex in which the water molecules form a nearly cubic cage around the plutonium ion with a total symmetry of D_{2d}, and 2.585 Å (axial) and 2.491 Å (equatorial) for a D_{3h} nine-coordinate tricapped trigonal prismatic complex. These values were in good agreement with a subsequent crystal structure determination of $[Pu(H_2O)_9][CF_3SO_3]_3$ (Fig. 17.33), which contains an isolated $Pu(H_2O)_9^{3+}$ ion with Pu–O distances of 2.574 Å (axial) and 2.476 Å (equatorial) (Matonic *et al.*, 2001). Earlier solution EXAFS studies, which are not as definitive concerning coordination number as the X-ray crystallography, had concluded that Pu–O = 2.51 Å and the coordination number was 9 or 10 for Pu^{3+} (Ankudinov *et al.*, 1998; Gropen, 1999).

Yang *et al.* (2001) performed quantum mechanical and molecular dynamics (MD) calculations on the Th^{4+} ion using DFT (B3LYP) methodology and AMBER force fields. In the aqueous phase, calculated using a polarized continuum model (PCM), they found a C_{4v} nine-water capped-square-antiprism complex to be the most stable. Their calculated Th–O bond distance was 2.54 Å. These results compare reasonably well with experimental EXAFS measurements, for which a coordination number of 9–11 and a bond length of 2.45 Å were found (Moll *et al.*, 1999). The MD simulations lead to a well-defined
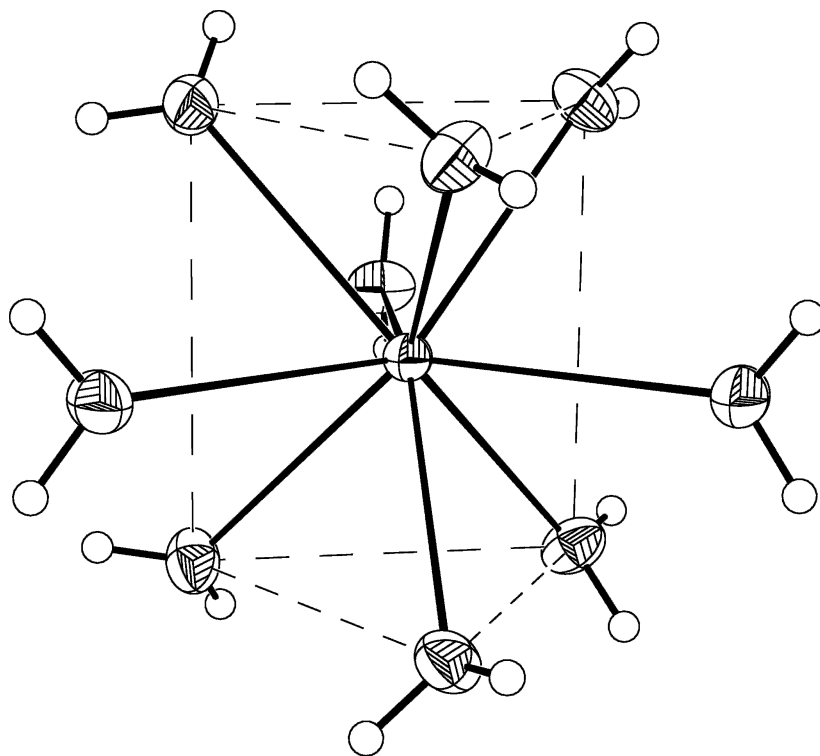
Fig. 17.33 *The structure of the* $[Pu(H_2O)_9]^{3+}$ *ion from the X-ray crystal structure of* $[Pu(H_2O)_9][CF_3SO_3]_3$ *(reproduced from Matonic et al., 2001).*

second shell consisting of 18.9 water molecules at a distance of 4.75 Å from the metal ion. In a further study, Tsushima *et al.* (2003) concluded that incorporation of the second shell in the geometry optimizations improves the Th–O bond distance to 2.50 Å. Mochizuki and Tsushima (2003) performed RECP-based B3LYP calculations with a conductive PCM and found a reduction in the calculated bond length to 2.47 and 2.48 Å. They also performed DIRAC four-component all-electron calculations of the $Ac(H_2O)_n^{3+}$ ($n = 1, 2, 4,$ and 6) complexes and the analogous Th^{4+} complexes. They found that the thorium complexes have a shorter metal–oxygen distance, larger stabilization energies, and larger amounts of ligand-to-metal electron donation. Mochizuki and Tatewaki (2002) performed similar calculations on the analogous Cm^{3+} complexes. They found the curium–oxygen bond distance to increase with the number of water molecules in the complex and the stabilization energy per water molecule was reduced. These studies provide important information about the solvation properties of actinides ions. Further theoretical calculations are needed to address the important chemical properties (e.g. charge-transfer or redox chemistry) of actinide ions in solutions.

17.8   UNSUPPORTED METAL–METAL BONDS CONTAINING ACTINIDE ATOMS

The rich manifold of s, p, d, and f orbitals on actinide atoms has led to numerous theoretical explorations on the possibility of forming discrete complexes that contain direct metal–metal bonds involving one or more actinide atoms. As noted earlier, one bonding motif that contains an unsupported (and therefore unambiguous) metal–metal bond involving an actinide atom is the $Cp_2^*(X)Th - RuCp(CO)_2 (X = Cl, I)$ system reported by Marks and coworkers in 1985 (Sternal *et al.*, 1985). This system was studied theoretically using quasi-relativistic Xα-SW calculations (Bursten and Novo-Gradac, 1987), which indicated that the $CpRu(CO)_2$ fragment in the molecule is best considered as an 'organometallic pseudohalide' that leads to a very polarized Ru–Th bond characteristic of 'early–late' heterodimetallic complexes (Gade, 2000). The conclusions of this theoretical study were applied in the synthesis of other organometallic complexes that contain unsupported actinide–transition metal bonds, such as the $Cp_3An–MCp(CO)_2$ (An = Th, U; M = Fe, Ru) complexes (Sternal and Marks, 1987). Mass spectrometric evidence has been presented for the formation of cationic complexes that contain direct An–M bonds from the reaction of Th^+ and U^+ with $Fe(CO)_5$ (da Conceicao Vieira *et al.*, 2001). The proposed complexes, $[AnFe(CO)_n]^+$ (An = Th, U) have the potential to lead to more covalent An–Fe bonding because of the lower oxidation state of the actinide centers, but theoretical studies are yet to be done for this structurally uncharacterized system.

Gagliardi (2003) recently exploited the pseudohalide characteristics of Au atoms as ligands to explore the structure and bonding in UAu_4 at the DFT and CASPT2 levels of theory. It is predicted that UAu_4 has a geometry slightly distorted from tetrahedral with U–Au bond lengths of 2.72 Å. The molecule is predicted to have a triplet ground state, analogous to the uranium tetrahalides. The U–Au bond is predicted to be ionic, although a comparison of the atomic populations of UAu_4 with those of other MAu_4 (M = Ti, Zr, Hf, Th) complexes indicates that the U–Au bond should have greater covalency than the other systems. Gagliardi and Pyykkö (2004) extended the analogy between An–main group and An–transition metal bonding to explore the possibility of strong U–M bonding in species such as NUIr, which is electronically similar to NUN. NUIr is predicted to be a closed-shell molecule with a very short U–Ir bond of 2.15 Å at the CASPT2 level with an extended basis. The bond is predicted to be polar, with a partial positive charge on U and partial negative charges on N and Ir, although less so than the other systems mentioned in this section. Similar results were obtained for the neutral isoelectronic molecules FURe, OUOs, and CUPt.

Truly covalent metal–metal bonds involving actinide atoms could be made in principle via direct actinide–actinide bonding in a symmetric discrete complex. To date, there are no well-characterized complexes that contain direct

actinide–actinide bonds; indeed, such systems remain as an experimental 'holy grail' in actinide chemistry. Most of the attention to the bonding and electronic structure of actinide–actinide bonded systems has focused on homonuclear diatomic molecules. March *et al.* have used simple models to predict that homonuclear diatomics of the heavy elements are unlikely to exist (Mucci and March, 1985; Pucci and March, 1986). Contrary to this prediction, the diatomic molecule U_2 has been detected in the gas phase via mass spectrometry (Gorokhov *et al.*, 1974; Gingerich, 1980), and was proposed to have a dissociation enthalpy of 52 ± 5 kcal mol^{-1}. This molecule has been the subject of several theoretical studies. Bursten and Ozin (1984) first examined the electronic structure of U_2 and Np_2 at an assumed bond distance of 2.2 Å using the quasi-relativistic Xα-SW method. They proposed that these molecules could form ϕ bonds via the 'face-to-face' interaction of the An 5fϕ AOs. Pepper and Bursten (1990) later used CASSCF and single-reference CI calculations to explore the bonding in U_2. They found a complex electronic structure for this molecule, including a relatively low-spin short-bond-length (SBL) state, and completely spin-uncoupled long-bond-length (LBL) state. Interestingly, they found the LBL minimum (at ca. 3.0 Å) to be lower in energy than the SBL minimum (at ca. 2.2 Å), although they expressed concerns about the lack of inclusion of spin–orbit effects in their calculations. Archibong and Ray (1999) have used DFT, CISD, and CCSD(T) calculations with RECPs to explore the possible existence of the Pu_2 diatomic molecule. They find that the molecule is bound, but that the Pu 5f electrons are localized, which leads to a rather weak interaction. The predicted Pu–Pu bond length, 4.4–4.5 Å depending on the method, is quite long and the predicted ground state is $^{13}\Sigma_g$ in the absence of spin–orbit effects.

Most recently, Gagliardi and Roos (2005) have reexamined the bonding in the U_2 molecule using CASSCF/CASPT2 methodology that includes spin–orbit effects. They find that the molecule has a very complex electronic structure: six of the 12 valence electrons fully occupy 7sσ and 6dπ bonding orbitals, one electron each occupy the 6dσ and 6dδ orbitals, one electron each occupy the weakly bonding 5fπ and 5fδ orbitals, and the last two electrons are essentially localized in the 5fϕ atomic orbitals on the two U atoms. They therefore describe the bonding in the molecule as having "three strong 'normal' electron-pair bonds, two fully developed one-electron bonds, two weak one-electron bonds, and two localized electrons," leading to the prediction of a net quintuple bond in the molecule. Fig. 17.34 depicts the active MOs of U_2 used to construct this unusual bond, and the occupation number of each from the CASPT2 calculations. With the inclusion of spin–orbit coupling, they predict a U–U bond length of 2.43 Å and a bond dissociation energy of 30.5 kcal mol^{-1}. It is highly unusual that a molecule with a quintuple bond possesses a dissociation energy lower than that of most systems with single bonds, which emphasize the weakness and complexity of the actinide–actinide bonds.

$7s\sigma_g(2.00)$ $6d\pi_u(4.00)$

$6d\sigma_g(0.97)$ $6d\delta_g(0.98)$ $5f\pi_u(0.63)$ $5f\pi_g(0.37)$

$5f\delta_g(0.63)$ $5f\delta_u(0.37)$ $5f\phi_u(1.00)$ $5f\phi_g(1.00)$
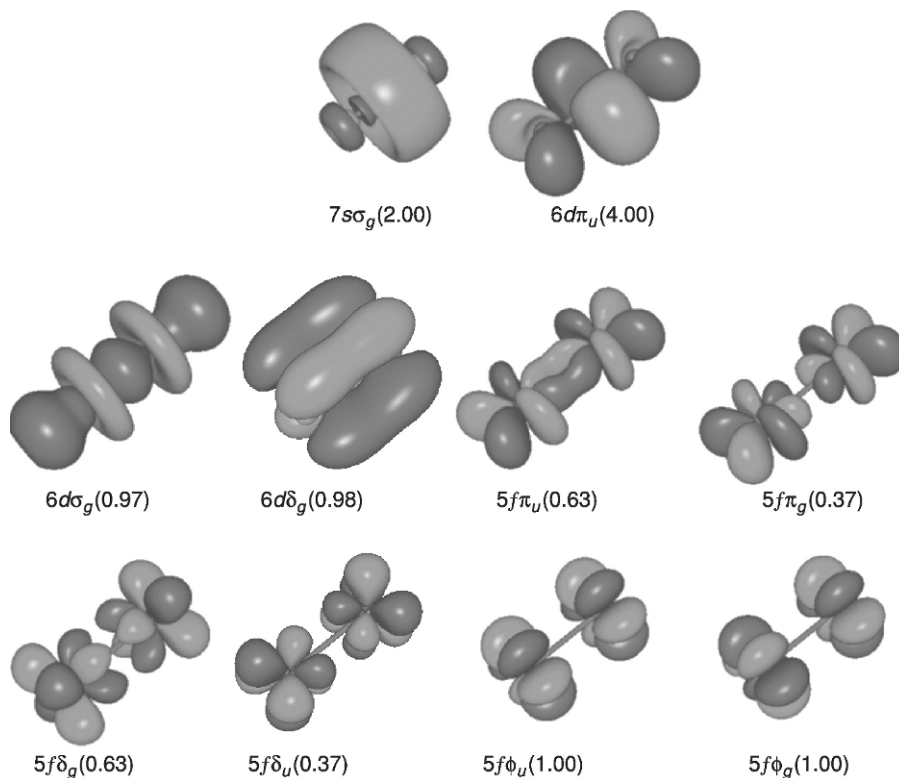
Fig. 17.34 *The active MOs that form the bond in U_2 from CASPT2 calculations. The number in parentheses is the electron occupation of the orbital in the ground state (reproduced from Gagliardi and Roos*, 2005).

17.9 CONCLUDING COMMENTS

We hope that this chapter has given the reader a sense of the challenges and complexity of obtaining and describing the electronic structure of discrete actinide-containing systems. As was stated at the outset, the large number of active atomic orbitals on actinide atoms and ions, the necessarily large number of electrons, the need to include relativistic effects, and the generally large coordination numbers all serve to make the electronic structure of molecular actinide complexes appreciably more complicated than that of transition-metal systems (and, perforce, purely organic systems). We have attempted to show the reader how recent advances in computational resources coupled with new theoretical methodologies have led to great progress in the quantitative description of actinide electronic structure. In particular, the growth of density functional methods and new electron correlation techniques during the last

10–15 years has greatly facilitated advances in this field, particularly with respect to the calculation of geometries, vibrational frequencies, and ground state metal–ligand interactions.

In spite of the progress that has been made, there are areas of actinide electronic structure that still require a great deal of development so as to allow computational actinide chemistry to be an even stronger partner to the experimental studies of actinide science. Very recent developments have led to better descriptions of the electronic structure of excited states of actinide systems, to improved treatment of dynamic correlation effects with the inclusion of scalar and spin–orbit relativistic effects, and to more effective combining of quantum mechanics and molecular mechanics methods (QM/MM methods) for the theoretical analysis of very large actinide molecular systems, such as those that are relevant to the interaction of actinide atoms and ions with biomolecules. These new capabilities portend an even greater role that theoretical studies will play in the understanding of experimental observations and the prediction of new properties of actinide systems.

Improved methods and enhanced computational capabilities will enable higher quality calculations of the types of actinide systems discussed in this chapter. They will also allow computational actinide chemists to address the 'next generation' of actinide electronic structure problems, including the interaction of actinide-containing molecules with realistically modeled solvents and surfaces and the complex equilibria exhibited in actinide chemistry (particularly aqueous actinide chemistry). We anticipate that the next decade will be one of continued growth in the scope and utility of theoretical actinide chemistry. Continuing efforts to improve relativistic electronic structural methodologies within DFT and electron correlation techniques, coupled with ever-increasing computational capabilities, will provide new, more powerful electronic structure codes for addressing actinide electronic structure. We expect that more reliable methods will be developed for exploring excited states of actinide systems, including the complex multiplets that are characteristic of the optical spectroscopy of actinide complexes. Improved methods for the calculation of the molecular energetics of actinide complexes could lead to predictive capabilities with thermodynamic accuracy. We are also hopeful that relativistic molecular electronic structure approaches will be improved to the point of allowing for the facile calculation of potential energy surfaces for actinide-containing molecules, including reaction transition states. It will be an exciting time for our field.

LIST OF ABBREVIATIONS

ADF	Amsterdam density functional code
AIMP	*ab initio* model potential
An	Actinide

AO	atomic orbital
ACPF	averaged coupled-pair functional
AQCC	averaged quadratic coupled cluster
B3LYP	Becke's three parameter exchange functional plus the correlation functional of Lee, Yang and Parr
BDF	Beijing density functional code
BLYP	Becke–Lee–Yang–Parr functional
BP86	Becke–Perdew 86 functional
Bz	Benzene
CASPT2	complete active space plus second-order perturbation theory
CASSCF	complete active space self-consistent field
CCSD	coupled cluster with single and double excitations
CCSD(T)	coupled cluster singles, doubles and perturbative triples
Cht	cycloheptatrienyl
CISD	configuration interaction with single and double excitations
COT	cyclooctatetraene
Cp	cyclopentadienyl
Cp*	pentamethylcyclopentadienyl
DFT	density functional theory
DHF	Dirac–Hartree–Fock method
DKH	Douglas–Kroll–Hess hamiltonian
DV-Xα	discrete variational Xα method
ECP	effective core potential
EHMO	extended Hückel molecular orbital
Gaussian	Gaussian computational chemistry code
GGA	generalized gradient approximation
GVB	generalized valence bond
HF	Hartree–Fock
HFS	Hartree–Fock–Slater
HOMO	highest occupied molecular orbital
INDO	intermediate neglect of differential overlap
IR	infrared
LCAO	linear combination of atomic orbitals
LDA	local density approximation
LMCT	ligand-to-metal charge transfer
LUMO	lowest unoccupied molecular orbital
MCSCF	multi-configuration self-consistent field
MLCT	metal-to-ligand charge transfer
MO	molecular orbital
MP2	second-order Møller–Plesset perturbation theory
MRCI	multi-reference configuration interaction
MRCISD	multi-reference configuration interaction with single and double excitations
NESC	normalized elimination of the small components

Ng	noble gas
NWChem	Northwest computational chemistry code
PCM	polarized continuum model
PW91	Perdew–Wang 1991 functional
QR-SW-Xα	quasi-relativistic scattered wave Xα
RASSCF	restrictive active space self-consistent field
RESC	relativistic scheme by eliminating small components
RECP	relativistic effective core potential
REX	relativistic extended Hückel
SCF	self-consistent field
SO	spin–orbit
SOCI	spin–orbit configuration interaction
SO-MRCISD	spin-orbit multi-reference configuration interaction singles and doubles
SW-Xα	scattered-wave Xα method
TD-DFT	time-dependent density functional theory
TMCOT	tetramethylcyclooctatetraene
Tp	tetrapyrrole
ZORA	zeroth-order regular approximation (to the Dirac equation)

REFERENCES

Aaberg, M., Ferri, D., Glaser, J., and Grenthe, I. (1983) *Inorg. Chem.,* **22**, 3986–9.
Abramowitz, S., Acquista, N., and Thompson, K. R. (1971) *J. Phys. Chem.,* **75**, 2283–5.
Abramowitz, S. and Acquista, N. (1972) *J. Phys. Chem.,* **76**, 648–9.
ADF: Scientific Computing and Modeling (SCM) NV, *Theoretical Chemistry*, Vrije Universiteit, Amsterdam, The Netherlands. http://www.scm.com

Alcock, N. W. and Esperas, S. (1977) *J. Chem. Soc.*, *Dalton Trans.*, 893–6.

Allen, G. C., Baerends, E. J., Vernooijs, P., Dyke, J. M., Ellis, A. M., Feher, M., and Morris, A. (1988) *J. Chem. Phys.,* **89**, 5363–72.

Allen, P. G., Veirs, D. K., Conradson, S. D., Smith, C. A., and Marsh, S. F. (1996) *Inorg. Chem.,* **35**, 2841–5.

Allen, P. G., Bucher, J. J., Shuh, D. K., Edelstein, N. M., and Reich, T. (1997) *Inorg. Chem.,* **36**, 4676–83.

Amberger, H. D. (1983) *J. Less Common Metals,* **93**, 233–41.

Andersen, R. A., Boncella, J. M., Burns, C. J., Blom, R., Haaland, A., and Volden, H. V. (1986) *J. Organomet. Chem.,* **312**, C49–52.

Andersson, K., Malmqyist, P.-A., and Roos, B. O. (1992) *J. Chem. Phys.,* **96**, 1218–26.

Andrews, L., Liang, B. Y., Li, J., and Bursten, B. E. (2000a) *Angew. Chem. Int. Edn.,* **39**, 4565–7; *Angew. Chem.*, **112**, 739–41.

Andrews, L., Zhou, M. F., Liang, B. Y., Li, J., and Bursten, B. E. (2000b) *J. Am. Chem. Soc.,* **122**, 11440–9.

Andrews, L. and Citra, A. (2002) *Chem. Rev.,* **102**, 885–912.

Andrews, L., Liang, B. Y., Li, J., and Bursten, B. E. (2003) *J. Am. Chem. Soc.,* **125**, 3126–39.

Andrews, L., Liang, B. Y., Li, J., and Bursten, B. E. (2004) *New J. Chem.,* **28**, 289–94.

Ankudinov, A. L., Conradson, S. D., de Leon, J. M., and Rehr, J. J. (1998) *Phys. Rev. B,* **57**, 7518–25.

Archibong, E. F. and Ray, A. K. (1999) *Phys. Rev. A,* **60**, 5105–7.

Archibong, E. F. and Ray, A. K. (2000) *J. Mol. Struct.* (*Theochem*), **530**, 165–70.

Arfken, G. (1985) *Mathematical Methods for Physicists,* Academic Press, New York.

Arliguie, T., Lance, M., Neirlich, M., Vigner, J., and Ephritikhine, M. (1995) *J. Chem. Soc.*, *Chem. Commun.*, 183–4.

Arney, D. S. J., Burns, C. J., and Smith, D. C. (1992) *J. Am. Chem. Soc.,* **114**, 10068–9.

Avdeef, A., Raymond, K. N., Hodgson, K. O., and Zalkin, A. (1972) *Inorg. Chem.,* **11**, 1083–8.

Balasubramanian, K. and Pitzer, K. S. (1987) *Adv. Chem. Phys.,* **67**, 287–319.

Balasubramanian, K. (1989) *J. Phys. Chem.,* **93**, 6585–96.

Balasubramanian, K. (1994) in *Handbook on the Physics and Chemistry of Rare Earths,* vol. 18 (eds. K. A. Gschneidner and L. Eyring), North-Holland, Amsterdam, p. 29–158.

Balasubramanian, K. (1997) *Relativistic Effects in Chemistry, Part A: Theory and Techniques,* John Wiley, New York.

Barandiarán, Z. and Seijo, L. (2003) *J. Chem. Phys.,* **119**, 3785–90.

Bartlett, R. J. (1981) *Ann. Rev. Phys. Chem.,* **32**, 359–401.

Bartlett, R. J. (1989) *J. Phys. Chem.,* **93**, 1697–708.

Basile, L. J., Sullivan, J. C., Ferraro, J. R., and LaBonville, P. (1974) *Appl. Spectrosc.,* **28**, 142–5.

Batista, E. R., Martin, R. L., and Hay, P. J. (2004a) *J. Chem. Phys.,* **121**, 11104–11.

Batista, E. R., Martin, R. L., Hay, P. J., Peralta, J. E., and Scuseria, G. E. (2004b) *J. Chem. Phys.,* **121**, 2144–50.

Beattie, I. R. (1999) *Angew. Chem. Int. Edn.,* **38**, 3294–306.

Becke, A. D. (1988) *Phys. Rev. A,* **38**, 3098–100.

Becke, A. D. (1993a) *J. Chem. Phys.,* **98**, 1372–7.

Becke, A. D. (1993b) *J. Chem. Phys.,* **98**, 5648–52.

BERTHA: Grant, I. P. (1999) in *Supercomputers, Collision Processes and Applications* (eds. K. L. Bell, K. A. Berrington, D. S. F. Crothers, and K. T. Taylor), Plenum, New York, pp. 213–24.

Bethe, H. (1929) *Ann. Physik,* **3**, 133–208.

Blaudeau, J.-P., Zygmunt, S. A., Curtiss, L. A., Reed, D. T., and Bursten, B. E. (1999) *Chem. Phys. Lett.,* **310**, 347–54.

Blaudeau, J.-P., Bursten, B. E., and Pitzer, R. M. unpublished results.

Bleaney, B. (1955) *Discuss. Faraday Soc.,* **19**, 112–18.

Boerrigter, P. M., Baerends, E. J., and Snijders, J. G. (1988) *Chem. Phys.,* **122**, 357–74.

Bolvin, H., Wahlgren, U., Gropon, O., and Marsden, C. (2001a) *J. Phys. Chem. A,* **105**, 10570–6.

Bolvin, H., Wahlgren, U., Moll, H., Reich, T., Geipel, G., Fanghänel, T., and Grenthe, I. (2001b) *J. Phys. Chem. A,* **105**, 11441–5.

Bond, G. C. (2000) *J. Mol. Catal. A,* **156**, 1–20.

Bondybey, V. E., Smith, A. M., and Agreiter, J. (1996) *Chem. Rev.,* **96**, 2113–34.

Boring, M., Wood, J. H., and Moskowitz, J. W. (1975) *J. Chem. Phys.,* **63**, 638–42.

Boring, M. and Wood, J. H. (1979) *J. Chem. Phys.,* **71**, 392–9.

Breit, G. (1932) *Phys. Rev.,* **39**, 616–24.

Brennan, J. G., Andersen, R. A., and Robbins, J. L. (1986) *J. Am. Chem. Soc.,* **108**, 335–6.

Brennan, J. G., Cloke, F. G. N., Sameh, A. A., and Zalkin, A. (1987) *J. Chem. Soc., Chem. Commun.*, 1668–9.

Brennan, J. G., Green, J. C., and Redfern, C. M. (1989) *J. Am. Chem. Soc.,* **111**, 2373–7.

Brown, K. L. and Kaltsoyannis, N. (1999) *J. Chem. Soc., Dalton Trans.*, 4425–30.

Budantseva, N. A., Fedosseey, A. M., Bessonov, A. A., and Grigoriev, M. S. (2000) *Radiochim. Acta,* **88**, 291–5.

Burns, J. H. (1973) *J. Am. Chem. Soc.,* **95**, 3815–17.

Burns, C. J. and Bursten, B. E. (1989) *Comments Inorg. Chem.,* **9**, 61–93.

Bursten, B. E. and Fang, A. (1983) *J. Am. Chem. Soc.,* **105**, 6495–6.

Bursten, B. E. and Ozin, G. A. (1984) *Inorg. Chem.,* **23**, 2910–11.

Bursten, B. E., Casarin, M., Di Bella, S., Fang, A., and Fragalà, I. L. (1985) *Inorg. Chem.,* **24**, 2169–73.

Bursten, B. E. and Fang, A. (1985) *Inorg. Chim. Acta,* **110**, 153–60.

Bursten, B. E. and Novo-Gradac, K. J. (1987) *J. Am. Chem. Soc.,* **109**, 904–5.

Bursten, B. E. and Strittmatter, R. J. (1987) *J. Am. Chem. Soc.,* **109**, 6606–8.

Bursten, B. E., Rhodes, L. F., and Strittmatter, R. J. (1989a) *J. Am. Chem. Soc.,* **111**, 2756–8.

Bursten, B. E., Rhodes, L. F., and Strittmatter, R. J. (1989b) *J. Am. Chem. Soc.,* **111**, 2758–66.

Bursten, B. E. and Strittmatter, R. J. (1991) *Angew. Chem. Int. Edn. Engl.,* **30**, 1069–85.

Bursten, B. E., Drummond, M. L., and Li, J. (2003) *Faraday Discuss.,* **124**, 1–24, 457–8.

Capone, F., Colle, Y., Hiernaut, J. P., and Ronchi, C. (1999) *J. Phys. Chem. A,* **103**, 10899–906.

Carnall, W. T. and Crosswhite, H. M. (1986) in *Chemistry of the Actinide Elements*, vol. 2 (eds. J. J. Katz, G. T. Seaborg, and L. R. Morss), Chapman & Hall, London, ch 16.

Carnall, W. T. (1992) *J. Chem. Phys.,* **96**, 8713–26.

Carstens, D. H. W., Gruen, D. M., and Kozlowski, J. F. (1972) *High Temp. Sci.,* **4**, 436–44.

Casida, M. E., Jamorski, C., Casida, K. C., and Salahub, D. R. (1998) *J. Chem. Phys.,* **108**, 4439–49.

Castellato, U., Vigato, A., and Vidali, M. (1981) *Coord. Chem. Rev.,* **36**, 183–265.

Castro-Rodrigues, I., Nakai, H., Gantzel, P., Zakharov, L. N., Rheingold, A. L., and Meyer, K. (2003a) *J. Am. Chem. Soc.,* **125**, 15734–5.

Castro-Rodrigues, I., Olsen, K., Gantzel, P., and Meyer, K. (2003b) *J. Am. Chem. Soc.,* **125**, 4565–71.

Chang, C., Pelissier, M., and Durand, P. (1986) *Phys. Scr.,* **34**, 394–404.

Chang, A. H. H. and Pitzer, R. M. (1989) *J. Am. Chem. Soc.,* **111**, 2500–7.

Chang, A. H. H., Zhao, K., Ermler, W. C., and Pitzer, R. M. (1994) *J. Alloys Compd.,* **213–214**, 191–5.

Chang, Q. (2002) MS Thesis, The Ohio State University.

Christe, K. O. (2001) *Angew. Chem. Int. Edn.,* **40**, 1419–21.

Christiansen, P. A., Lee, Y. S., and Pitzer, K. S. (1979) *J. Chem. Phys.,* **71**, 4445–50.

Christiansen, P. A., Ermler, W. C., and Pitzer, K. S. (1985) *Ann. Rev. Phys. Chem.,* **36**, 407–32.

Clark, D. L., Hobart, D. E., and Neu, M. P. (1995) *Chem. Rev.,* **95**, 25–48.

Clark, D. L., Conradson, S. D., Ekberg, S. A., Hess, N. J., Neu, M. P., Palmer, P. D., Runde, W., and Tait, C. D. (1996) *J. Am. Chem. Soc.,* **113**, 2089–90.

Clark, D. L. (1999) Presented at the Symposium of Heavy Element Complexes: The Convergence of Theory and Experiment, 217th ACS National Meeting, Anaheim, CA.

Clark, D. L., Conradson, S. D., Donohoe, R. J., Keogh, D. W., Morris, D. E., Palmer, P. D., Rogers, R. D., and Tait, C. D. (1999) *Inorg. Chem.,* **38**, 1456–66.

Clavaguéra-Sarrio, C., Brenner, V., Hoyau, S., Marsden, C. J., Millié, P., and Dognon, J.-P. (2003a) *J. Phys. Chem. B,* **107**, 3051–60.

Clavaguéra-Sarrio, C., Hoyau, S., Ismail, N., and Marsden, C. J. (2003b) *J. Phys. Chem. A,* **107**, 4515–25.

Clavaguéra-Sarrio, C., Vallet, V., Maynau, D., and Marsden, C. J. (2004) *J. Chem. Phys.,* **121**, 5312–21.

Cloke, F. G. N. and Hitchcock, P. B. (2002) *J. Am. Chem. Soc.,* **124**, 9352–3.

Cloke, .F. G. N., Green, J. C., and Kaltsoyannis, N. (2004) *Organometallics,* **23**, 832–5.

Connick, R. E. and Hugus, Z. Z. Jr (1952) *J. Am. Chem. Soc.,* **74**, 6012–15.

Conradson, S. D. (1998) *Appl. Spectrosc.,* **52**, 252A–79A.

Cornehl, H. H., Heinemann, C., Marcalo, J. Pires de Matos, P., and Schwarz, H. (1996) *Angew. Chem. Int. Edn. Engl.,* **35**, 891–4.

Cory, M. G., Köstimeier, S., Kotzian, M., Rösch, N., and Zerner, M. (1994) *J. Chem. Phys.,* **100**, 1353–65.

Cotton, F. A. (1990) *Chemical Applications of Group Theory,* John Wiley, New York.

Coulson, C. A. and Lester, G. R. (1956) *J. Chem. Soc.*, 3650–9.

Coupez, B. and Wipff, G. (2003) *Inorg. Chem.,* **42**, 3693–703.

Cowan, R. A. and Griffin, G. C. (1976) *J. Opt. Soc. Am. B.,* **66**, 1010–14.

Cramer, R. E., Edelmann, F., Mori, A. L., Roth, S., Gilje, J. W., Tatsumi, K., and Nakamura, A. (1988) *Organometallics,* **7**, 841–9.

Craw, J. S., Vincent, M. A., Hillier, I. H., and Wallwork, A. L. (1995) *J. Phys. Chem.,* **99**, 10181–5.

Crosswhite, H. M. and Crosswhite, H. (1984) *J. Opt. Soc. Am. B,* **1**, 246–54.

da Conceicao Vieira, M., Marcalo, J., and Pires de Matos, A. (2001) *J. Organomet. Chem.,* **632**, 126–32.

Dallinger, R. F., Stein, P., and Spiro, T. G. (1978) *J. Am. Chem. Soc.,* **100**, 7865–70.

David, F. H. and Vokhmin, V. (2001) *J. Phys. Chem. A,* **105**, 9704–9.

de Jong, W. A. and Nieuwpoort, W. C. (1996) *Int. J. Quantum Chem.,* **58**, 203–16.

de Jong, W. A., Harrison, R. J., and Dixon, D. A. (2001a) *J. Chem. Phys.,* **114**, 48–53.

de Jong, W. A., Harrison, R. J., Nichols, J. A., and Dixon, D. A. (2001b) *Theo. Chem. Acta,* **107**, 22–6. (Erratum: *Theo. Chem. Acta,* **107**, 318)

De Kock, R. L., Baerends, E. J., Boerrigter, P. M., and Snijders, J. G. (1984) *Chem. Phys. Lett.,* **105**, 308–16.

Del Mar, Conejo, M., Parry, J. S., Carmona, E., Schultz, M., Brennan, J. G., Beshouri, S. M., Andersen, R. A., Rogers, R. D., Coles, S., and Hursthouse, M. (1999) *Chem. Eur. J.,* **5**, 3000–9.

Den Auwer, C., Simoni, E., Conradson, S., and Madic, S. (2003) *Eur. J. Inorg. Chem.*, **21**, 3843–59.

Denning, R. G., Norris, J. O. W., and Brown, D. (1982a) *Mol. Phys.,* **46**, 287–323.

Denning, R. G., Norris, J. O. W., and Brown, D. (1982b) *Mol. Phys.,* **46**, 325–64.

Denning, R. G. (1992) *Struct. Bond.* (*Berlin*), **79**, 215–76.

Desclaux, J.-P. (1973) *At. Data Nucl. Data Tables,* **12**, 311–406.

Devillers, C. and Ramsay, D. A. (1971) *Can. J. Phys.,* **49**, 2839–58.

Di Bella, S., Gulino, A., Lanza, G., Fragalà, I. L., and Marks, T. J. (1993) *J. Phys. Chem.,* **97**, 11673–6.

Di Bella, S., Lanza, G., Fragalà, I. L., and Marks, T. J. (1996) *Organometallics,* **15**, 205–8.

Diaconescu, P. L., Arnold, P. L., Baker, T. A., Mindiola, D. J., and Cummins, C. C. (2000) *J. Am. Chem. Soc.,* **122**, 6108–9.

Diaconescu, P. L. and Cummins, C. C. (2002) *J. Am. Chem. Soc.,* **124**, 7660–1.

Diamond, R. M., Street, K. Jr, and Seaborg, G. T. (1954) *J. Am. Chem. Soc.,* **76**, 1461–9.

Dieke, G. H. (1968) in *Spectra and Energy Levels of Rare Earth Ions in Crystals* (eds. H. M. Crosswhite and H. Crosswhite), Interscience, New York.

DIRAC: Department of Chemistry, University of Southern Denmark, Odense M., Denmark. http://dirac.chem.sdu.dk

Dirac, P. A. M. (1929) *Proc. R. Soc. London, Ser. A,* **123**, 714–33.

Docrat, T. I., Mosselmans, J. F. W., Charnock, J. M., Whiteley, M. W., Collison, D., Livens, F. R., Jones, C., and Edmiston, M. J. (1999) *Inorg. Chem.,* **38**, 1879–82.

Dolg, M., Fulde, P., Stoll, H., Preuss, H., Chang, A., and Pitzer, R. M. (1995) *Chem. Phys.,* **195**, 71–82.

Dolg, M. and Stoll, H. (1996) in *Handbook on the Physics and Chemistry of Rare Earths,* vol. 22 (eds. K. A. Gschneidner and L. Eyring), Elsevier Science B.V., Amsterdam, pp. 607–729.

Dolg, M. and Fulde, P. (1998) *Chem. Eur. J.,* **4**, 200–4.

Dolg, M. (2001) *J. Chem. Inf. Comput. Sci.,* **41**, 18–21.

Dolg, M. (2002) *Theor. Comput. Chem.* **11**, 793–862.

Domanov, V. P., Buklanov, G. V., and Lebanov, Y. V. (2002) *Radiochemistry,* **44**, 114–20.

Douglas, M. and Kroll, N. M. (1974) *Ann. Phys.* (*N.Y.*), **82**, 89–155.

Dyall, K. G. (1997) *J. Chem. Phys.,* **106**, 9618–26.

Dyall, K. G. (1999) *Mol. Phys.,* **96**, 511–18.

Dyall, K. G. (2001) *J. Chem. Phys.,* **115**, 9136–43.

Dyall, K. G. (2005) *Chem. Phys.,* **311**, 19–24.

Edelstein, N. M., Allen, P. G., Bucher, J. J., Shuh, D. K., Sofield, C. D., Sella, A., Russo, M., Kaltsoyannis, N., and Maunder, G. (1996) *J. Am. Chem. Soc.,* **118**, 13115–16.

Eisenstein, J. C. and Pryce, M. H. L. (1955) *Proc. R. Soc. London,* **A229**, 20–38.

Eisenstein, J. C. (1956) *J. Chem. Phys.,* **25**, 142–6.

Elliott, R. J. (1953) *Phys. Rev.,* **89**, 659–60.

Ellis, D. E., Rosén, A., and Walch, P. F. (1975) *Int. J. Quantum Chem. Symp.,* **9**, 351–8.

Ellis, D. E., Rosen, A., and Gubanov, V. A. (1982) *J. Chem. Phys.,* **77**, 4051–60.

Ermler, W. C., Ross, R. B., and Christiansen, P. A. (1988) *Adv. Quantum Chem.,* **19**, 139–82.

Ermler, W. C., Ross, R. B., and Christiansen, P. A. (1991) *Int. J. Quantum Chem.,* **40**, 829–46.

Evans, W. J., Kozimor, S. A., Nyce, G. W., and Ziller, J. W. (2003) *J. Am. Chem. Soc.,* **125**, 13831–5.

Evans, W. J., Kozimor, S. A., Ziller, J. W., and Kaltsoyannis, N. (2004) *J. Am. Chem. Soc.,* **126**, 14533–47.

Fischer, R. D. (1963) *Theor. Chim. Acta* (*Berlin*), **1**, 418–31.

Foldy, L. L. and Wouthuysen, S. A. (1950) *Phys. Rev.,* **78**, 29–36.

Foldy, L. L. (1956) *Phys. Rev.,* **102**, 568–81.

Fuchs, M. S. K., Shor, A. M., and Rosch, N. (2002) *Int. J. Quantum. Chem.,* **86**, 485–501.

Gabelnick, S. D., Reedy, G. T., and Chasanov, M. G. (1973a) *J. Chem. Phys.,* **58**, 4468–75.

Gabelnick, S. D., Reedy, G. T., and Chasanov, M. G. (1973b) *Chem. Phys. Lett.,* **19**, 90–3.

Gabelnick, S. D., Reedy, G. T., and Chasanov, M. G. (1973c) *J. Chem. Phys.,* **59**, 6397–404.

Gade, L. H. (2000) *Angew. Chem. Int. Edn.,* **39**, 2658–78.

Gagliardi, L., Handy, N. C., Ioannou, A. G., Skylaris, C.-K., Spencer, S., Willetts, A., and Simper, A. M. (1998) *Chem. Phys. Lett.,* **283**, 187–93.

Gagliardi, L. and Roos, B. O. (2000) *Chem. Phys. Lett.,* **331**, 229–34.

Gagliardi, L., Grenthe, I., and Roos, B. O. (2001a) *Inorg. Chem.,* **40**, 2976–8.

Gagliardi, L., Roos, B. O., Malmqvist, P., and Dyke, J. M. (2001b) *J. Phys. Chem. A,* **105**, 10602–6.

Gagliardi, L., Schimmelpfennig, B., Maron, L., Wahlgren, U., and Willetts, A. (2001c) *Chem. Phys. Lett.,* **344**, 207–12.

Gagliardi, L. and Roos, B. O. (2002) *Inorg. Chem.,* **41**, 1315–19.

Gagliardi, L., Skylaris, C.-K., Willets, A., Dyke, J. M., and Barone, V. (2002) *Chem. Phys.,* **2**, 3111–14.

Gagliardi, L. (2003) *J. Am. Chem. Soc.,* **125**, 7504–5.

Gagliardi, L., La Manna, G., and Roos, B. O. (2003) *Faraday Discuss.,* **124**, 63–8.

Gagliardi, L. and Pyykkö, P. (2004) *Angew. Chem. Int. Edn.,* **43**, 1573–6.

Gagliardi, L., Heaven, M. C., Krogh, J. W., and Roos, B. O. (2005) *J. Am. Chem. Soc.,* **127**, 86–91.

Gagliardi, L. and Roos, B. (2005) *Nature,* **433**, 848–51.

GAMESS: "General Atomic and Molecular Electronic Structure System," Schmidt, M. W., Baldridge, K. K., Boatz, J. A., Elbert, S. T., Gordon, M. S., Jensen, J. H., Koseki, S., Matsunaga, N., Nguyen, K. A., Su, S. J., Windus, T. L., Dupuis, M., and Montgomery, J. A. (1993) *J. Comput. Chem.,* **14**, 1347–63.

Gao, J., Liu, W., Song, B., and Liu, C. (2004) *J. Chem. Phys.,* **121**, 6658–66.

Garcia-Hernandez, M., Lauterbach, C., Kruger, S., Matveev, A., and Rösch, N. (2002) *J. Comput. Chem.,* **23**, 834–46.

GAUSSIAN: GAUSSIAN03, Frisch, M. J. *et al.*, Gaussian, Inc., Wallingford, CT. http://www.gaussian.com

Geoffrey, G. L. and Bassner, S. L. (1988) *Adv. Organomet. Chem.,* **28**, 1–83.

Gingerich, K. A. (1967) *J. Chem. Phys.,* **47**, 2192–3.

Gingerich, K. A. (1980) *Symp. Faraday Soc.,* **14**, 109–25.

Glueckauf, E. and McKay, H. A. C. (1950) *Nature,* **165**, 594–5.

Gorokhov, L. N., Emel'yanov, A. M., and Khodeev, Y. S. (1974) *Teplofiz. Vys. Temp.,* **12**, 1307–9.

Gourier, D., Caurant, D., Arliguie, T., and Ephritikhine, M. (1998) *J. Am. Chem. Soc.,* **120**, 6084–92.

Grant, I. P. and Quiney, H. M. (2000) *Int. J. Quantum. Chem.,* **80**, 283–97.

Green, D. W., Gabelnick, S. D., and Reedy, G. T. (1976) *J. Chem. Phys.,* **64**, 1697–705.

Green, D. W. and Reedy, G. T. (1976) *J. Chem. Phys.,* **65**, 2921–2.

Green, D. W. and Reedy, G. T. (1978a) *J. Chem. Phys.,* **69**, 544–51.

Green, D. W. and Reedy, G. T. (1978b) *J. Chem. Phys.,* **69**, 552–5.

Green, D. W. and Reedy, G. T. (1979) *J. Mol. Spectrosc.,* **74**, 423–34.

Green, D. W. (1980) *Int. J. Thermophys.,* **1**, 61–71.

Green, D. W., Reedy, G. T., and Gabelnick, S. D. (1980) *J. Chem. Phys.,* **73**, 4207–16.

Green, J. C., Green, M. L. H., Kaltsoyannis, N., Mountford, P., Scott, P., and Simpson, S. J. (1992) *Organometallics,* **11**, 3353–61.

Green, J. C., Kaltsoyannis, N., Mac Donald, M. A., and Sze, K. H. (1994) *J. Am. Chem. Soc.,* **116**, 1994–2004.

Gropen, O. (1999) *J. Phys. Chem. A,* **103**, 8257–64.

Gulino, A., Ciliberto, E., Di Bella, S., Fragalà, I., Seyam, A. M., and Marks, T. J. (1992) *Organometallics,* **11**, 3248–57.

Gulino, A., Di Bella, S., Fragalà, I. L., Casarin, M., Seyam, A. M., and Marks, T. J. (1993) *Inorg. Chem.,* **32**, 3873–9.

Hamermesh, M. (1989) *Group Theory and its Application to Physical Problems,* Dover, Mineola, New York.

Han, Y. and -K. Hirao, K. (2000) *J. Chem. Phys.,* **113**, 7345–50.

Han, J., Kaledin, L. A., Goncharov, V., Komissarov, A. V., and Heaven, M. C. (2003) *J. Am. Chem. Soc.,* **125**, 7176–7.

Hay, P. J., Wadt, W. R., Kahn, L. R., Raffenetti, R. C., and Phillips, D. H. (1979) *J. Chem. Phys.,* **71**, 1767–79.

Hay, P. J. (1983) *J. Chem. Phys.,* **49**, 5468–82.

Hay, P. J. and Wadt, W. R. (1985) *J. Chem. Phys.,* **82**, 270–83.

Hay, P. J., Ryan, R. R., Salazar, K. V., Wrobleski, D. A., and Sattelberger, A. P. (1986) *J. Am. Chem. Soc.,* **108**, 313–15.

Hay, P. J. and Martin, R. L. (1998) *J. Chem. Phys.,* **109**, 3875–81.

Hay, P. J., Martin, R. L., and Schreckenbach, G. (2000) *J. Phys. Chem. A,* **104**, 6259–70.

Hay, P. J. (2003) *Faraday Discuss.,* **124**, 69–83.

Hayes, R. G. and Edelstein, N. M. (1972) *J. Am. Chem. Soc.,* **94**, 8688–91.

Heinemann, C. and Schwarz, H. (1995) *Chem. Eur. J.,* **1**, 7–11.

Herzberg, G. (1944) *Atomic Spectra and Atomic Structure,* Dover, New York.

Herzberg, G. (1989) *Molecular Spectra and Molecular Structure Volume I – Spectra of Diatomic Molecules,* Krieger, Malaber, FL.

Herzberg, G. (1991) *Molecular Spectra and Molecular Structure Volume III – Electronic Spectra and Electronic Structure of Polyatomic Molecules,* Krieger, Malaber, FL.

Hess, B. A. (2003) *Relativistic Effects in Heavy-Element Chemistry and Physics,* JohnWiley, Chichester.

Hildenbrand, D. and Lau, K. H. (1991) *J. Chem. Phys.,* **94**, 1420–5.

Himmel, H.-J., Downs, A. J., and Greene, T. M. (2002) *Chem. Rev.,* **102**, 4191–241.

Hirao, K., and Ishikawa, S., (eds.) (2004) *Recent Advances in Relativistic Molecular Theory, Recent Advances in Computational Chemistry*, vol 5, World Scientific, Singapore.

Hirata, S., Yanai, T., de Jong, W. A., Nakajima, T., and Hirao, K. (2004) *J. Chem. Phys.,* **120**, 3297–310.

Hohenberg, and P. Kohn, W. (1964) *Phys. Rev. B,* **136**, 864–71.

Hong, G., Schautz, F., and Dolg, M. (1999) *J. Am. Chem. Soc.,* **121**, 1502–12.

Hong, G., Dolg, M., and Li, L. (2000) *Int. J. Quantum. Chem.,* **80**, 201–9.

Hong, G., Dolg, M., and Li, L. (2001) *Chem. Phys. Lett.,* **334**, 396–402.

Hunt, and R. D. Andrews, L. (1993) *J. Phys. Chem.,* **98**, 3690–6.

Hunt, R. D., Yustein, J. T., and Andrews, L. (1993) *J. Chem. Phys.,* **98**, 6070–4.

Huzinaga, and S. Cantu, A. A. (1971) *J. Chem. Phys.,* **55**, 5543–9.

Huzinaga, S., Seijo, L., Barandiarán, Z., and Klobukowski, M. (1987) *J. Chem. Phys.,* **86**, 2132–45.

Infante, and I. Visscher, L. (2004a) *J. Comput. Chem.,* **25**, 386–92.

Infante, and I. Visscher, L. (2004b) *J. Chem. Phys.,* **121**, 5783–8.

Ionova, G. V., Mironov, V. S., Spitsyn, V. I., and Pershina, V. G. (1981) *Radiokhimiya,* **23**, 6–11.

Ismail, N., Heully, J.-L., Saue, T., Daudey, J.-P., and Marsden, C. J. (1999) *Chem. Phys. Lett.,* **300**, 296–302.

Jacox, M. E. (1994) *Chem. Phys.,* **189**, 149–70.

Jacox, M. E. (2003) *J. Phys. Chem. Ref. Data,* **32**, 1–441.

Jamorski, C., Casida, M. E., and Salahub, D. R. (1996) *J. Chem. Phys.,* **104**, 5134–47.

Jensen, W. B. (1982) *J. Chem. Educ.,* **59**, 634.

Jansen, G. and Hess, B. A. (1989) *Phys. Rev. A,* **39**, 6016–17.

Janiak, C. and Schumann, H. (1991) *Adv. Organomet. Chem.,* **33**, 291–393.

Jensen, F. (1999) *Introduction to Computational Chemistry,* John Wiley, New York.

Jensen, M. P. and Bond, A. H. (2002) *J. Am. Chem. Soc.,* **124**, 9870–7.

Jones, L. H. and Penneman, R. A. (1953) *J. Chem. Phys.,* **21**, 542–4.

Jones, L. H. and Ekberg, S. (1977) *J. Chem. Phys.,* **67**, 2591–5.

Jørgensen, C. K. (1970) *Prog. Inorg. Chem.,* **12**, 101–58.

Jørgensen, C. K. and Reisfeld, R. (1983) *J. Electrochem. Soc.,* **130**, 681–4.

Joubert, L. and Maldivi, P. (2001) *J. Phys. Chem. A,* **105**, 9068–76.

Kaltsoyannis, N. (1995) *J. Chem. Soc., Dalton Trans.*, 3727–30.

Kaltsoyannis, N. and Bursten, B. E. (1995) *Inorg. Chem.,* **34**, 2735–44.

Kaltsoyannis, N. (1997) *J. Chem. Soc.*, *Dalton Trans.*, 1–11.

Kaltsoyannis, N. and Bursten, B. E. (1997) *J. Organomet. Chem.,* **528**, 19–33.

Kaltsoyannis, N. and Scott, P. (1998) *Chem. Commun.*, 1665–6.

Kaltsoyannis, N. and Scott, P. (1999) *The f-Elements,* Oxford University Press, Oxford.

Kaltsoyannis, N. and Russo, M. R. (2002) *J. Nucl. Sci. Technol.,* Suppl. 3, 393–9.

Kaltsoyannis, N. (2003) *Chem. Soc. Rev.,* **32**, 9–16.

Karraker, D. G., Stone, J. A., Jones, E. R. Jr, and Edelstein, N. M. (1970) *J. Am. Chem. Soc.,* **92**, 4841–5.

Karraker, D. G. (1973) *Inorg. Chem.,* **12**, 1105–8.

Katz, J. J., Seaborg, G. T., and Morss, L. R. (eds.) (1986) *Chemistry of the Actinide Elements,* vol. 2, Chapman & Hall, London.

Katzin, L. I. (1950) *Nature,* **166**, 605.

Kimura, M., Schomaker, V., Smith, D. W., and Weinstock, B. (1968) *J. Chem. Phys.,* **48**, 4001–12.

Kiplinger, J. L., John, K. D., Morris, D. E., Scott, B. L., and Burns, C. J. (2002) *Organometallics,* **21**, 4306–8.

Knappe, P. and Rösch, N. (1990) *J. Chem. Phys.,* **92**, 1153–62.

Koch, W. and Holthausen, M. C. (2001) *A Chemist's Guide to Density Functional Theory,* Wiley-VCH, Weinheim.

Koelling, D. D., Ellis, D. E., and Artlett, R. J. (1976) *J. Chem. Phys.,* **65**, 3931–40.

Kohn, W. and Sham, L. J. (1965) *Phys. Rev.,* **140**, A1133.

Korobkov, I., Gambarotta, S., Yap, G. P. A., Thompson, L., and Hay, P. J. (2001) *Organometallics,* **20**, 5440–5.

Koster, G. F., Dimmock, J. O., Wheeler, R. G., and Staz, H. (1963) *Properties of the Thirty-Two Point Groups,* MIT Press, Cambridge, MA.

Kot, W. K., Shalimoff, G. V., Edelstein, N. M., Edelman, M. A., and Lappert, M. F. (1988) *J. Am. Chem. Soc.,* **110**, 986–7.

Kovács, A. and Konings, R. J. M. (2004) *J. Mol. Struct.* (*Theochem*), **684**, 35–42.

Küchle, W., Dolg, M., Stoll, H., and Preuss, H. (1994) *J. Chem. Phys.,* **100**, 7535–42.

Kushto, G. P., Souter, P. F., Andrews, L., and Neurock, M. (1997) *J. Chem. Phys.,* **106**, 5894–903.

Kushto, G. P., Souter, P. F., and Andrews, L. (1998) *J. Chem. Phys.,* **108**, 7121–30.

Kushto, G. P. and Andrews, L. (1999) *J. Phys. Chem. A,* **103**, 4836–44.

Lander, G. H., Fisher, E. S., and Bader, S. D. (1994) *Adv. Phys.,* **43**, 1–111.

Lauher, J. W. and Hoffmann, R. (1976) *J. Am. Chem. Soc.,* **98**, 1729–42.

Leary, H. J., Rooney, T. A., Cater, E. D., and Friedrich, H. B. (1971) *High Temp. Sci.,* **3**, 433–43.

Lee, Y. S., Ermler, W. C., and Pitzer, K. S. (1977) *J. Chem. Phys.,* **67**, 5861–76.

Lee, C., Yang, W., and Parr, R. G. (1988) *Phys. Rev. B,* **37**, 785–9.

Levine, I. N. (2000) *Quantum Chemistry,* Prentice-Hall, Upper Saddle River, NJ.

Li, J. and Bursten, B. E. (1997) *J. Am. Chem. Soc.,* **119**, 9021–32.

Li, J. and Bursten, B. E. (1998) *J. Am. Chem. Soc.,* **120**, 11456–66.

Li, J. and Bursten, B. E. (1999) *J. Am. Chem. Soc.,* **121**, 10243–4.

Li, J., Bursten, B. E., Zhou, M., and Andrews, L. (2001) *Inorg. Chem.,* **40**, 5448–60.

Li, J., Bursten, B. E., Liang, B. Y., and Andrews, L. (2002) *Science,* **295**, 2242–5.

Li, J., Bursten, B. E., Andrews, L., and Marsden, C. J. (2004) *J. Am. Chem. Soc.,* **126**, 3424–5.

Liang, B. and Andrews, L. (2002) *J. Phys. Chem. A,* **106**, 4038–41.

Liang, B. Y., Andrews, L., Li, J., and Bursten, B. E. (2002) *J. Am. Chem. Soc.,* **124**, 9016–17.

Liang, B. Y., Andrews, L., Li, J., and Bursten, B. E. (2003) *Chem. Eur. J.,* **9**, 4781–8.

Liang, B. Y., Andrews, L., Li, J., and Bursten, B. E. (2004) *Inorg. Chem.,* **43**, 882–94.

Liang, B., Hunt, R. D., Kushto, G. P., Andrews, L., Li, J., and Bursten, B. E. (2005) *Inorg. Chem.,* **44**, 2159–68.

Liu, W., Dolg, M., and Fulde, P. (1997) *J. Chem. Phys.,* **107**, 3584–91.

Liu, W., Wang, F., and Li, L. (2004) Recent advances in molecular theory, in *Recent Advances in Computational Chemistry,* vol. 5 (eds. K. Hirao and S. Ishikawa), World Scientific, Singapore, pp. 257–82.

Lue, C. J., Jin, J., Ortiz, M. J., Rienstra-Kiracofe, J. C., and Heaven, M. C. (2004) *J. Am. Chem. Soc.,* **126**, 1812–15.

MAGIC: Willetts, A., Gagliardi, L., Ioannou, A. G., Simper, A. M., Skylaris, C.-K., Spencer, S., and Handy, N. C. (2000) *Int. Rev. Phys. Chem.,* **19**, 327–62.

Majumdar, D., Balasubramanian, K., and Nitsche, H. (2002) *Chem. Phys. Lett.,* **361**, 143–51.

Makhyoun, M. A., El-Issa, B. D., and Salsa, B. A. (1987) *J. Mol. Struct.* (*Theochem*), **38**, 241–8.

Malli, G. L. (ed.) (1983) *Relativistic Effects in Atoms, Molecules and Solids,* NATO ASI Ser. B, 87, Plenum, New York.

Malmqvist, P.-A., Roos, B. O., and Schimmelpfennig, B. (2002) *Chem. Phys. Lett.,* **357**, 230–40.

Marian, C. M. (2001) *Rev. Comput. Chem.,* **17**, 99–204.

Marks, T. J. (1976) *Acc. Chem. Res.,* **9**, 223–30.

Marks, T. J. (1979) *Prog. Inorg. Chem.,* **25**, 223–333.

Marks, T. J. and Fischer, R. D. (eds.) (1979) *Organometallics of the f-Elements,* NATO Advanced Study Institutes, Series C, *Mathematical and Physical Sciences*, 44, Reidel, Dordrecht.

Marks, T. J. (1982) *Science,* **217**, 989–97.

Maron, L., Leininger, T., Schimmelpfennig, B., Vallet, V., Heully, J.-L., Teichteil, C., Gropen, O., and Wahlgren, U. (1999) *Chem. Phys.,* **244**, 195–201.

Maron, L., Perrin, L., Eisenstein, O., and Andersen, R. A. (2002) *J. Am. Chem. Soc.,* **124**, 5614–15.

Matonic, J. H., Scott, B. L., and Neu, M. P. (2001) *Inorg. Chem.,* **40**, 2638–9.

Matsika, S. and Pitzer, R. M. (2000) *J. Phys. Chem. A,* **104**, 4064–8.

Matsika, S., Pitzer, R. M., and Reed, D. T. (2000) *J. Phys. Chem. A,* **104**, 11983–92.

Matsika, S. and Pitzer, R. M. (2001) *J. Phys. Chem. A,* **105**, 637–45.

Matsika, S., Zhang, Z., Brozell, S. R., Blaudeau, -P., J.Wang, Q., and Pitzer, R. M. (2001) *J. Phys. Chem. A,* **105**, 3825–8.

Matsuoka, O. and Watanabe, Y. (2004) Recent advances in relativistic molecular theory, in *Recent Advances in Computational Chemistry,* vol. 5 (eds. K. Hirao and Y. Ishikawa), World Scientific, Singapore, pp. 247—55.

Matthews, J. R. (1987) *J. Chem. Soc., Faraday Trans. 2,* **83**, 1273–85.

Mazzanti, M., Wietzke, R., Pécaut, J., Latour, J.-M., Maldivi, P., and Remy, M. (2002) *Inorg. Chem.,* **41**, 2389–99.

McDowell, R. S., Asprey, L. B., and Paine, R. T. (1974) *J. Chem. Phys.,* **61**, 3571–80.

McGlynn, S. P. and Smith, J. K. (1961) *J. Mol. Spectrosc.,* **6**, 164–87.

Mochizuki, Y. and Tatewaki, H. (2002) *J. Chem. Phys.,* **116**, 8838–42.

Mochizuki, Y. and Tatewaki, H. (2003) *J. Chem. Phys.,* **118**, 9201–7.

Mochizuki, Y. and Tsushima, S. (2003) *Chem. Phys. Lett.,* **372**, 114–20.

MOLFDIR: Visscher, L., Visser, O., Aerts, P. J. C., Merenga, H., and Nieuwpoort, W. C. (1994) *Comput. Phys. Commun.,* **81**, 120–44. http://theochem.chem.rug.nl/~broer/Molfdir/Molfdir.html

Moll, H., Denecke, M. A., Jalilehvand, F., Sandström, M., and Grenthe, I. (1999) *Inorg. Chem.,* **38**, 1795–9.

Møller, C. and Plesset, M. S. (1934) *Phys. Rev.,* **46**, 618–22.

Motegi, K., Nakajima, T., Hirao, K., and Seijo, L. (2001) *J. Chem. Phys.,* **114**, 6000–6.

Mucci, J. F. and March, N. H. (1985) *J. Chem. Phys.,* **82**, 5099–101.

Nakajima, T. and Hirao, K. (1999) *Chem. Phys. Lett.,* **302**, 383–91.

Nash, C. S. and Bursten, B. E. (1995) *New J. Chem.,* **19**, 669–75.

Nash, C. S., Bursten, B. E., and Ermler, W. C. (1997) *J. Chem. Phys.,* **106**, 5133–42.

Nash, C. S. and Bursten, B. E. (1999) *J. Am. Chem. Soc.,* **121**, 10830–1.

Nash, C. S., Bursten, B. E., and Ermler, W. C. (1999) *J. Chem. Phys.,* **111**, 2347 (erratum).

Navaza, A., Charpin, P., Vigner, D., and Heger, G. (1991) *Acta Crystallogr.,* **C47**, 1842–5.

Neuefeind, J., Soderholm, L., and Skanthakumar, S. (2004) *J. Phys. Chem. A,* **108**, 2733–9.

NWChem: William R. Wiley Environmental Molecular Sciences Laboratory, Pacific Northwest National Laboratory, Richland, Washington.http://www.emsl.pnl.gov/docs/nwchem/nwchem.html

Ohishi, M., Suzuki, H., Ishikawa, S., Yamada, C., Kanamori, H., Irvine, W. M., Brown, R. D., Godfrey, P. D., and Kaifu, N. (1991) *Astrophys. J.,* **380**, L39–42.

Onoe, J., Takeuchi, K., Nakamatsu, H., Mykoyama, T., Sekine, R., Kim, B. I., and Adachi, H. (1993) *J. Chem. Phys.,* **99**, 6810–17.

Ortiz, J. V. (1986) *J. Am. Chem. Soc.,* **108**, 550–1.

Ortiz, J. V., Hay, P. J., and Martin, R. L. (1992) *J. Am. Chem. Soc.,* **114**, 2736–7.

Paine, R. T., McDowell, R. S., Asprey, L. B., and Jones, L. H. (1976) *J. Chem. Phys.,* **64**, 3081–3.

PARAGAUSS: Belling, T., Grauschopf, T., Krüger, S., Nörtemann, F., Staufer, M., Mayer, M., Nasluzov, V. A., Birkenheuer, U., Hu, A., Matveev, A. V., Shor, A. M., Fuchs-Rohr, M. S. K., Neyman, K. M., Ganyushin, D. I., Kerdcharoen, T., Woiterski, A., Gordienko, A. B., Majumder, S., and Rösch, N., Technische Universi•tät München, München, Germany, 2004.

Parry, J., Carmona, E., Coles, S., and Hursthouse, M. (1995) *J. Am. Chem. Soc.,* **117**, 2649–50.

Parry, J. S., Cloke, F. G. N., Coles, S. J., and Hursthouse, M. B. (1999) *J. Am. Chem. Soc.,* **121**, 6867–71.

Paulovic, J., Nakajima, T., Hirao, K., and Seijo, L. (2002) *J. Chem. Phys.,* **117**, 3597–604.

Paulovic, J., Nakajima, T., Hirao, K., Lindh, R., and Malmqvist, P. A. (2003) *J. Chem. Phys.,* **119**, 798–805.

Pepper, M. and Bursten, B. E. (1990) *J. Am. Chem. Soc.,* **112**, 7803–4.

Pepper, M. and Bursten, B. E. (1991) *Chem. Rev.,* **91**, 719–41.

Peralta, J. E. and Scuseria, G. E. (2004) *J. Chem. Phys.,* **120**, 5875–81.

Perdew, J. P., Chevary, J. A., Vosko, S. H., Jackson, K. A., Pederson, M. R., Singh, D. J., and Fiolhais, C. (1992) *Phys. Rev. B,* **46**, 6671–87.

Perdew, J. P. and Wang, Y. (1992) *Phys. Rev. B,* **45**, 13244–9.

Pershina, V. G., Ionova, G. V., and Spitsyn, V. I. (1982) *Radiokhimiya,* **24**, 154–63.

Pershina, V. G. (1996) *Chem. Rev.,* **96**, 1977–2010.

Petersilka, M., Grossmann, U. J., and Gross, E. K. U. (1996) *Phys. Rev. Lett.,* **76**, 1212–15.

Pierloot, K. (2003) *Mol. Phys.,* **101**, 2083–94.

Pitzer, K. S. (1979) *Acc. Chem. Res.,* **12**, 271–5.

Pitzer, R. M. and Winter, N. W. (1988) *J. Phys. Chem.,* **92**, 3061–3.

Pople, J. A., Seeger, R., and Krishna, R. (1977) *Int. J. Quantum. Chem. Symp.,* **11**, 149–63.

Powell, R. E. (1968) *J. Chem. Educ.,* **45**, 558–63.

Privalov, T., Macak, P., Schimmelpfennig, B., Fromager, E., Grenthe, I., and Wahlgren, U. (2004) *J. Am. Chem. Soc.,* **126**, 9801–8.

Pucci, R. and March, N. H. (1986) *Phys. Rev. A,* **33**, 3511–14.

Purvis, G. D. and Bartlett, R. J. (1982) *J. Chem. Phys.,* **76**, 1910–18.

Pyykkö, P. (1978) *Adv. Quantum Chem.,* **11**, 353–409.

Pyykkö, P. and Desclaux, J.-P. (1979) *Acc. Chem. Res.,* **12**, 276–81.

Pyykkö, P. and Lohr, L. L. Jr (1981) *Inorg. Chem.,* **20**, 1950–9.

Pyykkö, P. and Toivonen, H. (1983) *Tables of Representation and Rotation Matrices for the Relativistic Irreducible Representations of 38 Point Groups, Acta Acad. Aboensis,* Ser. B, No. 2, Åbo Akademi, Åbo, Finland.

Pyykkö, P. (1986) Relativistic theory of atoms and molecules. A bibliography 1916–1985, in *Lecture Notes in Chemistry*, vol. 41, Springer-Verlag, Berlin.

Pyykkö, P. (1988) *Chem. Rev.,* **88**, 563–94.

Pyykkö, P., Laakkonen, L. J., and Tatsumi, K. (1989) *Inorg. Chem.,* **28**, 1801–5.

Pyykkö, P. and Zhao, Y. (1991) *Inorg. Chem.,* **30**, 3787–8.

Pyykkö, P. (1993) Relativistic theory of atoms and molecules II. A bibliography 1986–1992, in *Lecture Notes in Chemistry*, vol. 60, Springer-Verlag, Berlin.

Pyykkö, P., Li, J., and Runeberg, N. (1994) *J. Phys. Chem.,* **98**, 4809–13.

Pyykkö, P. (2000a) *Science,* **290**, 117–18.

Pyykkö, P. (2000b) Relativistic theory of atoms and molecules III. A bibliography 1993–1999, in *Lesture Notes in Chemistry*, vol. 76, Springer-Verlag, Berlin.

Pyykkö, P., Runeberg, N., Straka, M., and Dyall, K. G. (2000) *Chem. Phys. Lett.,* **328**, 415–19.

Raghavachari, K., Trucks, G. W., Pople, J. A., and Head-Gordon, M. (1989) *Chem. Phys. Lett.,* **157**, 479–83.

Reich, T., Bernhard, G., Geipel, G., Funke, H., Heining, C., Rosber, A., Matz, W., Schnell, N., and Nitsche, H. (2000) *Radiochim. Acta,* **88**, 633–7.

Reynolds, L. T. and Wilkinson, G. (1956) *J. Inorg. Nucl. Chem.,* **2**, 246–53.

Roesky, P. W. (2001) *Eur. J. Inorg. Chem.*, 1653–60.

Roos, B. O., Widmark, P.-O., and Gagliardi, L. (2003) *Faraday Discuss.,* **124**, 57–62.

Roos, B. O. and Malmqvist, P.-A. (2004) *Phys. Chem. Chem. Phys.,* **6**, 2919–27.

Rösch, N. and Streitweiser, A. J. (1983) *J. Am. Chem. Soc.,* **105**, 7237–40.

Rösch, N., Kruger, S., Mayer, M., and Nasluzov, V. A. (1996) *Theor. Comput. Chem.,* **4**, 497–566.

Roussel, P. and Scott, P. (1998) *J. Am. Chem. Soc.,* **120**, 1070–1.

Roussel, P., Errington, W. B., Kaltsoyannis, N., and Scott, P. (2001) *J. Organomet. Chem.,* **635**, 69–74.

Sankaran, K., Sundararajan, K., and Viswanathan, K. S. (2001) *J. Phys. Chem. A,* **105**, 3995–4001.

Saue, T., Fægri, K., Helgaker, T., and Gropen, O. (1997) *Mol. Phys.,* **91**, 937–50.

Schlosser, F., Kruger, S., and Rösch, N. (2003) *Eur. J. Inorg. Chem.*, **17**, 3144–51.

Schneider, W. F., Strittmatter, R. J., Bursten, B. E., and Ellis, D. E. (1991) in *Density Functional Methods in Chemistry* (eds. J. K. Labanowski and J. W. Andzelm), Springer-Verlag, New York, pp. 247–60.

Schreckenbach, G., Hay, P. J., and Martin, R. L. (1998) *Inorg. Chem.,* **37**, 4442–51.

Schreckenbach, G., Hay, P. J., and Martin, R. L. (1999) *J. Comput. Chem.,* **20**, 70–90.

Schreckenbach, G. (2000) *Inorg. Chem.,* **39**, 1265–74.

Schwarz, W. H. E. (1990) in *Theoretical Models of Chemical Bonding* (ed. Z. B. Maksic), Springer-Verlag, Berlin p. 595.

Schwerdtfeger, P. (ed.) (2002) *Relativistic Electronic Structure Theory: Part I, Fundamentals Theoretical and Computational Chemistry,* vol. 11, , Elsevier Science B. V., Amsterdam.

Schwerdtfeger, P. (ed.) (2004) *Relativistic Electronic Structure Theory, Part II: Applications Theoretical and Computational Chemistry,* vol. 14, Elsevier Science B. V., Amsterdam.

Seidel, S. and Seppelt, K. (2000) *Science,* **290**, 117–18.

Seijo, L. and Barandiarán, Z. (1999) in *Computational Chemistry: Reviews of Current Trends*, vol. 4, (ed. J. Leszczynski), World Scientific, Singapore, pp. 55–152.

Seijo, L. and Barandiarán, Z. (2001) *J. Chem. Phys.,* **115**, 5554–60.

Seijo, L., Barandiarán, Z., and Harguindey, E. (2001) *J. Chem. Phys.,* **114**, 118–29.

Seijo, L., Barandiarán, Z., and Ordejon, B. (2003) *Mol. Phys.,* **101**, 73–80.

Seip, H. M. (1965) *Acta Chem. Scand.,* **19**, 1955–68.

Seyferth, D. (2004) *Organometallics,* **23**, 3562–83.

Shavitt, I. (1977) in *Methods of Electronic Structure Theory* (ed. H. F. Schaefer III), Plenum, New York, pp. 189–276.

Shepard, R., Shavitt, I., Pitzer, R. M., Comeau, D. C., Pepper, M., Lischka, H., Szalay, P. G., Ahlrichs, R., Brown, F. B., and Zhao, J. G. (1988) *Int. J. Quantum Chem., Quantum Chem. Symp.,* **22**, 149–65.

Slater, J. L., Sheline, R. K., Lin, K. C., and Weltner, J. W. (1971) *J. Chem. Phys.,* **55**, 5129–30.

Slater, J. C. (1974) *The Self-Consistent Field for Molecules and Solids,* McGraw-Hill, New York.

Smith, G. M., Suzuki, H., Sonnenberger, D. C., Day, V. W., and Marks, T. J. (1986) *Organometallics,* **5**, 549–61.

Soderlind, P. (1998) *Adv. Phys.,* **47**, 959–98.

Solar, J. P., Burghard, H. P. G., Banks, R. H., Streitwieser, A. Jr., and Brown, D. (1980) *Inorg. Chem.,* **19**, 2186–8.

Sonnenberg, J. L., Hay, P. J., Martin, R. L., and Bursten, B. E. (2005) *Inorg. Chem.,* **44**, 2255–62.

Spencer, S., Gagliardi, L., Handy, N. C., Ioannou, A. G., Skylaris, C.-K., Willets, A., and Simper, A. M. (1999) *J. Phys. Chem. A,* **103**, 1831–7.

Sternal, R. S., Brock, C. P., and Marks, T. J. (1985) *J. Am. Chem. Soc.,* **107**, 8270–2.

Sternal, R. S. and Marks, T. J. (1987) *Organometallics,* **6**, 2621–3.

Straka, M., Dyall, K. G., and Pyykko, P. (2001) *Theor. Chem. Acc.,* **106**, 393–403.

Straka, M., Patzschke, M., and Pyykko, P. (2003) *Theor. Chem. Acc.,* **109**, 232–40.

Streitwieser, A. J. and Müller-Westerhoff, U. (1968) *J. Am. Chem. Soc.,* **90**, 7364.

Streitwieser, A. Jr. (1979) in *Organometallics of the f-Elements* (eds. T. J. Marks and R. D. Fischer), Reidel, Dortrecht, pp. 149–77.

Streitwieser, A. Jr. (1984) *Inorg. Chim. Acta,* **94**, 171–7.

Streitwieser, A. Jr. and Kinsley, S. A. (1985) *NATO ASI Ser. C,* **155**, 77–114 and references therein.

Strittmatter, R. J. and Bursten, B. E. (1991) *J. Am. Chem. Soc.,* **113**, 552–9.

Szabo, A. and Ostlund, N. S. (1989) *Modern Quantum Chemistry: Introduction to Advanced Electronic Structure Theory,* McGraw-Hill, New York.

Tague, T. J., Andrews, L., and Hunt, R. D. (1993) *J. Phys. Chem.,* **97**, 10920–4.

Tait, C. D. (1999) The Convergence of Theory and Experiment, Presented at the Symposium of Heavy Element Complexes, 217th ACS National Meeting, Anaheim, CA.

Tatsumi, K. and Hoffmann, R. (1980) *Inorg. Chem.,* **19**, 2656–8.

Tatsumi, K. and Nakamura, A. (1984) *J. Organomet. Chem.,* **272**, 141–53.

Tatsumi, K., Nakamura, A., Hofmann, P., Stauffert, P., and Hoffmann, R. (1985) *J. Am. Chem. Soc.,* **107**, 4440–51.

Tatsumi, K. and Nakamura, A. (1987) *J. Am. Chem. Soc.,* **109**, 3195–206.

Teichteil, C., Pelissier, M., and Spiegelmann, F. (1983) *Chem. Phys.,* **81**, 273–82.

Teichteil, C. and Spiegelmann, F. (1983) *Chem. Phys.,* **81**, 283–96.

Tsushima, S. and Suzuki, A. (1999) *J. Mol. Struct*. (*Theochem*), **487**, 33–8.

Tsushima, S., Yang, T., Mochizuki, Y., and Okamoto, Y. (2003) *Chem. Phys. Lett.,* **375**, 204–12.

TURBOMOLE: Quantum Chemistry Group, University of Karlsruhe, Karlsruhe, Germany. http://www.turbomole.com

Vallet, V., Maron, L., Schimmelpfennig, B., Leininger, T., Teichteil, C., Gropen, O., Grenthe, I., and Wahlgren, U. (1999a) *J. Phys. Chem. A,* **103**, 9285–9.

Vallet, V., Schimmelpfennig, B., Maron, L., Teichteil, C., Leininger, T., Gropen, O., Grenthe, I., and Wahlgren, U. (1999b) *Chem. Phys.,* **244**, 185–93.

Vallet, V., Maron, L., Teichteil, C., and Flament, J.-P. (2000) *J. Chem. Phys.,* **113**, 1391–402.

Vallet, V., Wahlgren, U., Schimmerlpfenning, B., Szabo, Z., and Grenthe, I. (2001) *J. Am. Chem. Soc.,* **123**, 11999–2008.

Vallet, V., Privalov, T., Wahlgren, U., and Grenthe, I. (2004) *J. Am. Chem. Soc.,* **126**, 7766–7.

Van der Sluys, W. G., Burns, C. J., and Sattelberger, A. P. (1989) *Organometallics,* **8**, 855–7.

van Gisbergen, S. J. A., Snijders, J. G., and Baerends, E. J. (1995) *J. Chem. Phys.,* **103**, 9347.

van Lenthe, E., Baerends, E. J., and Snijders, J. G. (1993) *J. Chem. Phys.,* **99**, 4597–610.

van Lenthe, E., Baerends, E. J., and Snijders, J. G. (1994) *J. Chem. Phys.,* **101**, 9783–92.

van Wezenbeek, E. M., Baerends, E. J., and Snijders, J. G. (1991) *Theor. Chem. Acc.,* **81**, 139–55.

van Wullen, C. (1999) *J. Comput. Chem.,* **20**, 51–62.

Vázquez, J., Bo, C., Poblet, M. M., de Pablo, J., and Bruno, J. (2003) *Inorg. Chem.,* **42**, 6136–41.

Volkoy, Y. F. and Kapshuhof, I. I. (1976) *Radiokhimiya,* **18**, 284.

Wadt, W. R. (1981) *J. Am. Chem. Soc.,* **103**, 6053–7.

Wahlgren, U., Schimmelpfennig, B., Jusuf, S., Stromsnes, H., Gropen, O., and Maron, L. (1998) *Chem. Phys. Lett.,* **287**, 525–30.

Wahlgren, U., Moll, H., Grenthe, I., Schimmelpfennig, B., Maron, L., Vallet, V., and Gropen, O. (1999) *J. Phys. Chem. A,* **103**, 8257–64.

Wang, F., Hong, G. Y., and Li, L. M. (2000) *Chem. Phys. Lett.,* **316**, 318–23.

Wang, Q. and Pitzer, R. M. (2001) *J. Phys. Chem. A,* **105**, 8370–5.

Wang, X., Andrews, L., Li, J., and Bursten, B. E. (2004) *Angew. Chem. Int. Edn.,* **43**, 2554–7.

Warner, B. P., Scott, B. L., and Burns, C. J. (1998) *Angew. Chem. Int. Edn. Engl.,* **37**, 959–60.

Watts, J. D., Gauss, J., and Bartlett, R. J. (1993) *J. Chem. Phys.,* **98**, 8718–33.

Wigner (1959) *Group Theory and its Application to the Quantum Mechanics of Atomic Spectra,* Academic Press, New York.

Wilkinson, G., Rosenblum, M., Whiting, M. C., and Woodward, R. B. (1952) *J. Am. Chem. Soc.,* **74**, 2125–6.

Wilkinson, G. (1975) *J. Organomet. Chem.,* **100**, 273–8.

Williams, C. W., Blaudeau, J.-P., Sullivan, J. C., Antonio, M. R., Bursten, B. E., and Soderholm, L. (2001) *J. Am. Chem. Soc.,* **123**, 4346–7.

Wills, J. M. and Eriksson, O. (2000) *Los Alamos Sci.,* **26**, 129–51.

Winter, N. W. and Pitzer, R. M. (1985) *Springer Ser. Opt. Sci.* (*Tunable Solid State Lasers*), **47**, 164–71.

Wood, J. H. and Boring, A. M. (1978) *Phys. Rev. B,* **18**, 2701–11.

Wood, J. H., Boring, M., and Woodruff, S. B. (1981) *J. Chem. Phys.,* **74**, 5225–33.

Wybourne, B. G. (1965) *Spectroscopic Properties of the Rare Earths,* Interscience, New York.

Yabushita, S., Zhang, Z., and Pitzer, R. M. (1999) *J. Phys. Chem. A,* **103**, 5791–800.

Yang, C. Y., Johnson, K. H., and Horsley, J. A. (1978) *J. Chem. Phys.,* **68**, 1001–5.

Yang, T., Tsushima, S., and Suzuki, A. (2001) *J. Phys. Chem. A,* **105**, 10439–45.

Zhang, Z. and Pitzer, R. M. (1999) *J. Phys. Chem. A,* **103**, 6880–6.

Zhou, M. F. and Andrews, L. (1999) *J. Chem. Phys.,* **111**, 11044–9.

Zhou, M. F., Andrews, L., Li, J., and Bursten, B. E. (1999a) *J. Am. Chem. Soc.,* **121**, 9712–21.

Zhou, M. F., Andrews, L., Li, J., and Bursten, B. E. (1999b) *J. Am. Chem. Soc.,* **121**, 12188–9.

Zhou, M., Andrews, L., Ismail, N., and Marsden, C. (2000) *J. Phys. Chem. A,* **104**, 5495–502.

Zhou, M., Andrews, L., and Bauschlicher, C. W. Jr (2001) *Chem. Rev.,* **101**, 1931–62.

Ziegler, T., Tschinke, V., Baerends, E. J., Snijders, J. G., and Ravenek, W. (1989) *J. Phys. Chem.,* **93**, 3050–6.